การผลิตก๊าซไฮโดรเจนจากก๊าซชีวภาพด้วยกระบวนการร่วมระหว่างเคมิคอลลูปปิงแบบแยกน้ำและการรีฟอร์มมิงที่เสริมการดูดซับ: การวิเคราะห์และการออกแบบกระบวนการ

นายณัฐพร ไทรทอง

วิทยานิพนธ์นี้เป็นส่วนหนึ่งของการศึกษาตามหลักสูตรปริญญาวิศวกรรมศาสตรมหาบัณฑิต
สาขาวิชาวิศวกรรมเคมี ภาควิชาวิศวกรรมเคมี
คณะวิศวกรรมศาสตร์ จุฬาลงกรณ์มหาวิทยาลัย
ปีการศึกษา 2560

Hydrogen production from biogas by the combined process of chemical looping water splitting and sorption enhanced reforming process: process analysis and design

Mr. Natthaporn Saithong

A Thesis Submitted in Partial Fulfillment of the Requirements
for the Degree of Master of Engineering Program in Chemical Engineering
Department of Chemical Engineering
Faculty of Engineering
Chulalongkorn University
Academic Year 2017

Thesis Title	Hydrogen production from biogas by the combined process of chemical looping water splitting and sorption enhanced reforming process: process analysis and design
By	Mr. Natthaporn Saithong
Field of Study	Chemical Engineering
Thesis Advisor	Assistant Professor Amornchai Arpornwichanop, D.Eng.

Accepted by the Faculty of Engineering, Chulalongkorn University in Partial Fulfillment of the Requirements for the Master's Degree

.....Dean of the Faculty of Engineering
(Associate Professor Supot Teachavorasinskun, D.Eng.)

THESIS COMMITTEE

.....Chairman
(Professor Sarawut Rimdusit, Ph.D.)

.....Thesis Advisor
(Assistant Professor Amornchai Arpornwichanop, D.Eng.)

.....Examiner
(Palang Bumroongsakulsawat, Ph.D.)

.....External Examiner
(Assistant Professor Suthida Authayanun, Ph.D.)

ณัฐพร ไทรทอง : การผลิตก๊าซไฮโดรเจนจากก๊าซชีวภาพด้วยกระบวนการร่วมระหว่างเคมิคอลลูปปิงแบบแยกน้ำและการรีฟอร์มมิงที่เสริมการดูดซับ: การวิเคราะห์และการออกแบบกระบวนการ (Hydrogen production from biogas by the combined process of chemical looping water splitting and sorption enhanced reforming process: process analysis and design) อ.ที่ปรึกษาวิทยานิพนธ์หลัก: ผศ. ดร.อมรชัย อาภรณ์วิชานพ, 144 หน้า.

งานวิจัยนี้นำเสนอกระบวนการร่วมระหว่างกระบวนการเคมิคอลลูปปิงแบบรีฟอร์มมิงที่เสริมการดูดซับและกระบวนการเคมิคอลลูปปิงแบบแยกน้ำ (SECLR-WS) สำหรับการผลิตไฮโดรเจนจากก๊าซชีวภาพ ด้วยการใช้เหล็กออกไซด์เป็นตัวพาออกซิเจน และใช้แคลเซียมออกไซด์เป็นตัวดูดซับคาร์บอนไดออกไซด์ การจำลองกระบวนการ SECLR-WS จะอยู่บนพื้นฐานของวิธีการเชิงเทอร์โมไดนามิกส์ โดยการใช้โปรแกรมแอสเพนพลัส (Aspen Plus simulator) จากการศึกษาผลกระทบของตัวแปรดำเนินงานพบว่า ค่าสัดส่วนผลได้ของไฮโดรเจน ความบริสุทธิ์ของไฮโดรเจนในเตาปฏิกรณ์เชื้อเพลิง (FR) และค่าสัดส่วนการแปลงผันของมีเทน สามารถปรับปรุงได้ด้วยการเพิ่มค่าสัดส่วนไอน้ำที่ป้อนเข้าสู่เตาปฏิกรณ์ FR ต่อมีเทน (S_{FR}/CH_4) และค่าสัดส่วนแคลเซียมออกไซด์ต่อมีเทน (CaO/CH_4) การลดความเข้มข้นของคาร์บอนมอนอกไซด์ในสายผลิตภัณฑ์ไฮโดรเจนบริสุทธิ์สามารถทำได้โดยการเพิ่มความดันของเตาปฏิกรณ์ไอน้ำ (SR) สภาวะการดำเนินการที่เหมาะสมของกระบวนการ SECLR-WS สามารถเกิดขึ้นที่ อุณหภูมิของเตาปฏิกรณ์ FR เท่ากับ 606.9 ^oC และค่าสัดส่วน S_{FR}/CH_4 S_{SR}/CH_4 Fe_3O_4/CH_4 และ CaO/CH_4 เท่ากับ 2.35 2.33 0.92 และ 1.94 ตามลำดับ ประสิทธิภาพของกระบวนการ SECLR-WS ได้ถูกเปรียบเทียบกับกระบวนการเคมิคอลลูปปิงแบบรีฟอร์มมิงที่เสริมการดูดซับ (SECLR) และกระบวนการเคมิคอลลูปิงแบบแยกน้ำ (CLWS) นอกจากนี้ กระบวนการ SECLR-WS ได้ถูกปรับปรุงประสิทธิภาพเชิงความร้อนของกระบวนการด้วยการออกแบบเครือข่ายแลกเปลี่ยนความร้อนภายในกระบวนการด้วยการวิเคราะห์จุดพินช์ และได้วิเคราะห์ประสิทธิภาพเชิงความร้อนและเอกเซอร์จีของกระบวนการ เพื่อทำการระบุส่วนที่ใช้พลังงานอย่างไม่มีประสิทธิภาพภายในกระบวนการ จากการวิเคราะห์พบว่า ส่วนที่เกิดการสูญเสียเอกเซอร์จีมากที่สุดในกระบวนการคือเตาปฏิกรณ์ FR และ SR เนื่องจากมีการเกิดปฏิกิริยาเคมีในเตาปฏิกรณ์ดังกล่าว โดยกระบวนการ SECLR-WS มีประสิทธิภาพเชิงเอกเซอร์จี 72.30 % และสูญเสียเอกเซอร์จี 75152.8 kW

ภาควิชา วิศวกรรมเคมี ลายมือชื่อนิสิต .....

สาขาวิชา วิศวกรรมเคมี ลายมือชื่อ อ.ที่ปรึกษาหลัก .....

ปีการศึกษา 2560

5970160421 : MAJOR CHEMICAL ENGINEERING
KEYWORDS: CHEMICAL LOOPING PROCESS / SORPTION-ENHANCED REFORMING / WATER SPLITTING / HYDROGEN

NATTHAPORN SAITHONG: Hydrogen production from biogas by the combined process of chemical looping water splitting and sorption enhanced reforming process: process analysis and design. ADVISOR: ASST. PROF. AMORNCHAI ARPORNWICHANOP, D.Eng., 144 pp.

The integrated sorption-enhanced chemical looping reforming and water splitting (SECLR-WS) process was proposed for hydrogen (H_2) production from biogas using iron oxide as the oxygen carrier and calcium oxide (CaO) as a carbon dioxide (CO_2) adsorbent. The simulation of the SECLR-WS process was based on a thermodynamic approach and was performed using an Aspen Plus simulator. The sensitivity results showed that the H_2 yield (mole of H_2/mole of CH_4), H_2 purity in the fuel reactor (FR), and CH_4 conversion could be improved by increasing the steam feed to the FR to CH_4 (S_{FR}/CH_4) and CaO to CH_4 (CaO/CH_4) molar ratios. The molar concentration of carbon monoxide (CO) in the high-purity H_2 stream could be reduced by increasing the pressure in the steam reactor (SR). The H_2 yield in FR of 3.11 and in SR of 0.66 were obtained at the optimal operating condition at T_{FR} of 606.9 ^oC, S_{FR}/CH_4, S_{SR}/CH_4, Fe_3O_4/CH_4, and CaO/CH_4 molar ratio of 2.35, 2.33, 0.92, and 1.94, respectively. The performance of the optimal designed SECLR-WS process was compared with a sorption-enhanced chemical looping reforming (SECLR) and a chemical looping water splitting (CLWS) processes. The thermal efficiency of the optimal designed SECLR-WS process was further improved by heat exchanger network design based on a pinch analysis. In addition, the energy and exergy analyses of the optimal designed SECLR-WS process were conducted to identify the part of the inefficient energy usage of SECLR-WS process. The results indicated that the highest exergy destruction was occurred in the FR and SR due to the occurrence of several reactions in these units. The exergy efficiency of 76.83 % and 75152.8 kW exergy destruction can be obtained from the SECLR-WS process.

Department: Chemical Engineering Student's Signature .....
Field of Study: Chemical Engineering Advisor's Signature .....
Academic Year: 2017

ACKNOWLEDGEMENTS

First of all, I would like to express my sincere thanks to my thesis advisor, Assistant Professor Dr. Amornchai Arpornwichanop, for his invaluable recommendation as well as constant encouragement throughout the course of this research. I am most grateful for his teaching and suggestions for research methodology and point of view towards life. This thesis would not have been completed without his support that I have always received from him.

Moreover, I gratefully thanks the chairman, Dr. Varun Taepaisitphongse and Professor Dr. Sarawut Rimdusit, and the other member of the thesis committee, Dr. Palang Bumroongsakulsawat and Assistant Professor Dr. Suthida Authayanun, for their time and valuable suggestion in improving my research.

Furthermore, I would also like to thank the Department of Chemical Engineering, Chulalongkorn University for providing the scholarship during my Master's degree study and all my friends in the Computational Process Engineering Research Unit and the Control and System Engineering Research Center for their friendship and help.

Finally, I most gratefully thank my family, especially my father, Mr. Praphun Saithong, and my mother Mrs. Somjit Saithong, for their encouragement and support.

CONTENTS

Page

Page

LIST OF FIGURES

Page

LIST OF TABLES

NOMENCLATURES

a_{ji}	Number of atoms of element j in component i
b_j	Total number of atoms of element j
C_P	Heat capacity (kJ kg^{-1} $^oC^{-1}$)
CP	Heat capacity flow rate (kW $^oC^{-1}$)
CP_C	Heat capacity flow rate of cold streams (kW $^oC^{-1}$)
CP_H	Heat capacity flow rate of hot streams (kW $^oC^{-1}$)
ΔC^o_{Pi}	Standard-sate heat capacity change of reaction to form species i (kJ mol^{-1} K^{-1})
Ex	Exergy (kW)
$\overline{ex}_{ch,i}$	Standard specific molar chemical exergy of component i at T_0 and P_0 (kJ $kmol^{-1}$)
$ex_{ch,j}$	Chemical exergy of stream j (kJ $kmol^{-1}$)
Ex_d	Exergy destruction (kW)
$ex_{ph,j}$	Physical exergy of stream j (kJ $kmol^{-1}$)
Ex_Q	Exergy transfer by heat (kW)
Ex_S	Flow exergy (kW)
$ex_{S,j}$	Specific molar flow exergy of stream j (kJ $kmol^{-1}$)
$Ex_{S,j}$	Flow exergy of stream j (kW)
Ex_W	Exergy transfer by work (kW)
f_i	Fugacity of species I (atm)
f_i^o	Standard-sate fugacity of species I (atm)
F_j	Molar flow rate of stream j (kmol sec^{-1})
f_j^L	Mole fraction of liquid in stream j
f_j^S	Mole fraction of solid in stream j
f_j^V	Mole fraction of gas in stream j
G	Gibbs free energy (kJ)
G_i	Gibbs free energy of species i (kJ mol^{-1})
G_i^o	Standard-sate Gibbs free energy of species i (kJ mol^{-1})
G^t	Total Gibbs free energy (kJ)

ΔG_{fi}^{o}	Standard-state Gibbs free energy change of formation for species i (kJ mol^{-1})
ΔG_{f0i}^{o}	Standard-state Gibbs free energy change of formation for species i at reference temperature T_0 (kJ mol^{-1})
H	Enthalpy (kJ)
$h_{0,j}$	Specific molar enthalpy of stream j at T_0 and P_0 (kJ $kmol^{-1}$)
h_j	Specific molar enthalpy of stream j at T and P (kJ $kmol^{-1}$)
$\Delta\dot{H}$	Enthalpy change rate (kW)
ΔH_{f0i}^{o}	Standard-state enthalpy change of formation for species i at reference temperature T_0 (kJ mol^{-1})
ΔH_i	Net energy in each temperature interval (kW)
ΔH_R^{o}	Standard enthalpy change of reaction (kJ mol^{-1})
L	Lagrange function
LHV_{CH_4}	Lower heating value of methane (kJ $kmol^{-1}$)
LHV_{H_2}	Lower heating value of hydrogen (kJ $kmol^{-1}$)
$\dot{m}$	Mass flow rate (kg sec^{-1})
M	Total number of elements
N	Number of species
$\dot{N}_{CH_4,feed}$	Molar flow rate of methane in feed stream (kmol sec^{-1})
$\dot{N}_{H_2}$	Molar flow rate of hydrogen (kmol sec^{-1})
n_i	Mole of species i (mole)
N_U	Minimum heat exchanger unit
P	Pressure (atm)
P_e	Electric power (kW)
P^{o}	Standard-sate pressure (atm)
Q_{CAL}	Heat duty of the calcinator (kW)
Q_{FR}	Heat duty of the FR (kW)
Q_S	Heat transfer through the process (kW)
Q_{SR}	Heat duty of the SR (kW)
Q_{total}	Total energy input to the process (kW)

R	Gas constant (kJ mol^{-1} K^{-1})
$s_{0,j}$	Specific molar entropy of stream j at T_0 and P_0 (kJ $kmol^{-1}$)
S_{above}	Number of streams above the pinch temperature
S_{below}	Number of streams below the pinch temperature
S_i	Shifted temperature of interval i (^oC)
S_{i+1}	Shifted temperature of interval i+1 (^oC)
s_j	Specific molar etropy of stream j at T and P (kJ $kmol^{-1}$)
$S_{u,above}$	Number of utility above the pinch temperature
$S_{u,below}$	Number of utility below the pinch temperature
T	Temperature (^oC)
T_0	Reference temperature (^oC)
T_s	Supply temperature (^oC)
T_S	System temperature (^oC)
T_t	Target temperature (^oC)
W	Work transfer through the process (kW)
$x_{i,j}$	Mole fraction of component i in liquid phase in stream j.
y_i	Mole fraction of species i
$y_{i,j}$	Mole fraction of component i in gas phase in stream j.
$z_{i,j}$	Mole fraction of component i in solid phase in stream j.

Greek symbols

λ_j	Lagrange multiplier
η_{el}	Electric efficiency of fuel cell.
η_{ex}	Exergy efficiency (%)
$\eta_{ex,i}$	Exergy efficiency of unit i (%)
η_{th}	Thermal or energy efficiency (%)
ϕ_i	Fugacity coeffiient of species i
μ_i	Chemical potential of species i (kJ mol^{-1})

CHAPTER I
INTRODUCTION

1.1 Background and motivation

Hydrogen (H_2) has been regarded as an important alternative fuel which has high energy density and a heating value approximately three to four times higher than natural gas and coal (Phuluanglue, 2015). In addition, H_2 is considered as a clean and environmentally friendly fuel, it can be used as feedstock for synthesizing ammonia and methanol, in petrochemical processes, and it can also be used as a fuel in fuel cells to generate electricity (Balat and Kırtay, 2010). Typically, H_2 is produced from fossil fuels such as coal and natural gas, which are non-renewable energy sources, thus resulting in more greenhouse gas emissions (Muellerlanger *et al.*, 2007). Biogas is an attractive type of renewable fuel composed of 60-80 vol.% methane (CH_4), 40-20 vol.% carbon dioxide (CO_2), and a small amount of hydrogen sulfide (H_2S) (1-3 vol.%). Using of biogas as a feedstock in reforming process for hydrogen production has several advantages, such as reducing greenhouse gas emissions, easy producing from local crops and being compatible to the existing natural gas plant (Effendi *et al.*, 2005; Pipatmanomai *et al.*, 2009; Yang *et al.*, 2014).

Conventionally, H_2 is produced from the steam reforming process using natural gas as feedstock (Boyano *et al.*, 2011; Tugnoli *et al.*, 2008; Zeppieri *et al.*, 2010). In this process, CH_4 firstly reacts with steam to produce synthesis gas (syngas) which mainly consists of H_2 and carbon monoxide (CO), the produced syngas is later sent to the cleaning and purifying processes to produce high purity H_2. Although the steam-methane reforming (SMR) process is widely used, it is a high energy-consumed process, requiring several downstream units for H_2 purification. The catalyst deactivation due to coking is also found (Martínez *et al.*, 2014; Song *et al.*, 2015). As the high energy demand is a major problem of the SMR process, the chemical looping combustion (CLC) process has been developed. In the CLC process, two separate reactors: an air reactor (AR) and a fuel reactor (FR), are required. The metal oxygen carriers (OCs) transfer oxygen between the two reactors and react with the fuel in the

FR and with oxygen in the AR. This process generates heat from the oxidation reaction in the AR. Since in this process air and fuel come in contact indirectly, the combustion gas is not diluted by nitrogen (N_2). Therefore, the gas separation unit or the air separation unit, which consumes high amount of energy, is eliminated (Fan *et al.*, 2017; Ishida and Jin, 1996; Rydén *et al.*, 2008).

Presently, the concept of chemical looping, similar to the CLC process, has been introduced for H_2 production in several ways such as chemical looping H_2 generation (CLHG) (sometimes called chemical looping water splitting (CLWS)) and sorption-enhanced chemical looping reforming (SECLR). The CLWS process was developed from the CLC process to produce H_2, CO_2, and N_2 using iron oxides (Fe_xO_y) as OCs. The CLWS process, well-known as the steam-iron process, which was developed by Howard Lane and his co-workers was the oldest method used to produce high-purity H_2 in the industry (Lane, 1913; Messerschmitt, 1910; Thursfield *et al.*, 2012; Voitic and Hacker, 2016). The CLWS composed of three parts as shown in Figure. 1.1. First, hematite iron (III) oxide (Fe_2O_3), was reduced to wüstite ($Fe_{0.947}O$) by complete oxidation with fuel in the FR to obtain H_2O and CO_2. Subsequently, $Fe_{0.947}O$ was oxidized by H_2O in the steam reactor (SR) to form magnetite iron (II, III) oxide (Fe_3O_4) and produce H_2. In the AR, Fe_3O_4 was fully oxidized by the oxygen in the air and generated Fe_2O_3. The highly exothermic reaction in the AR produced the heat needed for the reduction reactions in the FR, therefore the system could be operated under autothermal conditions (Chiesa *et al.*, 2008; Edrisi *et al.*, 2014; Kathe *et al.*, 2016; Khan and Shamim, 2016; Xiang *et al.*, 2010). The H_2 generated in this process was sufficiently pure for utilization in fuel cell systems. Moreover, a gas separation unit was not required. Chiesa *et al.* (2008) analyzed the three-reactor chemical looping process for H_2 production. The results showed that the efficiency of the chemical looping process was the same as that of the steam reforming process. However, chemical looping was more environmentally friendly because the generated CO_2 could be completely captured. Edrisi *et al.* (2014) simulated and optimized the chemical looping process using iron-oxide-based OCs for H_2, N_2, and CO_2 production. The simulation showed that the high flow rate of the OCs can be used instead of the inert support to improve the heat transfer. However, the produced gas from FR usually contaminated

with H_2 and CO due to the effect of partial oxidation reaction, therefore, a gas separation unit was needed. In addition, the H_2 obtained from the SR was contaminated by CO_2 and CO because of carbon deposition on iron oxide in the reduction step (Chen *et al.*, 2012; Rydén and Arjmand, 2012; Karel Svoboda *et al.*, 2008; K. Svoboda *et al.*, 2007). Rydén and Arjmand (2012) conducted an experimental study on a steam-iron reaction using a two-compartment fluidized-bed reactor. The experiment showed that the natural gas reacting with iron oxide could produce syngas and CO_2. Chen *et al.* (2012) proposed an integrating steam-iron and CLC process to produce H_2 and electrical energy. The CLC process involved the combustion of the gas stream generated from the reduction of iron oxide using syngas.

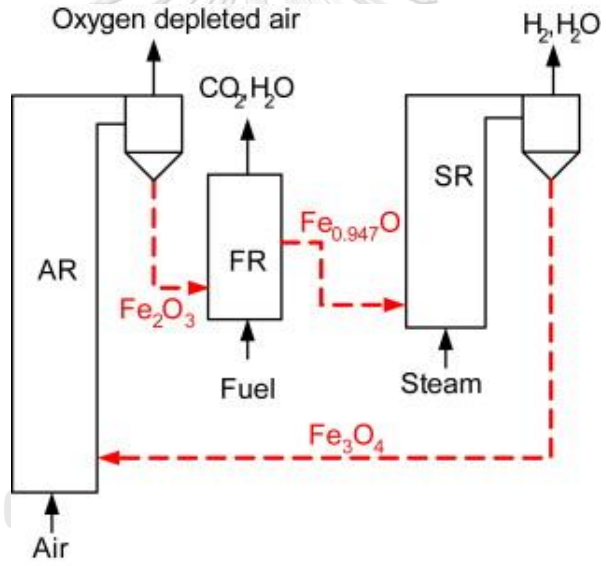

Figure 1.1 Schematic of the three reactors chemical looping water splitting for hydrogen generation (Xiang *et al.*, 2010).

Another H_2 production method based on the use of the chemical looping concept is the SECLR process which was developed from chemical looping reforming (CLR) to improve the steam reforming process using calcium oxide (CaO) as CO_2 adsorbent and metal oxides (MeO), such as nickel oxide (NiO), as OCs. The SECLR process requires three reactors as shown in Figure 1.2. Firstly, the NiO and CaO solid mixture

is fed to the FR to produce H_2-rich syngas. Syngas is produced when CH_4 reacts with H_2O and NiO during the steam reforming and partial oxidation reactions, respectively, while CaO adsorbs CO_2 simultaneously; thus, the water-gas shift reaction is shifted forward to provide higher yield of H_2. Afterward, the generated calcium carbonate ($CaCO_3$) is regenerated in the calcinator during an endothermic calcination reaction, while Ni from the FR is re-oxidized in the AR via the exothermic oxidation reaction. Therefore, the high temperature solid in the AR is used to maintain the operating temperature of three reactors under adiabatic operating conditions (Rydén and Ramos, 2012). A gas separation unit is not needed for this process because the generated CO_2 from steam reforming is captured by CaO. Hence, this process is less complex when compared with conventional steam reforming. Antzara *et al.* (2015) conducted the thermodynamic analysis of H_2 production using the SECLR process. They found that the sorption-enhanced process offered higher CH_4 conversion rates, H_2 purity, and yield at low temperature. Udomchoke *et al.* (2016) proposed a modified SECLR process involving the direct supply of the solid from the AR to FR to provide the heat for the reduction reaction. The modified process presented a significant impact on process control due to the broadened operating windows. However, the H_2 stream was still not pure enough to be used as a fuel for low-temperature polymer electrolyte membrane fuel cells (LT-PEMFC) (Phuluanglue *et al.*, 2017; Tippawan *et al.*, 2016; Udomchoke *et al.*, 2016; Yahom *et al.*, 2014). It should be noted that LT-PEMFC requires an extremely high purity H_2 stream which the CO concentration should be less than 20 ppm (Bhatia and Wang, 2004; Zamel and Li, 2011). Kasemanand *et al.* (2017) performed the exergy analysis of the SECLR integrated with high-temperature polymer electrolyte membrane fuel cells (HT-PEMFC). The results revealed that the main exergy destruction of SECLR and HT-PEMFC is found at the AR and the cathode of the fuel cell, respectively.

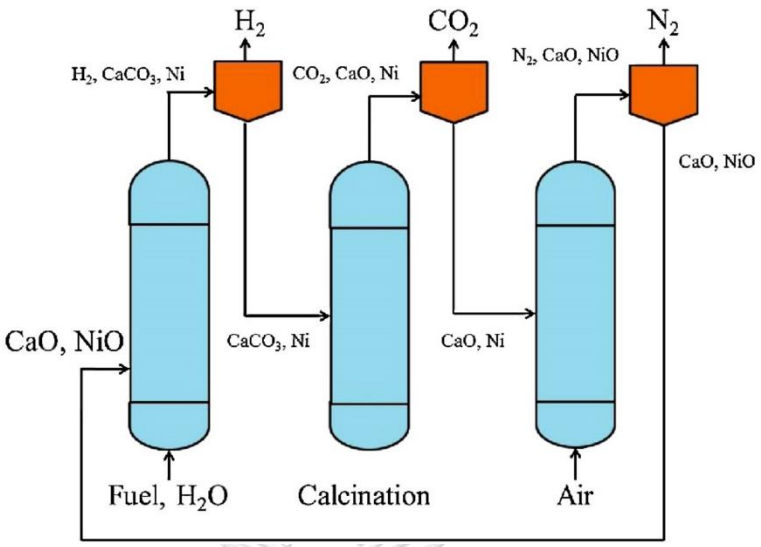

Figure 1.2 Schematic of sorption-enhanced chemical looping reforming (Yahom *et al.*, 2014).

The integration of the SECLR and CLWS processes is interesting and can be advantageous as it does not require a gas separation unit for the produced gas leaving the steam reforming reaction. Moreover, H_2-rich syngas and high purity H_2 are obtained from sorption-enhanced reforming and water-splitting reaction. The integrated of the SECLR and CLWS (SECLR-WS) process uses iron oxides, CaO, and H_2O as OC, CO_2 adsorbent, and oxidizing agent, respectively. The SECLR-WS process consists of three reactors i.e., FR, SR, and calcinator, as shown in Figure 1.3. Initially, Fe_3O_4 and CaO are fed into the FR to react with H_2O and fuel to produce H_2-rich syngas. Afterward, Fe_3O_4 and CaO are transformed into $Fe_{0.947}O$ and $CaCO_3$, respectively, and then the solid mixture is sent to the SR. In the SR, $Fe_{0.947}O$ is oxidized to Fe_3O_4 by H_2O and gaseous products H_2 and H_2O, are obtained. Subsequently, the solids from the SR, i.e., Fe_3O_4 and $CaCO_3$, are fed into the calcinator to regenerate and then supplied to the FR for the completion of the process cycle. Since CO_2 is captured by CaO in the FR, the separation of CO_2 from the gaseous product does not require a gas separation unit, and H_2-rich syngas is obtained. In addition, the purity of H_2 from the SR is high enough, so the H_2 thus obtained can be used in fuel cell systems to generate electricity.

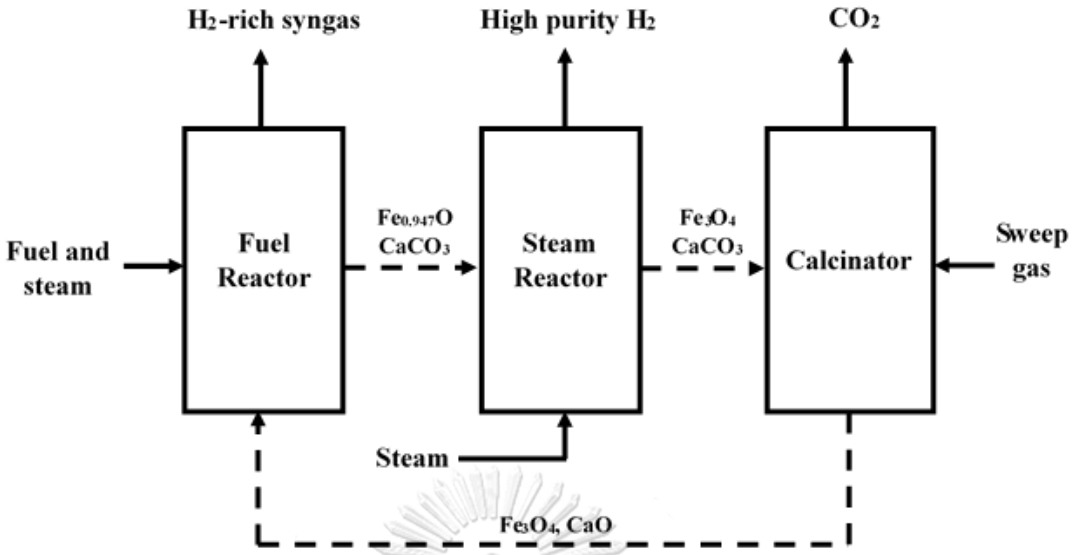

Figure 1.3 Schematic of the sorption-enhanced chemical looping reforming and water splitting process.

The objective of this study is to investigate the performance of the SECLR-WS process for H_2 production. Biogas as a renewable fuel was considered as feedstock. First, a thermodynamic approach is used to analyze the effects of operating parameters on the SECLR-WS regarding the H_2 yield and purity under steady-state condition. The key operating parameters considered are the temperature of FR and SR, steam feed to FR to CH_4 molar ratio, steam feed to SR to CH_4 malar ratio, Fe_3O_4 to CH_4 molar ratio, CaO to CH_4 molar ratio and CO_2 concentration in biogas feed stream. Then, the optimal operating conditions is determined based on two different objective functions, i.e., the maximization of H_2 production and the maximization of thermal efficiency. Performance of the optimal designed SECLR-WS process is compared to the SECLR and CLWS processes in terms of hydrogen purity and thermal efficiency of the process. Next, an energy-efficient SECLR-WS process including the optimum structure of heat exchanger is designed based on the pinch analysis to achieve the maximum heat recovery at the optimal operating conditions. Finally, the energy and exergy analysis of SECLR-WS are performed to identify the part of the SECLR-WS process with inefficient energy usage.

1.2 Objectives

To analyze and design the sorption-enhanced chemical looping reforming and water splitting integrated process for hydrogen production from biogas.

1.3 Scopes of work

1.3.1 The sorption-enhanced chemical looping reforming and water splitting integrated process (SECLR-WS) was simulated by using Aspen Plus program based on a thermodynamic approach.

1.3.2 Biogas with 60 mol% CH_4 and 40 mol% CO_2 is used as the main feedstock to produce hydrogen. The co-feed is H_2O, and iron oxide and CaO was used as an oxygen carrier and CO_2 adsorbent, respectively, for hydrogen production through SECLR-WS process.

1.3.3 Effects of operating parameters, i.e., operating temperatures of fuel reactor (T_{FR}) and that of steam reactor (T_{SR}), Fe_3O_4 to CH_4 (Fe_3O_4/CH_4) molar ratio, CaO to CH_4 (CaO/CH_4) molar ratio, steam feed to fuel reactor to CH_4 (S_{FR}/CH_4) molar ratio, steam feed to steam reactor to CH_4 (S_{SR}/CH_4) molar ratio and CO_2 molar concentration ($\%CO_2$) of feed stream, on the hydrogen purity and yield from fuel reactor and steam reactor and CH_4 conversion in the SECLR-WS process were investigated.

1.3.4 Optimization is performed to determine the optimum condition of the SECLR-WS process offering the maximum yield of H_2 from both fuel and steam reactors, and maximum thermal efficiency.

1.3.5 The performance of SECLR-WS process i.e., hydrogen purity, hydrogen yield and thermal efficiency is compared with those of the conventional SECLR and the CLWS processes.

1.3.6 Heat exchanger network of the SECLR-WS process is designed based on pinch analysis method to achieve the maximum heat recovery at the optimal operating condition.

1.3.7 The energy and exergy analysis of the SECLR-WS process are performed to determine the part of the process with inefficient energy usage.

CHAPTER II
LITERATURE REVIEWS

At present, hydrogen is a clean fuel that has been increased attention because it does not emit greenhouse gases after burning and it has a high energy density compared to other fuels. In this chapter, the literatures related to the H_2 production are summarized. The topic of the interested literatures are divided in two major parts i.e., the conventional hydrogen production process and the chemical looping concept for hydrogen production process.

2.1 Conventional hydrogen production

Hydrogen production process has been studied and developed extensively. However, there are only a few processes used in the industry such as steam-methane reforming process, partial oxidation process, autothermal reforming process, and steam-iron process. Hydrogen can be produced from the various feedstock. However, the most favored feedstock for hydrogen production is natural gas because it is available. (Rakib *et al*., 2010).

2.1.1 Steam-methane reforming process

The Steam-methane reforming process is the most widely used for hydrogen production in the industry. At present, around 40–50 % of the world's hydrogen is produced by the steam-methane reforming process (Dou *et al*., 2014). The basic steps in the steam-methane reforming process consists of the pretreatment process, the steam-methane reforming (SMR) process which CH_4 is converted to syngas, water-gas shift process and hydrogen purification process. In general, SMR reaction take places in the range of temperature and pressure around 750-900 ^oC and 50-600 psig, respectively, over the reforming catalysts. The steam to methane molar ratio of the feed is maintained around 2.5-6.0. The product gas from the reformer is cooled before it is fed to adjust the H_2 to CO ratio at the water-gas shift (WGS) reactor which normally operated at

300-400 ºC. The exhaust gas is then fed into the hydrogen purification process to separate CO_2 by pressure swing adsorption (PSA). The product gas from PSA process contains 98–99.99 mol% hydrogen (Hufton *et al.*, 1999). The process efficiency can increase by introducing recycle stream and flue gas to the furnace to supply heat to the reformer (Ogden, 2001).

However, the steam-methane reforming process has many drawbacks, such as highly energy demand and greenhouse gas emissions because the steam-methane reforming reaction is an endothermic thus the fuel is burned to supply heat to the reformer. In addition, the process is complicated from being comprised of multi-step reactions and separation to obtain high purity hydrogen (Martavaltzi *et al*., 2010).

2.1.2 Partial oxidation process

Partial oxidation process includes reacting natural gas or hydrocarbons with a restricted O_2. If the amount of supplied oxygen is too high, the product will be water and carbon dioxide. Generally, a non-catalytic reactor for partial oxidation operates under a temperature of 1150–1500 ºC and a pressure of 25–80 bar (Ritter and Ebner, 2007). Partial oxidation process has several advantages such as the reaction is exothermic, which does not require external heat source, the rate of reaction is faster than the SMR reaction, the size of the process is compact, and several feedstocks can be used (Steinberg and Cheng, 1989). However, the main drawback of this process is the requiring of pure oxygen from air separation unit, which is the expensive unit.

2.1.3 Autothermal reforming process

The autothermal reforming process is a combination of a steam-methane reforming process and a partial oxidation process within a single reactor. The advantage of this process is the SMR reaction can be heated directly through partial oxidation reaction thus the external heat source can be eliminated. To achieve an autothermal condition, the operating parameters must be appropriate. The molar ratio of oxygen to fuel and steam to carbon must be manipulated to control the temperature, a product gas

composition, and the side reaction in this system (Flytzani-Stephanopoulos and Voecks, 1983). However, the autothermal reforming process still requires an air separation unit to produce high purity O_2, which is expensive, and the process also produces less hydrogen than the steam-methane reforming process.

2.1.4 Steam-iron process

Steam-iron is an old process used to produce hydrogen in the industry which normally operates at temperatures between 750–850 ºC (Messerschmitt, 1910). The advantage of this process compared to other reforming processes is the ability to produce pure hydrogen using the two-steps redox cycle without another purification process, such as a water-gas shift process and PSA process (Takenaka *et al*., 2005). Although the process is less complicated, the gas separation unit is still required. Because of the contaminating of syngas in the gas product stream, which composes CO_2 and H_2O, from reduction step and the large consumption of energy for producing more high-pressure steam as feedstock (Bleeker *et al*., 2010).

2.2 Chemical looping method for hydrogen production

Chemical looping is a process that has the concept of dividing a reaction into subreactions and using the reaction medium, which reacts and was regenerated through such subreactions (Fan *et al.*, 2016).

The well-known chemical looping process is chemical looping combustion (CLC) process. The CLC process operates by using oxygen carriers (OC) instead of air in the combustion reaction to avoid direct contact between air and fuel. The combustion gases are not contaminated with N_2 and the air separation unit is not required. The CLC process operated by using two reactors, which are fuel reactor (FR) and air reactor (AR). The oxygen carriers react with the fuel in FR. The product gases are CO_2 and H_2O. Then, the oxygen carriers are re-oxidized by air in the AR before they are fed back to the FR. The reaction occurred in AR is an oxidation reaction of oxygen carriers, which in which the heat is released.

The CLC process has been applied to the electricity and hydrogen generation as a source of heat. Lyngfelt *et al*. (2001) proposed a circulating fluidized bed boiler design. The system consists of two connected fluidized beds i.e., a high-velocity riser and a low-velocity bubbling fluidized bed using a metal oxide as a bed material. Design based on the limited experimental of oxygen carriers, it was found that the rate of the reduction and oxidation are fast enough. The design of the reactor size is reasonable and feasible. In addition, yield and conversion are appropriate. Oxygen carriers have a sufficient amount of oxygen and the transfer rate of the oxygen carriers is also appropriate.

Fan *et al.* (2017) investigated the ex-situ coal gasification chemical looping combustion integrated with combined cooling, heating and power generation (CCHP-CLC). Syngas from the coal gasification process entered the chemical looping combustion process to produce heat and CO_2 can be separated without extra energy consumed. The parameters that affect the system, such as steam-to-coal mass ratio (S/C), the oxygen-to-coal mass ratio (O/C) and operating pressure and temperature of chemical looping combustion process, were analyzed to find out an optimal operating condition by using the Aspen Plus program. From the parameteric analysis, the optimal condition was achieved at the S/C of 0.05, O/C of 0.75, the pressure of 5 bar and the temperature of 1200 ^{o}C. The energy efficiency in terms of useful energy output to the required energy input was 58.20 % and 60.34 % in summer and winter respectively.

The CLC is also applied in a steam-methane reforming process. This concept was proposed by Ryden and Lyngfelt (2006), who studied the hydrogen production through the integrated steam reforming process and CLC process using natural gas as a feedstock. The endothermic reforming reactions take place in a bubbling fluidized bed reactor. The heat-contained oxygen carriers are used as a heating media for steam reforming reaction.

Fan *et al.* (2016) studied and compared the performance of the steam-methane reforming (SMR) process with that of the integrated of CLC and steam-methane reforming process (CLC-SMR) by performing exergy analysis. Modeling of the considered processes was done in Aspen Plus program. The SMR and CLC-SMR process models can be shown in Figure 2.1. The result showed that the overall exergy

efficiency of the CLC-SMR process was 9.5 % higher than that of SMR. Moreover, the exergy of combustion of the CLC-SMR process was found to be 1.47 % higher than that of the latter. Regarding economic analysis, the CLC-SMR was found to be economically feasible.

Although the integrated CLC and steam-methane reforming process can enhance the H_2 production performance, it requires a complex H_2 purification process, which composes of the high-temperature water-gas shift (HT-WGS) reactor, low-temperature water-gas shift (LT-WGS) reactor, and the PSA process. In addition, the design requires the reformer in the fluidized environment which it has a serious corrosion problem.

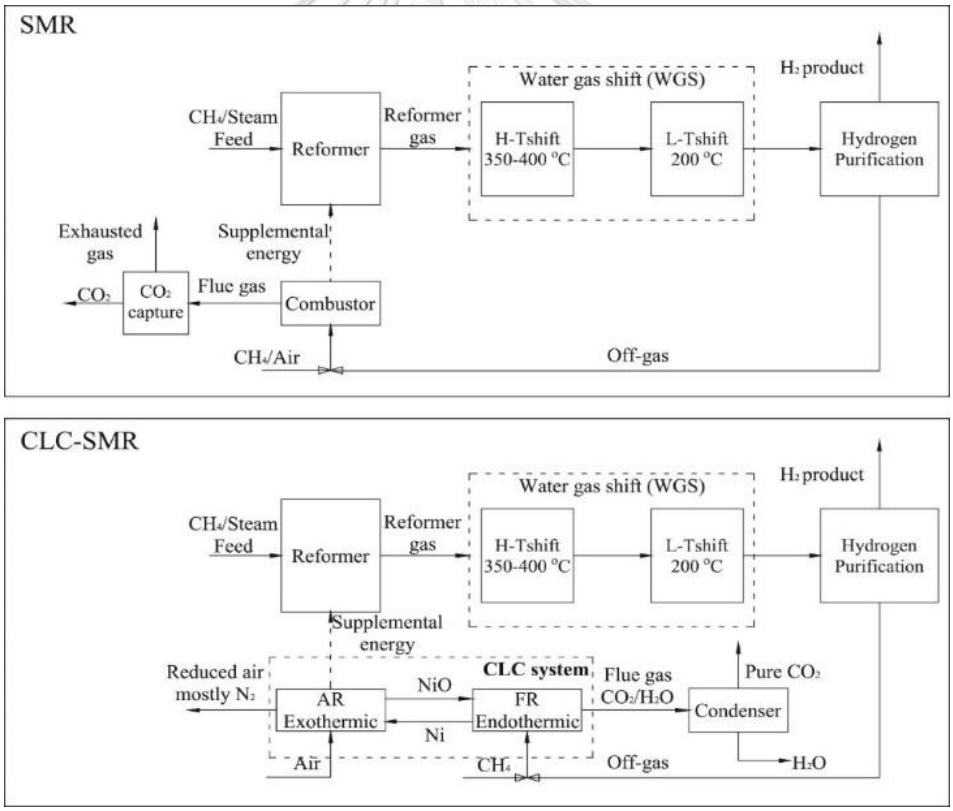

Figure 2.1 Schematic diagram of SMR and CLC-SMR process. (Fan *et al.* (2016))

2.2.1 Sorption-enhanced chemical looping reforming process

Chemical looping reforming (CLR) process differs from the CLC process in terms of the product. The main product of CLC process is heat while that of CLR process is syngas. In CLR process, restricted amount of oxygen carrier is fed to react with fuel to form syngas via partial oxidation reaction. The product gas leaving FR is fed to WGS reactor and PSA unit in order to produce high purity H_2.

Ryden *et al*. (2006) studied a continuous chemical looping reforming reactor. The reactor consists of two inter-connected fluidized reactors, as shown in Figure 2.2. The natural gas and NiO were used as a feedstock and oxygen carrier, respectively. The NiO is mixed with inert solids of 60 % by weight. The oxygen carriers were reduced by the natural gas within FR and then re-oxidized by air within AR. The product gas from FR consisted of CO, CO_2, H_2O, and H_2. The various parameters were investigated, such as the composition of product gas leaving FR, the carbon formation in FR, the leakage between FR and AR, and the O_2 ratio. Based on the experiment in the various condition, it was found that the natural gas conversion of 100 % could be achieved and the product gas with high yield of H_2 and CO was obtained. In addition, the combined feed of natural gas and steam could increase the H_2 production while decrease the carbon formation on oxygen carrier.

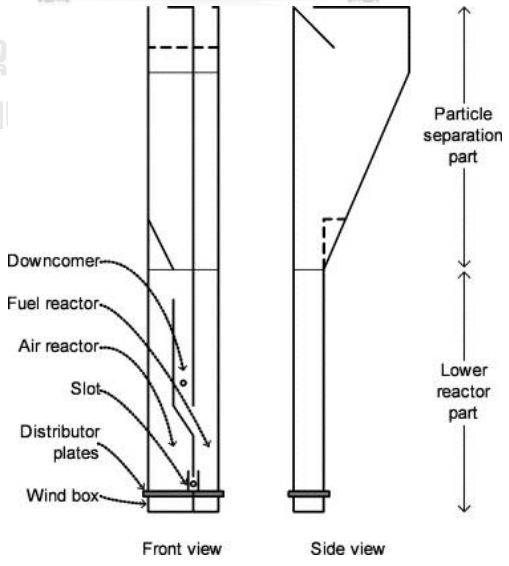

Figure 2.2 Schematic description of chemical looping reforming reactor (Ryden *et al.*, 2006).

Ortiz *et al*. (2010) investigated the production of hydrogen by autothermal chemical looping reforming process using pressurized fluidized bed reactor. NiO was used as an oxygen carrier. The effect of pressure, the reduction temperature, and the oxygen carrier-to-fuel (NiO/CH_4) molar ratio on CH_4 conversion, product gas composition, and carbon formation, were studied. The experiment was divided into two parts: reduction test and oxidation test using a semi-continuous fluidized bed reactor. It was found that the pressure did not affect the gas outlet composition. More than 98 % of methane conversion could be achieve in all considered conditions.

Lima da Silva *et al*. (2012) analyzed the efficiency of the polymer electrolyte membrane fuel cells (PEMFC) system integrated with the CLR system using biogas as a feedstock. The performance of PEMFC system integrated with different reforming processes, such as steam reforming process (SR), autothermal reforming process (ATR), and partial oxidation process (POX) was investigated and compared. The thermodynamic analysis was carried out by using minimize Gibbs free energy method. It was found that the PEMFC system integrated with the SR required the highest energy, whereas the PEMFC system integrated with CLR, POX, and ATR could be operate under the autothermal condition. The PEMFC systems integrated with the CLR process provided equal voltage and energy as the PEMFC system integrated with the SR process and can also reduce CO_2 emissions. The optimal operating condition of PEMFC system integrated with reforming process was determined.

The CLR process has advantages over the CLC-SMR process due to it is not necessary to design the reformer in the fluidized environment, which it has a serious corrosion problem, but there are still required the hydrogen purification process, which composes WGS and PSA process. Thus, the CLR process has been improved by using the concept of integrating the separation and regeneration into the single reactor, which is called sorption-enhanced process.

Ding and Alpay (2000) investigated the steam-methane reforming reaction with the addition of a hydrotalcite-based CO_2 adsorbent and Ni-based catalyst. From the experiment and theoretical studies, it was found that the CO_2 adsorbent enhanced the steam-methane reforming reaction by shifting the reaction equilibrium of reforming and water-gas shift reactions. The conversion was found to increase when the operating

pressure and reactor space time increase. However, the opposite trend was found when steam to methane ratio increase.

Hydrogen production through sorption-enhanced chemical looping reforming process (SECLR) using waste cooking oil as a feedstock within a packed bed reactor was investigated by Pimenidou *et al*. (2010). An experiment was conducted in packed bed reactor using a Ni catalyst with in-situ CO_2 capture by using dolomite, which was fully carbonated and had a composition of 21.3 wt.% MgO, 30.7 wt.% CaO, 0.3 wt.% SiO_2, 0.27 wt.% Fe_2O_3, 0.1 wt.% Al_2O_3, and 47.33 wt.% CO_2. The feed is alternated between fuel-steam and air. It was found that 98 % purity of hydrogen was obtained at 600 ^oC and 1 atm. The system with CO_2 adsorbent has a higher conversion than the one without CO_2 adsorbent. The result also showed that CO_2 could completely captured by dolomite.

Rydén and Ramos (2012) studied hydrogen production with CO_2 capture by a SECLR process using NiO as an oxygen carrier and CaO as a CO_2 adsorbent. The process consisted of three reactors: reforming reactor, calcination reactor and air reactor. In the reforming reactor, fuel was partially oxidized by the oxygen carrier while CO_2 was captured by the CaO. This process can produce the high purity H_2, N_2 and CO_2 without the need for gas separation unit. The study indicated that, the SECLR system could operate under the autothermal conditions and the H_2 with purity higher than 98 % was achieved at the operating pressure of 1 bar.

Yahom *et al*. (2014) simulated the SECLR process by Aspen Plus program. The product gas composition was calculated based on the Gibbs free energy minimization method. It was found that the involved CO_2 capture could enhance the yield and purity of H_2. Moreover, it allowed the reaction to take place at lower temperature. The optimal operating conditions offered high purity H_2 (> 90 %) of the SECLR process was achieved at temperature ranging of 500–600 ^oC, NiO/CH_4, and CaO/CH_4 molar ratios greater than 1, and H_2O/CH_4 molar ratio greater than 2, while that of the CLR process was found at 800 °C, H_2O/CH_4 molar ratio is 3, and NiO/CH4 molar ratio is 1, at these condition, approximately 75 % yield of high purity H_2 was achieved.

Although the SECLR process has the advantage of in-situ CO_2 capture without extra energy demand and it also does not require WGS and PSA process to purify hydrogen. However, hydrogen produced by the process is not pure enough to use in some systems, such as PEMFC.

2.2.2 Chemical looping water splitting process

Messerschmitt (1910) and Lane (1913) proposed the steam-iron process using iron oxide as an oxygen carrier. This is an old process used for hydrogen production in industry. At present, the steam-iron process is known as chemical looping water splitting process (CLWS). The traditional steam-iron process is divided into two parts. The first part, iron oxide in magnetite state (Fe_3O_4) is reduced to wüstite state ($Fe_{0.947}O$) by hydrocarbon fuel, and generates H_2O and CO_2. Then, the iron oxide in wüstite state enters the second part, where the iron oxide in wüstite state is oxidized by H_2O to form the iron oxide in magnetite state. The product is H_2 and H_2O and the iron oxide in magnetite state is then recycled.

Bleeker *et al*. (2007) studied hydrogen production by a steam-iron process using pyrolysis oil as a feed. The experiments were divided into two cases, once-through and the continuous process. The redox reaction was carried out over ammonia catalyst. The results showed that the hydrogen obtained from the oxidation reaction was 0.84 Nm^3/kg dry pyrolysis oil and the gases obtained during the reduction process had a heating value around 38 % of the feed stream.

Cormos (2010) studied the IGCC power generation and hydrogen production by chemical looping hydrogen production using iron oxide as an oxygen carrier. The syngas from gasification process was used to reduce the iron oxide in Fe_3O_4 to $Fe_{0.947}O$, which it is re-oxidized by H_2O to produce hydrogen, as shown in Figure 2.3. This process could generate 400 MW of electricity and produce 0 to 200 MW of hydrogen. The effect of operating parameters i.e., gasifier feeding condition (slurry feed vs. dry feed) and type of gasification reactor, on process efficiency was investigated. The process integration and product distribution analysis were also performed. The study found that the chemical looping process could be used in CO_2 captured better than

classical technologies like gas-liquid absorption because it had less effect on the process efficiency.

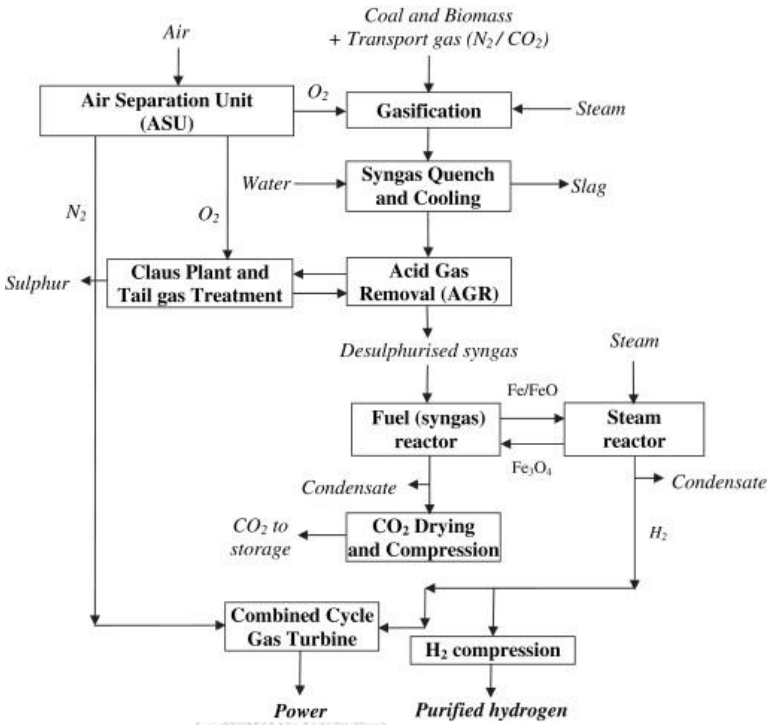

Figure 2.3 Layout of IGCC scheme for co-generation of hydrogen and electricity with carbon capture and storage using an iron-based chemical looping system (Cormos, 2010).

Chen *et al*. (2012) simulated an integrated steam-iron and chemical looping combustion process for hydrogen and electricity production using Aspen Plus program. The concept of the process was shown in Figure 2.4. The role of the CLC process in integrated process is combustion of the gas stream, which is a mixture of H_2, CO, CO_2, and H_2O, from Fe-FR. In this study, the effect of iron oxide recycle rate, steam flow rate to Fe-SR, and reactor temperature were examined. The results showed that net power efficiency of 14.15 % and the hydrogen efficiency of 33.61 % could be achieved at the Fe-SR, Fe-FR, Ni-FR, and Ni-AR temperature of 815 ^oC, 815 ^oC, 900 ^oC, and 1050 ^oC respectively. At this condition, the external heat source was not required, and

the generated CO_2 was completely capture. It also found that the ratio of hydrogen to electricity could be controlled by adjusting the iron oxide recycle rate.

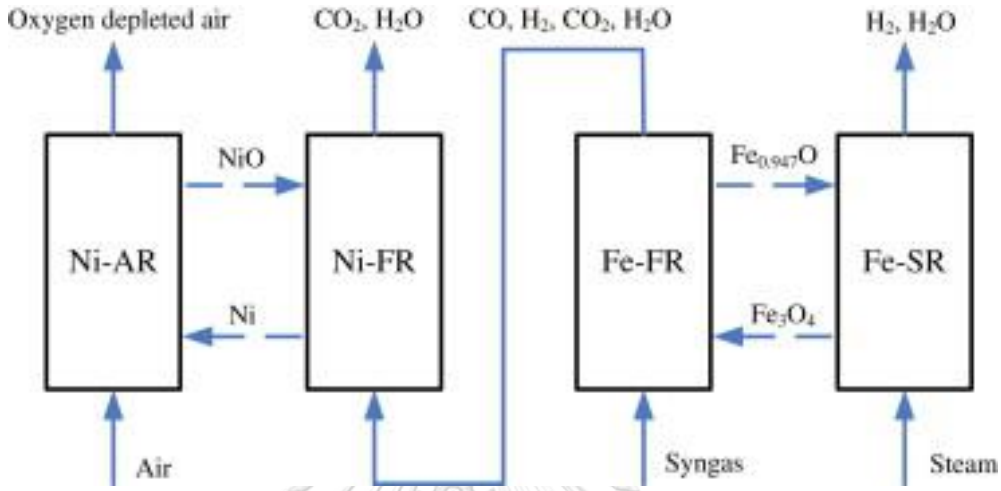

Figure 2.4 Conceptual scheme of the Fe looping and the Ni looping for hydrogen generation with inherent separation of CO_2 (Chen *et al.*, 2012).

Although the chemical looping water splitting process has the advantage of producing high purity hydrogen simultaneously with CO_2 capture, however, the process also has the disadvantage in thermodynamic limitation leading to low hydrogen production and the gas product stream from FR is contaminated by H_2 and CO. Therefore, the three-reactors chemical looping water splitting process was later developed. This process consists of FR, the steam reactor (SR), and AR. Additional the AR can be eliminated the thermodynamic limitation by using the iron oxide in hematite state (F_2O_3) instead of iron oxide in magnetite state to react with CH_4. The iron oxide in hematite state can be obtained from complete oxidation of iron oxide in magnetite state with air. The complete oxidation reaction is an exothermic reaction, which can provide heat to the system for an autothermal operation (Abad, 2015).

Chiesa *et al*. (2008) studied the three-reactors chemical looping process for hydrogen production. The process consists of three reactors, as shown in Figure 2.5. The chemical looping system was integrated with electricity and steam generation

processes. The study compares this process with the conventional process used in the industry, such as steam reforming process. It was found that the three-reactors chemical looping process offered the same efficiency as the steam reforming process, however, it offered better environmental benefit. Regarding the CO_2 capture performance, the generated CO_2 was completely captured in chemical looping process, whereas less than 80 % of CO_2 was captured in conventional process.

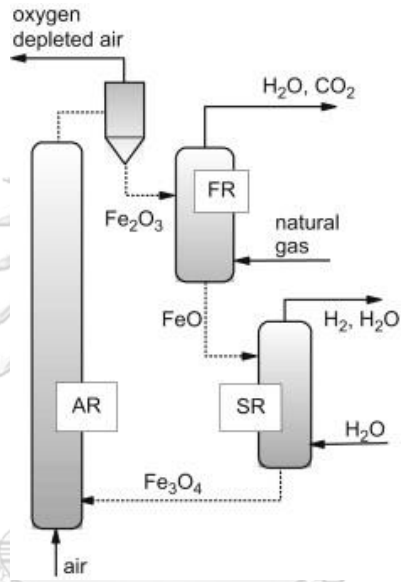

Figure 2.5 Concept scheme of the chemical looping (Chiesa *et al.*, 2008).

The production of H_2, N_2, and CO_2 by chemical looping using iron-based oxygen carrier and methane as a feed was studied by Edrisi *et al*. (2014). The optimal operating conditions offering maximum yield of H_2 was investigated. The study found that, at the optimal operating conditions, the production of H_2, N_2, and CO_2 of 2.65, 2.533 and 0.99 mol/mol CH_4, respectively, could be achieved. At this condition, the process efficiency is 80.2 % was obtained. The use of iron oxide instead if inert support could improve the energy utilization of the system. Moreover, the authors suggested that the re-oxidation stage should be divided into two steps to get the pure N_2.

Kathe *et al*. (2016) analyzed and simulated a chemical looping for hydrogen production process from natural gas using iron oxide as an oxygen carrier. The study

began by analyzing the oxidizer and the reducer thermodynamic phase diagrams to find the optimal operating conditions in an autothermal operation for complete loop simulation. The simulation carried out by using the Aspen Plus program for calculating a cooling load, a water requirement and net parasitic energy consumption (such as pump and compressor), and the other parameters for analyzing the thermal efficiency of the process. The study found that the chemical looping process could increase a cold gas efficiency and a thermal efficiency by 5 % and 6 %, respectively, higher than the SMR. Moreover, 90 % of generated CO_2 could be captured. In addition, Kathe *et al*. (2016) also proposed a model for increasing the efficiency of hydrogen production by separating two solid stream, leaving from the reducer, as shown in Figure 2.6, to reduce the amount of iron oxide in the oxidizer, so the H_2O/Fe molar ratio is increased, resulting in an increase in the rate of reaction.

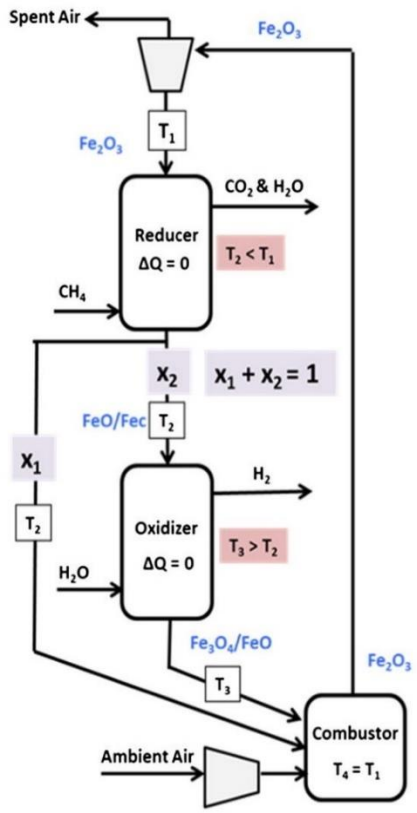

Figure 2.6 Split stream reactor loop variation for the chemical looping system (Kathe *et al.*, 2016).

Although the three-reactors CLWS process can overcome the thermodynamic limitation of the steam-iron process, it still has the disadvantage. The problem is the carbon formation on iron oxide in reduction state resulting in the CO and CO_2 contaminate in hydrogen product stream. The three-reactors CLWS process requires syngas, which mainly contained H_2 and CO, as a feed to produce the CO_2 and H_2O. The use of other hydrocarbon feedstocks lead to produce the product gas containing H_2, CO, CO_2 and H_2O, therefore the gas separation unit is required. Therefore, the system is usually integrated with the syngas production process, such as gasification (Abad *et al.*, 2007; K. Svoboda *et al.*, 2007). Thus, the hydrogen and syngas production using iron oxide as an oxygen carrier was studied.

Rydén and Ramos (2012) conducted an experiment on a steam-iron reaction experiment using a two-compartment fluidized-bed reactor at 800 – 900 ^oC and atmospheric pressure by using three types of feedstocks i.e., CO, syngas, and natural gas, in reduction step and using steam for oxidation step. The experiments showed that the CO and syngas reacted rapidly with oxygen carriers and the composition of gas product was close to the thermodynamic equilibrium. Iron oxide could react with steam completely. It also found that using natural gas as a feed offered syngas and CO_2 products.

Go *et al*. (2009) studied the production of hydrogen and syngas by chemical looping concept using methane as a feedstock. H_2 was produce from the SR without purification unit, while the syngas was produce from the FR. Then the produced gas was used to produce the liquid hydrocarbon via Fisher-Tropsch process. The parameters such as the reaction temperature, gas velocity, and reactant concentration, which affected to the iron oxide reactivity in fluidized bed reactor, were studied. The study found that the optimal operating conditions for the FR was achieved at the CH_4 concentration (C_{CH4}) > 25% and superficial gas velocity (U_g) of 0.0287 m/s and the SR is C_{CH4} > 50% and U_g of 0.0402 m/s. The average molar ratio of $H_2/(2CO+3CO_2)$ was 0.65 and pure hydrogen without CO contamination could be achieved when SR operates under 1173 K.

From the literature review mentioned above, the CLWS process can be applied to the hydrogen and syngas production. However, CO_2 must be separated to obtain a syngas with downstream process specification.

CHAPTER III
THEORY

3.1 Biogas

Biogas is a combustible gas produced by an anaerobic digestion process. A composition of biogas is similar to natural gas as shown in Table 3.1. It can be produced from a variety of feedstock such as animal waste, household wastes, crops residue, waste water, etc. Therefore, the biogas production is low cost and it can be used as alternative fuels. In recently, biogas is used in many applications, such as combustion to produce electricity and heat, improve quality for natural gas process, and it can be improved to be compressed biogas (CBG) or liquid biogas (LBG) for used instead of other fuels. The heat from direct combustion of biogas is low efficiency. While the use of biogas as a feedstock in reforming process for hydrogen production has several advantages, such as reducing greenhouse gas emissions, biogas can be easily produced from local crops can be used in existing natural gas plants (Authayanun *et al*., 2014; Pipatmanomai *et al*., 2009; Yang et al., 2014).

3.2 Hydrogen production process from biogas

Hydrogen production by methane through the reforming process generally consists of five types: 1. Steam-methane reforming (SMR) 2. Partial oxidation (POX) 3. Autothermal reforming (ATR) 4. Dry reforming (DR) and 5. Dry oxidation reforming (DOR). Currently, SR, POX, and ATR process are mostly used for hydrogen production by using natural gas as a feedstock. The appropriate reforming process should be selected by considering the natural gas composition. Normally, the production of hydrogen by biogas or methane usually operates at 600–1,000 ^{o}C with a catalyst.

Table 3.1 Composition of biogas from an anaerobic digestion-plant and natural gas in the Netherlands. (Schomaker *et al.* (2000))

Component	Dimension	Natural Gas	Biogas
CH_4	vol.%	85	55-70
CO_2	vol.%	0.89	30-45
C_2H_6	vol.%	2.85	-
C_3H_8	vol.%	0.37	-
C_4H_{10}	vol.%	0.14	-
N_2	vol.%	14.35	-
O_2	vol.%	< 0.5	-
H_2S	mg/m^3	< 5	0-15
NH_3	mg/m^3	-	0-450

3.3 Sorption-enhanced chemical looping reforming and water splitting process.

The sorption enhanced chemical looping reforming and water splitting process (SECLR-WS) is a combination of the SECLR process and the CLWS process, using iron oxide as an oxygen carrier and CaO as the CO_2 adsorbent. The SECLR-WS process consists of three reactors: a fuel reactor, steam reactor, and the calcinator, as shown in Figure 1.3, and the main reactions occurring are shown in Eqs. (3.1)–(3.8) (Fraser *et al.*, 2006; Go *et al.*, 2009; Yahom *et al.*, 2014). The fuel such as CH_4 and steam are fed to the fuel reactor for steam-methane reforming and partial oxidation reactions, Eq. (3.1) and (3.4), respectively. The gas product is CO and H_2. An iron oxide in Fe_3O_4 form is reduced to $Fe_{0.947}O$ by the endothermic reaction. At the same time, the CO_2 produced by the complete oxidation of methane, Eq. (3.5), is adsorbed by CaO according to carbonation, Eq. (3.3), resulting the equilibrium of water-gas shift reaction, Eq. (3.2), shift to the product side. Then the $Fe_{0.947}O$ and $CaCO_3$ enter the steam reactor to re-oxidize $Fe_{0.947}O$ to Fe_3O_4 by using the steam as an oxidant according

to Eq. (3.6). The product gas from the steam reactor is H_2O and H_2. After that, Fe_3O_4 and $CaCO_3$ are fed to the calcinator. This will produce CO_2 from calcining the $CaCO_3$, and then Fe_3O_4 and CaO are returned to the fuel reactor for the complete loop.

Fuel reactor

Steam-methane reforming (SMR)

$$CH_4 + H_2O \rightarrow CO + 3H_2 \qquad \Delta H_R^o = +206.2 \text{ kJ/mol} \quad (3.1)$$

Water-gas shift

$$CO + H_2O \leftrightarrow CO_2 + H_2 \qquad \Delta H_R^o = -41.1 \text{ kJ/mol} \quad (3.2)$$

Carbonation

$$CaO + CO_2 \leftrightarrow CaCO_3 \qquad \Delta H_R^o = -178.7 \text{ kJ/mol} \quad (3.3)$$

Partial oxidation of methane

$$1.202Fe_3O_4 + CH_4 \leftrightarrow 3.807Fe_{0.947}O + CO + 2H_2 \qquad \Delta H_R^o = +294.6 \text{ kJ/mol} \quad (3.4)$$

Complete oxidation of methane

$$4.807Fe_3O_4 + CH_4 \leftrightarrow 15.228Fe_{0.947}O + CO_2 + 2H_2O \qquad \Delta H_R^o = +518.5 \text{ kJ/mol} \quad (3.5)$$

Steam reactor

Steam-iron (or water-splitting)

$$3.808Fe_{0.947}O + H_2O \leftrightarrow 1.202\,Fe_3O_4 + H_2 \qquad \Delta H_R^o = -88.1 \text{ kJ/mol} \quad (3.6)$$

Oxidation of CO

$$3.8071Fe_{0.947}O + CO_2 \leftrightarrow 1.2018Fe_3O_4 + CO \qquad \Delta H_R^o = -47.34 \text{ kJ/mol} \quad (3.7)$$

Calcinator

Calcination

$$CaCO_3 \leftrightarrow CaO+CO_2 \qquad \Delta H_R^o = 178.7 \quad kJ/mol \quad (3.8)$$

3.4 Minimization of Gibbs free energy method

The Gibbs free energy is the thermodynamic property which usually used to identify the equilibrium state. The Gibbs free energy is the value which defined by the enthalpy (H) minus the multiple of temperature and entropy (S) as shown in Eq. (3.9)

$$G \equiv H - TS \qquad (3.9)$$

where G is the Gibbs free energy, H is the enthalpy, S is the entropy, and T is the temperature of the system.

The thermodynamic analysis of the process under an equilibrium condition can be performed by minimization of Gibbs free energy method. The total Gibbs free energy (G^t) of N species of the system at a temperature and pressure is determined by Eq. (3.10):

$$G^t = \sum_{i=1}^{N} n_i G_i = \sum_{i=1}^{N} n_i \mu_i = \sum_{i=1}^{N} (n_i G_i^o + n_i RT \ln \frac{f_i}{f_i^o}) \text{ at T, P} \qquad (3.10)$$

where G_i^o is the Gibbs free energy of species i at standard condition, n_i is the mole of species i, N is the number of species, R is the universal gas constant, f_i is the fugacity of species i, f_i^o is the fugacity of species i at standard condition, μ_i is the chemical potential of species i, and G_i is the Gibbs free energy of species i. T and P are the temperatures and the pressure of the system.

The G_i^o is set equal to zero for all the element at standard state, and the G_i^o is set to equal the Gibbs free energy change of formation for species i at standard condition (ΔG_{fi}^o), which determined by Eq. (3.11). For the gas phase, f_i defined by Eq. (3.12) and f_i^o is equal to standard state pressure of 1 bar.

$$\frac{\Delta G_{fi}^{o}}{RT} = \frac{\Delta G_{f0i}^{o} - \Delta H_{f0i}^{o}}{RT_0} + \frac{\Delta H_{f0i}^{o}}{RT} + \frac{1}{T}\int_{T_0}^{T} \frac{\Delta C_{Pi}^{o}}{R} dT - \int_{T_0}^{T} \frac{\Delta C_{Pi}^{o}}{R} \frac{dT}{T} \tag{3.11}$$

$$f_i = y_i \phi_i P \tag{3.12}$$

where y_i is the mole fraction of species i, which determined by Eq. (13) and ϕ_i is the fugacity coefficient of species i. T_0 is the reference temperature. ΔG_{f0i}^{o} and ΔH_{f0i}^{o} is the Gibbs free energy and enthalpy change of formation for species i at reference standard condition, respectively. ΔC_{Pi}^{o} is the heat capacity change of reaction to form species i.

As the process proceeds, the total Gibbs free energy decreases until the equilibrium condition is reached when the total Gibbs free energy is minimum. So, the equilibrium composition and the other thermodynamic value can be calculated by solving the optimization problem, Eq. (3.13).

$$\min_{n_i} (G^t)_{T,P} \tag{3.13}$$

For the conservation of atomic species, the n_i must be satisfied the constraints following Eq. (3.14):

$$\sum_{i=1}^{N} a_{ji} n_i = b_j \quad \text{for } 1 \le j \le M \tag{3.14}$$

where a_{ji} is the number of atoms of element j in component i, b_j is the total number of atoms of element j, and M is the total number of elements.

From the substitution of Eq. (3.11) and (3.12) to (3.10), the optimization can be performed as follows:

$$\min_{n_i} (G^t)_{T,P} = \sum_{i=1}^{N} (n_i \Delta G_{fi}^{o} + n_i RT \ln \frac{y_i \phi_i P}{P^o})$$

$$\text{subject to } \sum_{i=1}^{N} a_{ji} n_i - b_j = 0$$

The problem is to find the set of n_i which minimizes G^t for specified T and P, and satisfy the constraints. In general, the method to solve this problem is Lagrange

multiplier method. For an example problem, the single-phase ideal gas reaction at 1 bar and high temperature, the ϕ_i and P/P^o is unity. Thus the problem can be reduced to the following form;

$$\min_{n_i}(G^t)_{T,P} = \sum_{i=1}^{N}(n_i\Delta G_{fi}^o + n_i RT\ln y_i) = \sum_{i=1}^{N}(n_i\Delta G_{fi}^o + n_i RT\ln\frac{n_i}{\sum_i^N n_i})$$

$$\text{subject to } \sum_{i=1}^{N} a_{ji}n_i - b_j = 0$$

By defining a quantity λ_j, called the Lagrange multiplier and applied to the constraints in the example problem to get the Lagrange function (L) as shown in Eq. (3.15)

$$L(n_1, n_2, ..., n_N, \lambda_1, \lambda_2, ..., \lambda_M) = \sum_{i=1}^{N}(n_i\Delta G_{fi}^o + n_i RT\ln\frac{n_i}{\sum_i^N n_i}) + \sum_{1}^{M}(\lambda_j(\sum_{i=1}^{N} a_{ji}n_i - b_j)) \quad (3.15)$$

To find the set of n_i and λ_j which minimize the problem, the necessary conditions are generated following;

$$\frac{\partial L}{\partial n_1} = 0, \frac{\partial L}{\partial n_2} = 0, ..., \frac{\partial L}{\partial n_N} = 0$$
$$\frac{\partial L}{\partial \lambda_1} = 0, \frac{\partial L}{\partial \lambda_2} = 0, ..., \frac{\partial L}{\partial \lambda_M} = 0$$

The solution of n_i and λ_j of the example problem can be solved from the system equations above. But the method to solve the optimization problem, Lagrange multiplier, is very complicated when applied in Gibbs minimization method for a complicated process due to the complex step for calculating the value of ΔG_{f0i}^o and ϕ_i for real gas (Bonilla-Petriciolet *et al.*, 2011). Thus, the simulation software such as Aspen Plus is very useful to perform the thermodynamic analysis in complicated process. Aspen Plus can calculate the composition and the other thermodynamic value by Gibbs minimization method through an RGibbs module.

3.5 Pinch analysis

Energy consumption is a major problem for chemical processes. Generally, in the chemical process design, it is important to concern about how the maximum energy recovery can be obtained. Pinch technology is one of the widely used approaches to design the process to maximize energy recovery. The concept, pinch analysis, was first introduced by Linnhoff et al. and Umeda based on Hohmann's work (Linnhoff and Hindmarsh, 1983; Yoon *et al.*, 2007). The pinch analysis (or pinch technology) is the method to design heat exchanger networks of the process base on the thermodynamic which that guarantee the maximum heat recovery (Sahdev, 2012). The advantage of pinch analysis is that it can improve the efficiency of the process without the need for advance or complex operating units but to generate the heat integration system. The concept of the pinch analysis is to find the minimum energy target (also called energy target, which that the maximum energy recovery can be obtained at this point) by matching hot streams and cold streams (Peters *et al.*, 2003). The finding minimum energy target by pinch analysis can be achieved in 2 methods, graphical method and problem table algorithm.

3.5.1 Graphical method for minimum energy target

One of the methods used to perform pinch analysis to determine the energy target is the graphical method. A graphical method is a basic method for pinch analysis. The first step of this method is to identify of the process stream of interest, the all process streams need to heat up are called cold streams, in contrast, the all process streams need to be cooled are called hot streams. The data of all process streams in the process of interest must be identified including flow rate, thermal properties, phase changes, the temperature ranges, and also enthalpy change. The example of 4 process streams data is shown in Table 3.2.

The important information of the process streams for pinch analysis is the enthalpy change of the streams, the initial (or supply) and final (or target) temperature of the streams, and the flow rate of the streams. Those data can be obtained by the mass

and energy balance from the process simulation or the measurement of the real existing process. The enthalpy change of the streams can be calculated by Eq. (3.16)

Table 3.2 The data of 4 process streams example (Kemp, 2011).

Process stream number and type	Heat capacity flow rate (kW/^{o}C)	Initial (supply) temperature (^{o}C)	Final (target) temperature (^{o}C)	Stream heat load (kW) (positive for heat release)
(1) cold	2.0	20	135	2.0(20-135) = -230
(2) hot	3.0	170	60	3.0(170-60) = 330
(3) cold	4.0	80	140	4.0(80-140) = -240
(4) hot	1.5	150	30	1.5(150-30) = 180

$$\Delta\dot{H} = \dot{m}C_P(T_s - T_t) = CP(T_s - T_t) \tag{3.16}$$

where $\Delta\dot{H}$ is the enthalpy change rate (or the amount of heat of the hot and cold streams can be exchanged), $\dot{m}$ is the mass flow rate, C_P is the heat capacity. T_s and T_t are the supply and target temperature and CP is the heat capacity flow rate define as the $\dot{m}C_P$ product. In this study, the value of CP in the stream is assuming constant, and the value of $\Delta\dot{H}$ is the amount of heat for changing the temperature (sensible heat) and phase (latent heat) of the streams.

When the data of the process streams are obtained, the next step is to construct a composite curve. The example of a construct of the hot composite curve, which is representing all hot streams, is shown in Figure 3.1. Consider the temperature and enthalpy diagram shown in Figure 3.1(a), which consists of 3 hot separated streams in temperature range T_1 to T_5. In the temperature range T_1 to T_2, only the stream B exits. Therefore, the enthalpy change in this range can be calculated from $CP_B(T_1\text{-}T_2)$. However, during temperature range of T_2 to T_3, the enthalpy changes within this range is equal to $(CP_A + CP_B + CP_C)$ $(T_2\text{-}T_3)$. In the temperature range of T_3 to T_4 and T_4 to T_5, the enthalpy change can be calculated by using this same method. When the

calculations are done in all temperature ranges, the hot composite curve is completed as shown in Figure 3.1(b). In the same way, the enthalpy changes in the temperature range of cold streams and the construction of the cold composite curve, which is representing all clod streams, can be done by this method.

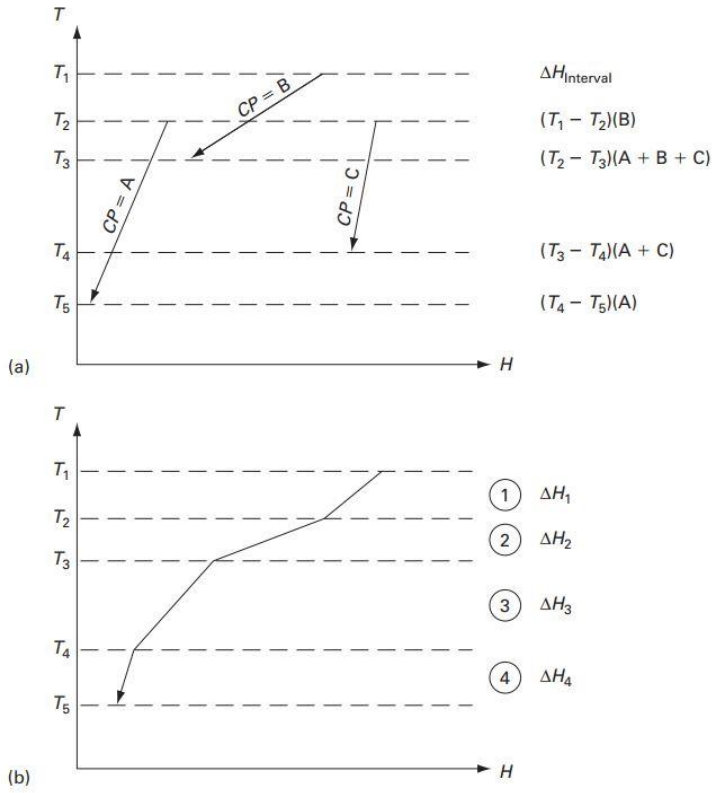

Figure 3.1 Example of the construction of hot composite curve (Kemp, 2011).

The hot and cold composite curve of the example according to the Table 3.2 is shown in Figure 3.2. The overlap of hot and cold composite curve represents the maximum heat can be exchanged within the process. The excess point (or overshoot) from the bottom of the hot composite represents the minimum cold utility required for cooling the hot streams, and the excess point from the top of the cold composite curve represents the minimum hot utility required for heating the cold streams. For the pinch analysis, the hot composite curve is fixed on the left side. And then, the cold composite curve is moved to the right, away from hot composite curve by fixing the temperature

and enthalpy change of the curves. This process proceeds until the specified of the minimum temperature different (ΔT_{min}) is obtained. The ΔT_{min} is the point that the different temperature of hot and cold composite curve is minimum in vertical distance or the point that the hot and cold composite curve is closest. The ΔT_{min} of the curve which represent the minimum cold and hot utility is called “pinch point”. For example shown in Figure 3.2, there is a ΔT_{min} of 10 °C. From the pinch analysis using the composite curve, the energy target or the minimum hot and cold utility can be obtained at the specific of the ΔT_{min} value. When ΔT_{min} is changed, the minimum energy required in the process is changed. The minimum energy required in the process is increased by increasing the ΔT_{min}. But the capital cost is reduced because of the increase in the driving force.

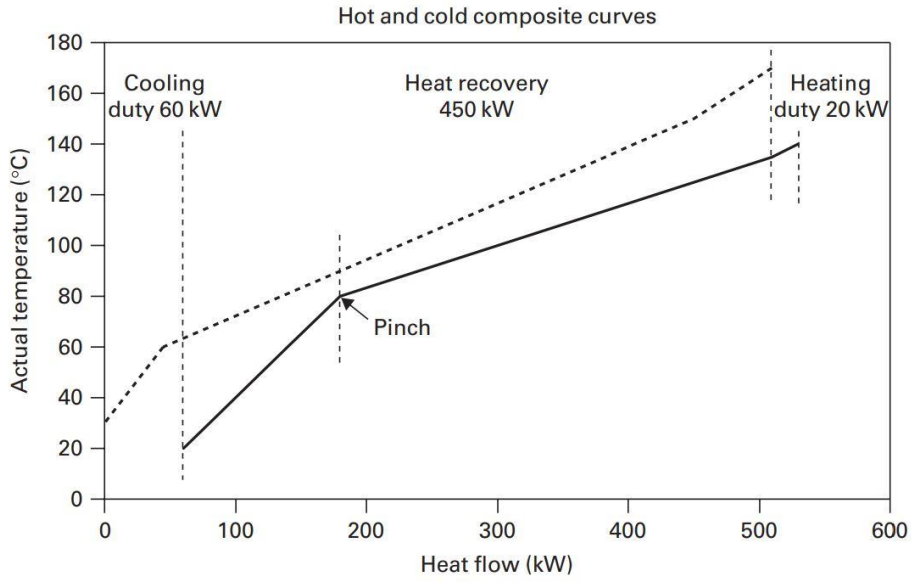

Figure 3.2 Composite curve of the four streams example according to the Table 3.2 (Kemp, 2011).

3.5.2 Problem table algorithm for minimum energy target

Although the graphical method can be used to find the minimum energy target when specifying ΔT_{min} , however, this method is difficult and inaccurate because the composite curve must be drawn. Another way to find the minimum energy target base on the pinch analysis is to use a problem table algorithm approach. It is a step-by-step calculation. It was introduced by Linnhoff and Flower in 1978.

The first step for the problem table algorithm is the setting of ΔT_{min} value. For the four process streams example according to the data are as shown in Table 3.2, the ΔT_{min} is set at 10 °C. Then, the supply and target temperature are shifted. For the hot streams, the temperature is shifted by half the ΔT_{min} (5 °C for this example) below and above for the cold streams as shown in Table 3.3. The schematic of the temperature in vertical scale of normal and shifted temperature change of each stream can be shown in Figure 3.3. By shifting the temperature in this way ensures that the heat exchangers between the hot and cold streams are possible in the interval temperature. For example, In the temperature interval 2 within the shifted temperature range between 145 °C and 140 °C, it can be seen that stream 2 and 4, which are hot streams, have a temperature change from 150 °C to 145 °C while stream 3, which is cold stream, has the temperature change from 135 °C to 140 °C. Thus, in this temperature interval, the hot stream temperature is higher than the cold stream throughout the interval. Therefore, we can calculate the net energy in each temperature interval according to Eq. (3.17). The results of the calculation can be shown in Table 3.4.

$$\Delta H_i = (S_i - S_{i+1})(\sum CP_H - \sum CP_C)_i \qquad (3.17)$$

where S_i and S_{i+1} are the shifted temperature of interval i and i+1. $\sum CP_H$ and $\sum CP_C$ are the summation of the heat capacity flow rate in hot and cold streams in the interval i.

Table 3.3 The data of 4 process streams example with shifted temperature according to the data in Table 3.2 (Kemp, 2011).

Stream number and type	CP (kW/K)	Actual temperature		Shifted temperature	
		T_s (°C)	T_t (°C)	S_s (°C)	S_t (°C)
1. cold	2	20	135	25	140
2. hot	3	170	60	165	55
3. cold	4	80	140	85	145
4. hot	1.5	150	30	145	25

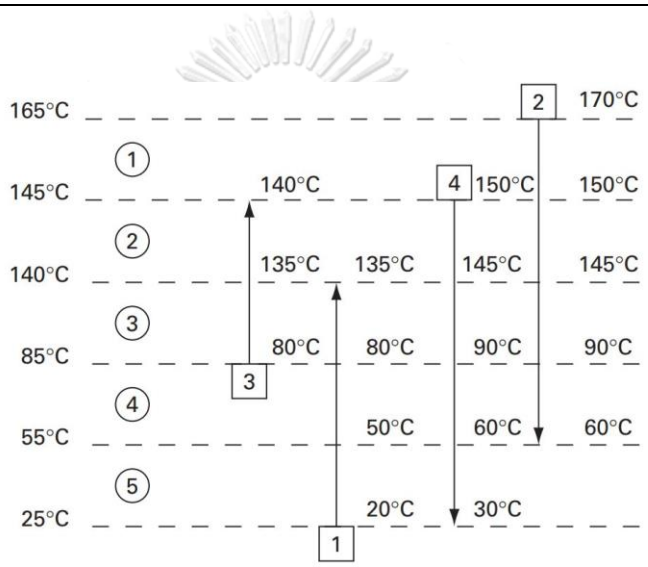

Figure 3.3 Stream and interval temperature according to the data in Table 3.2 (Kemp, 2011).

Table 3.4 The net enthalpy change in the temperature interval from the data according to Table 3.2 (Kemp, 2011).

Shifted temperature (°C)	Interval number	$S_i - S_{i+1}$ (°C)	$\sum CP_H - \sum CP_C$ (kW/°C)	ΔH_i (kW)
$S_1 = 165$				
	1	20	+3.0	+60
$S_2 = 145$				
	2	5	+0.5	+2.5

$S_3 = 140$				
	3	55	-1.5	-82.5
$S_4 = 85$				
	4	30	+2.5	+75
$S_5 = 55$				
	5	30	-0.5	-15
$S_6 = 25$				

The positive sign of the net enthalpy change means the surplus energy and the minus sign represents the deficit energy. Then, the next step is the cascade calculations. The assumption use for calculations is the temperature of net enthalpy change in each temperature interval i higher than interval i+1. Thus, the heat can be transfer from the interval i to i+1. The example of calculation between the temperature interval 1 and 2 can be performed, as shown in Figure 3.4. A surplus heat of 60 kW in interval 1 will be transfer to the interval 2 which has a surplus heat of 2.5 kW. Therefore, the net heat in the temperature interval 2 is the surplus of 62.5 kW. The heat is then transferred to the temperature interval 3. In the temperature interval 3, the heat deficit is 82.5 kW. The surplus heat of 62.5 kW from the temperature interval 2 range results in a net heat deficit of 20 kW, which will be transferred to the temperature interval 4. When this step is follow to the final, in the temperature interval 5, the net heat is the surplus heat of 40 kW which is transferred to the cold utility. The cascade calculation procedure can be shown in Figure 3.5(a). In the temperature interval of 3 and 4, the net heat transfer between interval 3 and 4 is a negative value of 20 kW which is not possible in thermodynamics. In order for the system to be thermodynamically feasible, 20 kW of heat must be sent from the hot utility unit, as shown in Figure 3.5(b). Finally, when the procedure end, the minimum of hot and cold utility for the system can be obtained at the given ΔT_{min}. As shown in the example, the minimum hot utility is 20 kW and the minimum cold utility is 60 kW. In addition, the pinch temperature can be found at a point where the heat transfer is zero. The pinch temperature is 85 °C or and 90°C for hot stream and 80 °C for cold stream. When compared with the graphical method described above, the answer and information is the same. But the problem table

algorithm is more convenient for large systems with high complexity. This is a numerical procedure which can be applied to computer-based calculations.

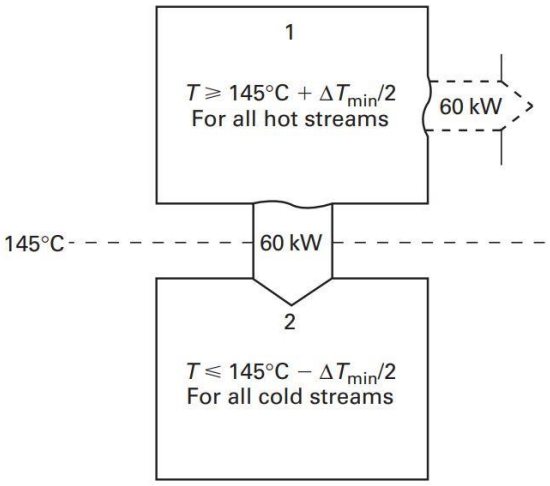

Figure 3.4 Transfer of the surplus heat from interval 1 to 2 (Kemp, 2011).

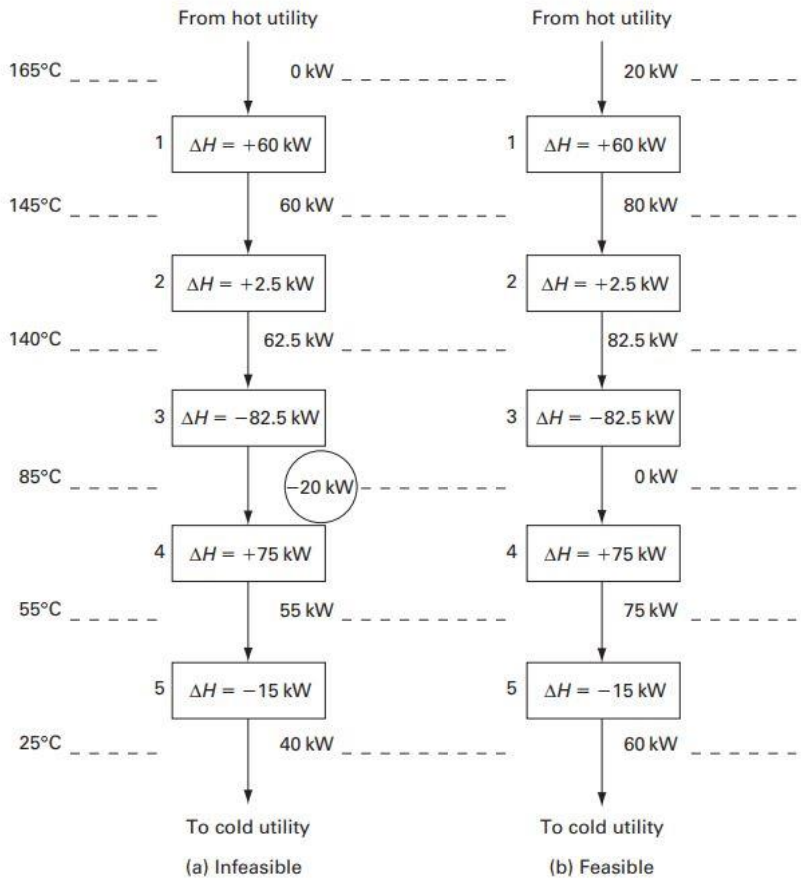

Figure 3.5 The cascade calculation of the example according to Table 3.2 (Kemp, 2011).

3.5.3 Heat exchanger network design

After the energy target is obtained, the heat exchange network design can be performed to meet the target energy. It starts by drawing a grid diagram of the process stream. The grid diagram of the example 4 process stream according to Table 3.2 is shown in Figure 3.6, this diagram was proposed by Linnhoff and Flower (1978). Initially, the table is divided into two parts: the above pinch and the below pinch. When considered above the pinch, only the hot utility is needed. Another meaning, above pinch, all hot streams can be cooled sufficiently by heat exchange with cold streams. Therefore, it is possible to find a match to cool the hot streams to a pinch temperature by using a heat exchanger with the cold streams and only the hot utility is needed for

the remaining cold streams. Thus, the design of heat exchanger network at above the pinch temperature must find matches to fulfill this condition.

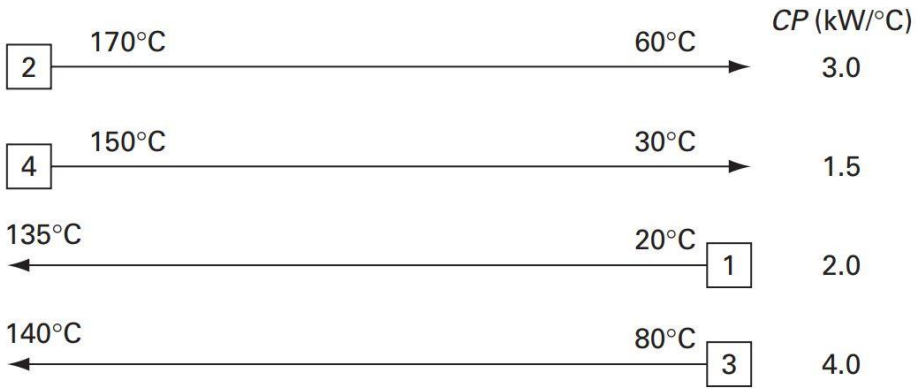

Figure 3.6 Grid diagram of the data according to Table 3.2 (Kemp, 2011).

The example for heat exchanger network design is presented by using the data of example in Table 3.2. The energy target from the graphical method and problem table algorithm of example process streams at ΔT_{min} of 10 ^{o}C is 80 kW, which are 20 kW hot utility and 60 kW cold utility. The design for matching hot and cold streams at above pinch temperature starts from the pinch temperature, according to the requirement criterion that the heat capacity flow rate of the hot stream is less than or equal to the cold stream as shown in Eq. (3.18). This criterion is used to avoiding the temperature different in exchange of hot and cold stream greater than ΔT_{min}. Consider hot stream 2 and cold stream 3 because of $CP_2 < CP_3$, so both of these streams can be matched. Above the pinch temperature, the hot stream 2 must discharge the heat of 240 kW while the cold stream 3 needs the heat to be heated of 240 kW. Therefore, the matching between stream 2 and 3 will provide the satisfy heat of both streams. Then consider hot stream 4 and cold stream 1, it found that $CP_4 < CP_1$ which can be matched. For heat exchange between stream 4 and stream 1, only stream 4 has been satisfy with 90 kW of cooling. But stream 1 is not satisfy heating load. By the 90 kW heat from stream 4, the temperature of stream 1 is change from 80 ^{o}C to 125 ^{o}C, while the target temperature of stream 1 is 135 ^{o}C. So, the stream 1 must be heated from external hot

utility with the amount of 20 kW to change the temperature from 125 ºC to 135 ºC. The hot and cold streams matching scheme is shown in Figure 3.7. It can be seen that the 20 kW heat from the hot utility is the same as the value from the energy target calculation.

$$CP_{HOT} \leq CP_{COLD} \tag{3.18}$$

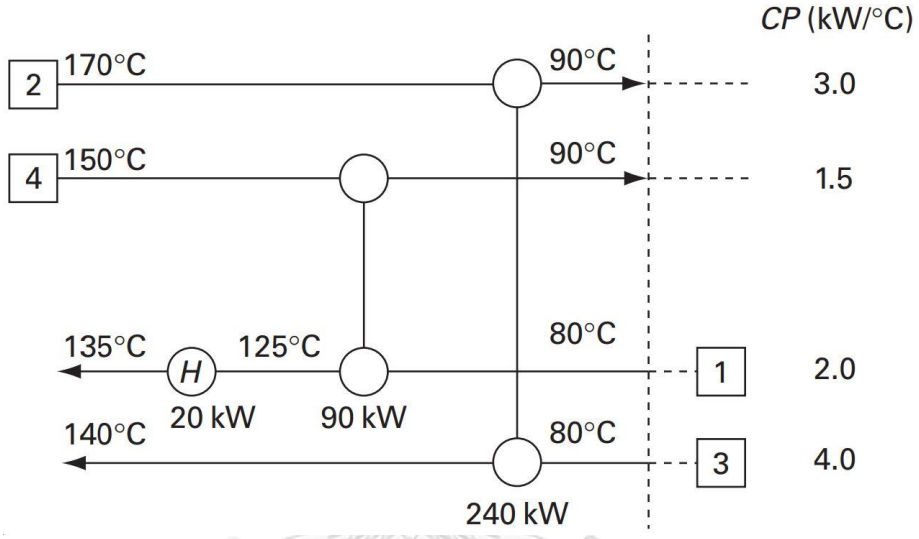

Figure 3.7 Above pinch heat exchanger network design for example data in Table 3.2 (Kemp, 2011).

Next, consider below pinch temperature, the heat exchanger network design is performed separately from the above pinch temperature design. The design starting from the pinch temperature by the requirement criterion that the heat capacity flow rate of the hot stream must be greater than or equal to the cold stream, as shown in Eq. (3.19). The design below pinch temperature is the same as the design of the above pinch temperature. The design is aimed to ensure that the cold stream is adequately heated to the pinch temperature and that the only cold utility is used with the hot stream. In this example, the matching starts from the cold stream 1 (the only cold stream below the pinch temperature), which must be matched to hot stream 2 because $CP_1 < CP_2$. Due to the only 90 kW of heat in the hot stream 2 can be exchange with cold stream 1, which

not satisfy the target temperature. The remaining of 30 kW must be discharge from the hot stream to cold stream 1 and the only hot stream is stream 4. Although, the CP criterion of cold stream 1 and hot stream 4 did not pass for this match, but this match is feasible because it is away from pinch. The cold stream 1 has been heated to 90 kW, the point is far from the pinch temperature, so it can be heated from hot stream 4. The feasible of this match can be checked using the balance of the heat exchange, as shown in Figure 3.8. When the match is complete, only hot stream 2 is not reach the target temperature. It must be cooling by using the external cold utility of 60 kW to be at 30 ^{o}C. The value of the cold utility requiring corresponds to the energy target calculation.

$$CP_{HOT} \geq CP_{COLD} \tag{3.19}$$

To complete the heat exchanger network design, putting the design of above and below the pinch temperature together, as shown in Figure 3.9. The design achieves the best heat transfer efficiency at ΔT_{min} of 10 °C. There are 6 heat exchangers (including heater and cooler unit).

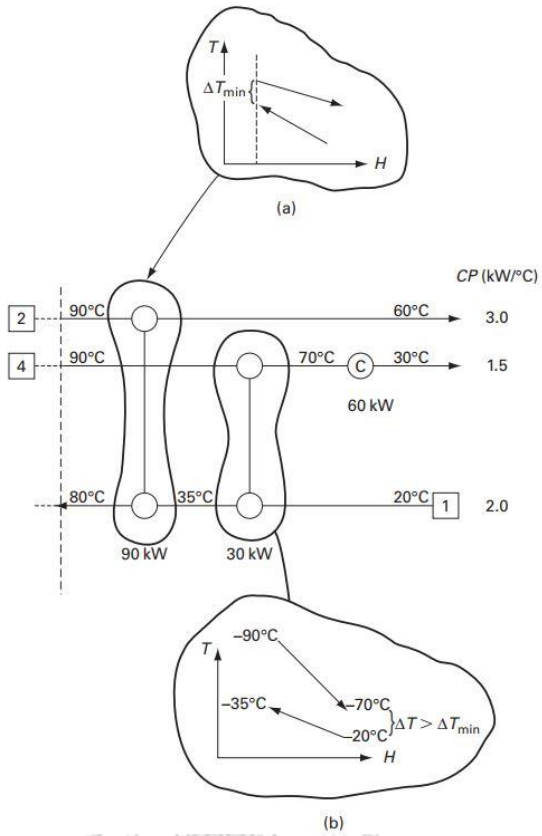

Figure 3.8 Below pinch heat exchanger network design for example data in Table 3.2 (Kemp, 2011).

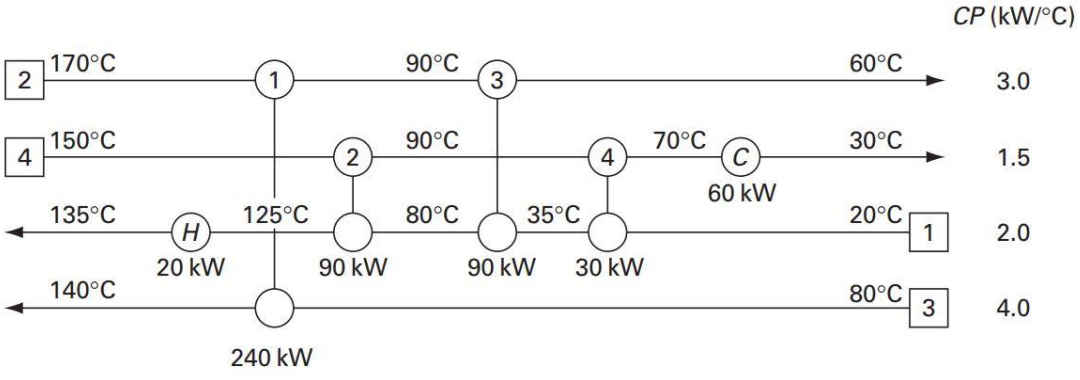

Figure 3.9 Complete heat exchanger network design for example data in Table 3.2 (Kemp, 2011).

3.6 Energy and exergy analysis

Energy analysis can be performed by using the thermal efficiency of the process based on the first law of thermodynamics. The thermal efficiency can be obtained by calculating the heat demand and the heat release through the energy balance, which is by the first law of thermodynamics. The energy analysis treats all the form of energy are an equivalence. It only analyzes the quantity of energy. For energy analysis of hydrogen production with the SECLR-WS process, thermal efficiency (or energy efficiency) can be calculated from the energy produced by the hydrogen product divided by the all energy input to the process (Dincer and Rosen, 2013). The total energy input to the system is the summation of the heat for the reactor, the heat for heating all feed streams, and the energy in the feed stream. The thermal efficiency of the system can be calculated following the Eq. (3.20).

$$\eta_{th}(\%) = \frac{Energy_{H_2\ product\ stream}}{Total\ energy\ to\ system} = \frac{\dot{N}_{H_2} \times LHV_{H_2}}{Q_{total} + (\dot{N}_{CH_4,\,feed} \times LHV_{CH_4})} \times 100 \qquad (3.20)$$

where $\dot{N}_{H_2}$ and $\dot{N}_{CH_4,feed}$ are the molar flow rate of H_2 in the product stream and CH_4 in biogas feed stream, respectively. LHV_{H_2} and LHV_{CH_4} are the lower heating value of H_2 and CH_4. Q_{total} is the total energy input to the process (including the duty of heater and duty of the reactor).

Energy analysis, based on the first law of thermodynamics, does not provide sufficient information on how much work is being lost to transform energy (Mukherjee *et al.*, 2015). Therefore, to evaluate the efficiency of the process, taking into account the irreversibility of the system, the exergy analysis is conducted. The exergy analysis is based on the first and second laws of thermodynamics. Exergy is the maximum useful work can be obtained when the system is operated under one initial state (T, P) to the equilibrium with the reference environment sate (T_0, P_0) (Zhu *et al.*, 2018). In this study, the reference environment state is T_0 = 25 ^oC and P_0 = 1 atm. The exergy analysis of the process can determine which parts of the process are inefficient in energy usage, resulting from the irreversibility of the system.

Energy is conserved and cannot be lost but can transform from one to another, which is based on the first law of thermodynamics, and from this point, the energy balance can be performed. The entropy and exergy balances are different from the energy; the system must always have to generate entropy. While the system is always destroyed the exergy. This is due to the irreversibility of the system as shown in Figure 3.10.

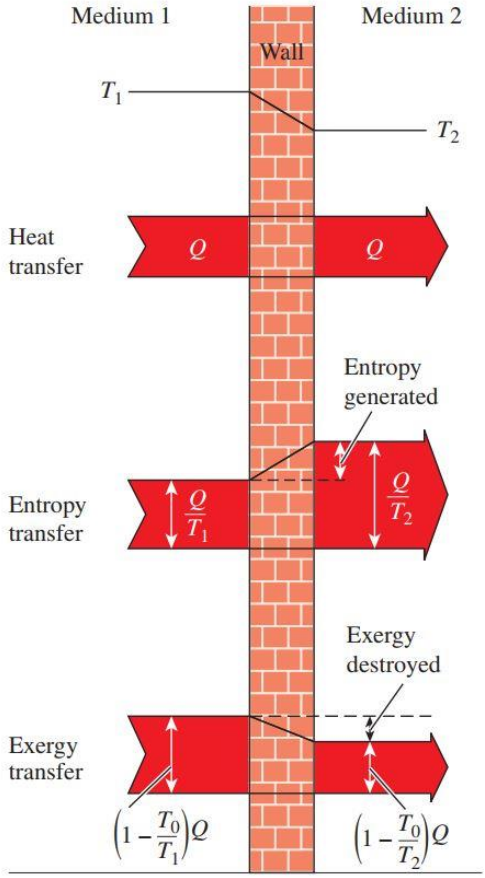

Figure 3.10 Energy, entropy, and exergy transfer through the wall (Boles and Yunus A. Cengel, 2014).

The exergy destruction can be calculated by exergy balance around the control volume at steady state operation with several input and output streams according to Eq. (3.21) (Kasemanand *et al.*, 2017).

$$(\sum Ex)_{in} = (\sum Ex)_{out} + Ex_d \quad (3.21)$$

where $(\sum \mathrm{Ex})_{\mathrm{in}}$ and $(\sum \mathrm{Ex})_{\mathrm{out}}$ are the summation of exergy in and exergy out, respectively, and Ex_{d} is the exergy destruction.

The transfer of the exergy is divided into three types: the exergy transfer by heat, exergy transfer by work, and the exergy transfer by mass (or flow exergy). The exergy transfer by kinetic and potential energy is neglect in this study because there are small when compared with the exergy transfer by heat and flow exergy in the thermal chemical process (Kasemanand *et al.*, 2017). The total exergy transfer can be calculated according to Eq. (3.22).

$$\sum Ex = \sum Ex_s + \sum Ex_Q + \sum Ex_W \quad (3.22)$$

where $\sum Ex_s$, $\sum Ex_Q$, and $\sum Ex_W$ are the total exergy transfer by mass, heat, and work, respectively.

The exergy transfer by heat and work can be calculated following the Eq. (3.23) and (3.24).

$$Ex_Q = (1 - \frac{T_0}{T_s})Q_s \quad (3.23)$$

$$Ex_W = W \quad (3.24)$$

where Ex_{Q} and Ex_{W} are the exergy transfer by heat and work, respectively. T_0 is the reference environment temperature, T_{S} is the system temperature. Q_{s} and W are the heat and work transfer through the process. When the heat and work transfer into the process, the exergy transfer by heat and work are included in the term of exergy transfer into the process. In contrast, when the heat and work release from the process, the exergy transfer by heat and work are included in the term of exergy transfer out of the process. In this study, the heat source to supply the process is not consideration, thus, when the unit operates by consuming the heat of Qs at Ts, the heat source assuming supply the heat at level of Ts.

The flow exergy can be calculated from the Eq. (3.25)

$$Ex_{S,j} = F_j \times ex_{S,j} \tag{3.25}$$

where $Ex_{S,j}$ is the flow exergy of stream j, F_j is the molar flow rate of stream j, and $ex_{S,j}$ is the specific molar flow exergy of stream j.

The flow exergy consists of two component, physical exergy and chemical exergy, according to Eq. (3.26). The physical exergy of stream j ($ex_{ph,j}$) is the useful work obtained by passing a stream in the general state (T, P) to the reference environment state (T_0, P_0), which can be determined by Eq.(3.27) (Querol *et al.*, 2013). The chemical exergy of stream j ($ex_{ch,j}$) is the useful work obtained by passing the substance from the reference environment state to the equilibrium with the reference environment state. The chemical exergy can be calculated from Eq. (3.28) (J.Y. *et al.*, 2004).

$$ex_{S,j} = ex_{ph,j} + ex_{ch,j} \tag{3.26}$$

$$ex_{ph,j} = (h_j - h_{0,j}) - T_0(s_j - s_{0,j}) \tag{3.27}$$

$$ex_{ch,j} = f_j^V(\sum y_{i,j}\overline{ex}_{ch,i} + RT_0\sum y_{i,j}\ln y_{i,j}) + f_j^L(\sum x_{i,j}\overline{ex}_{ch,i}) + f_j^S(\sum z_{i,j}\overline{ex}_{ch,i}) \tag{3.28}$$

where h_j and s_j are the specific molar enthalpy and entropy of stream j at T and P. $h_{0,j}$ and $s_{0,j}$ are the specific molar enthalpy and entropy of stream j at T_0 and P_0. f_j^V , f_j^L, and f_j^S are the mole fraction of gas, liquid, and solid, respectively, in stream j. $y_{i.j}$, $x_{i.j}$, and $z_{i.j}$ are the mole fraction of component i in gas, liquid, and solid phase, respectively, in stream j. $\overline{ex}_{ch,i}$ is the standard specific molar chemical exergy of component i at T_0 and P_0. $\overline{ex}_{ch,i}$ of the all components in the SECLR-WS process are shown in Table 3.5.

The exergy analysis is performed by using the exergy efficiency of the process (η_{ex}) and exergy of a single unit in the process ($\eta_{ex,i}$) and also the exergy destruction of the single unit in the process to explode the nearly real efficiency of the process. The definition of the exergy efficiency of the SECLR-WS process for the hydrogen production is the exergy of hydrogen product output divided by the total exergy input,

according to Eq. (3.29), which analogous to the thermal efficiency of the process (Dincer and Rosen, 2013). The exergy efficiency of the single unit in the process can be calculated by Eq. (3.30).

$$\eta_{ex}(\%) = \frac{Ex_{H_2\ product\ stream}}{(\sum Ex)_{in}} \tag{3.29}$$

$$\eta_{ex,i}(\%) = \frac{(\sum Ex)_{out}}{(\sum Ex)_{in}} = 1 - \frac{Ex_d}{(\sum Ex)_{in}} \tag{3.30}$$

Table 3.5 Standard chemical exergy (Szargut, 2005).

Substance	Phase	Standard chemical exergy (kJ/kmol)
CH_4	g	831600
H_2O	g	9500
CO	g	275100
CO_2	g	19870
H_2	g	236090
Fe_3O_4	s	116300
$Fe_{0.947}O$	s	111300
CaO	s	110200
$CaCO_3$	s (aragonite)	1000
H_2O	l	900

CHAPTER IV
MODELING OF THE SORPTION-ENHANCED CHEMICAL LOOPING REFORMING AND WATER SPLITTING PROCESS

Process model is a useful tool for understanding the behavior of chemical processes. In this chapter, the modeling and simulation of the sorption-enhanced chemical looping reforming and water splitting (SECLR-WS) process are explained. The SECLR-WS process is simulated by using Aspen Plus program. The Aspen Plus is a flowsheeting based model using a sequential modular approach. Basically, the sequential modular is a computational strategy which perform the simulation of the process by performing the calculation sequence (unit-by-unit). Detailed flowsheet development for the SECLR-WS process are given in this chapter, including major assumptions, a module of a unit, and stream information. In addition, the validation of SECLR-WS simulation against the experimental data reported in the literature is presented.

4.1 Model of the SECLR-WS

Modeling of the sorption-enhanced chemical looping reforming and water splitting process (SECLR-WS) was performed by using Aspen Plus simulator. In the process, the equilibrium reactor is simulated using the equilibrium RGibbs reactor. The gaseous equilibrium composition in the reactor can be calculated using the minimization of Gibbs free energy method which does not require specific information of the reaction in the system. However, the input composition for the calculation must be appropriated. In this study, the biogas feed, which mainly composes of CH_4 and CO_2, and steam were considered reactants. Magnetite iron oxide and CaO were used as oxygen carrier and CO_2 adsorbent, respectively. Therefore, the possible gaseous components were H_2, CH_4, CO_2, and CO, and the solid components were $CaCO_3$, CaO, Fe_3O_4, and $Fe_{0.947}O$ (Go *et al.*, 2009; Rydén and Ramos, 2012). The summarize specification of components in this system is summarized in Table 4.1. The system was operated under isothermal and isobaric conditions. The thermodynamic properties were

determined based on the SOLIDS property method using the vapor phase in the Redlich-Kwong-Soave equation of state with Boston-Mathias modification (ESRKS). The assumptions of the simulation were as follows: (1) the kinetic effects were not taken into consideration, (2) the shape and properties of the solids were disregarded, (3) the pressure drops and heat lost between units during the operation were neglected.

Table 4.1 Specification of components in SECLR-WS process.

Components	Type
H_2O	Conventional
H_2	Conventional
CO	Conventional
CO_2	Conventional
CaO	Solid
$CaCO_3$	Solid
Fe_3O_4	Solid
$Fe_{0.947}O$	Solid

The flow diagram of the SECLR-WS process for H_2 production from biogas is shown in Figure 4.1. The process involved three reactors: FR, SR, and calcinator and three cyclones. Biogas (BIOGAS), steam (STEAM-FR), and the mixture of Fe_3O_4 and CaO in the SOLID-RE stream were fed into the FR to produce H_2-rich syngas. The FR was operated under isothermal conditions at 500–800 °C and atmospheric pressure. The oxidation reaction, which included the partial (Eq. (3.4)) and complete (Eq. (3.5)) oxidation reactions, and the SMR reaction (Eq. (3.1)) took place in the FR. Magnetite iron oxide was reduced to wüstite during the oxidation reaction. At the same time, CO_2 produced during the complete oxidation reaction (Eq. (3.5)), was adsorbed by CaO during the carbonation reaction (Eq. (3.3)), resulting in the equilibrium of the water-gas shift reaction (Eq. (3.2)) shifting toward the product side. The gaseous products and solids from the FR (FR-CYC) were fed to the first cyclone (CYC1) to separate gases

from solids. The main product of the FR was H_2-rich syngas (SYNGAS). The solids stream from the FR (FEOCACO3): Fe_3O_4, $Fe_{0.947}O$, CaO, and $CaCO_3$, were fed to the second reactor, the SR. The SR was operated under isothermal conditions at 400–800 °C and atmospheric pressure. In the SR, wüstite iron oxide was re-oxidized to magnetite iron oxide using steam as oxidizing agent during the steam-iron reaction (Eq. (3.6)). The main gaseous product from the SR was high-purity H_2 (H2). The mixed gaseous and solid products that streamed from the SR (SR-CYC) were sent to the second cyclone (CYC2) for separation. Subsequently, the solids that streamed from the SR (CACO3FE3): Fe_3O_4, CaO, and $CaCO_3$ were fed to the calcinator (CAL) to regenerate $CaCO_3$ by calcinating (Eq. (3.8)) $CaCO_3$ into CaO. The calcinator was operated at T_{CAL} = 860 °C. The mixture of gases and solids that streamed from the calcinator (CLC-CYC3) was fed to the last cyclone (CYC3) to separate CO_2 gas from the solid Fe_3O_4 and CaO. The solids that streamed from CYC3 were fed back to the FR to complete the cycle of the process. The based case and the range of operating conditions considered in this study are shown in Table 4.2. The main reactions occurring in the combined process, SECLR-WS, are shown in chapter 3 (section 3.3) which according to Eqs. (3.1)-(3.8) (Fraser *et al.*, 2006; Go *et al.*, 2009; Yahom *et al.*, 2014).

Table 4.2 Base case simulation and studied range of the SECLR-WS process.

Parameter	Value	
	Base case condition	**Range of study**
Biogas feed stream		
CO_2 molar concentration (%)	40	0–90
Temperature (°C)	400	-
Pressure (atm)	1	-
Steam feed to FR		
Temperature (°C)	400	-

Pressure (atm)	1	-
Steam feed to SR		
Temperature (°C)	400	-
Pressure (atm)	1	-
Steam in FR to CH_4 molar ratio	2.2	0–8
Fe_3O_4 to CH_4 molar ratio	1	0–8
CaO to CH_4 molar ratio	1.66	0–8
Steam in SR to CH_4 molar ratio	2.87	0–8
FR temperature (°C)	600	500–800
SR temperature (°C)	500	400–800
Calcinator temperature (°C)	860	-

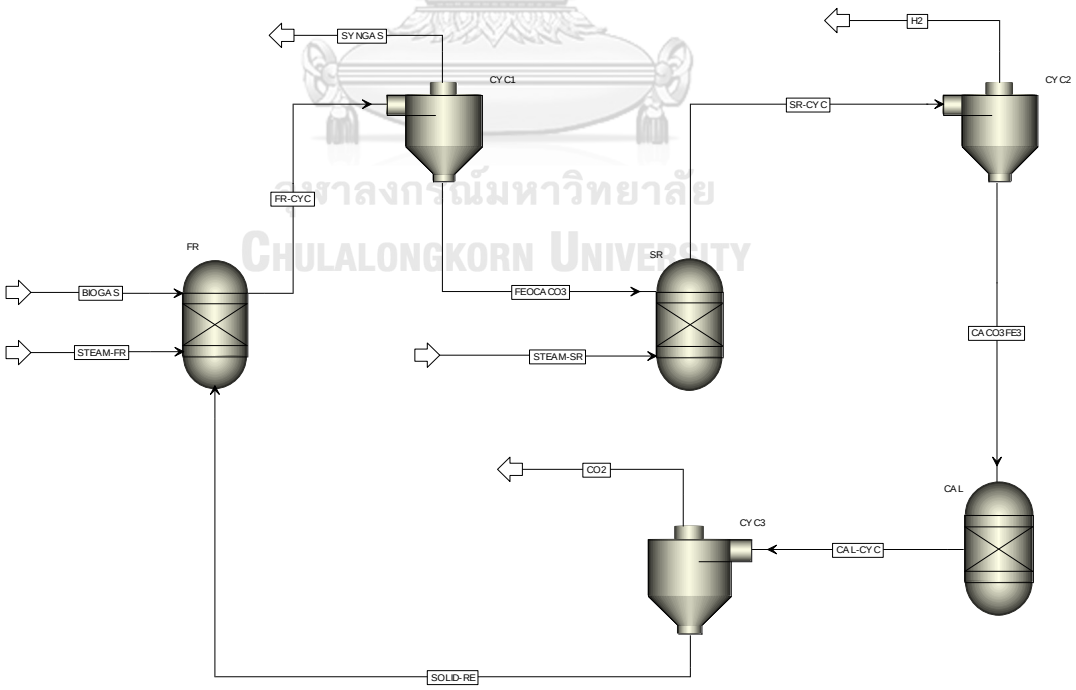

Figure 4.1 Simulation flow diagram of the combined process of sorption-enhanced chemical looping reforming and water splitting process (SECLR-WS).

The key operating parameters in the SECLR-WS process were the fuel and steam reactor temperatures (T_{FR} and T_{SR}, respectively) and the Fe_3O_4 to CH_4 (Fe_3O_4/CH_4) molar ratio, CaO to CH_4 (CaO/CH_4) molar ratio, steam feed to FR to CH_4 (S_{FR}/CH_4) molar ratio, and steam feed to SR (S_{SR}/CH_4) molar ratio (Eqs. (4.1)–(4.4), respectively), and CO_2 molar concentration (%CO_2) in the biogas feed stream. The performance of the process was expressed in terms of H_2 yield in the FR and SR, total H_2 yield, H_2 purity in the FR and SR, and CH_4 conversion, which were calculated using Eqs. (4.5)-(4.10), respectively.

$$Fe_3O_4/CH_4 \text{ molar ratio (mol/mol)} = \frac{\text{mol } Fe_3O_4 \text{ feed}}{\text{mol } CH_4 \text{ feed}} \quad (4.1)$$

$$CaO/CH_4 \text{ molar ratio (mol/mol)} = \frac{\text{mol CaO feed}}{\text{mol } CH_4 \text{ feed}} \quad (4.2)$$

$$S_{FR}/CH_4 \text{ molar ratio (mol/mol)} = \frac{\text{mol steam feed to FR}}{\text{mol } CH_4 \text{ feed}} \quad (4.3)$$

$$S_{SR}/CH_4 \text{ molar ratio (mol/mol)} = \frac{\text{mol steam feed to SR}}{\text{mol } CH_4 \text{ feed}} \quad (4.4)$$

$$H_2 \text{ yield in FR (mol/mol)} = \frac{\text{mol } H_2 \text{ produced in FR}}{\text{mol } CH_4 \text{ feed}} \quad (4.5)$$

$$H_2 \text{ yield in SR (mol/mol)} = \frac{\text{mol } H_2 \text{ produced in SR}}{\text{mol } CH_4 \text{ feed}} \quad (4.6)$$

$$\text{Total } H_2 \text{ yield (mol/mol)} = \frac{\text{mol } H_2 \text{ produced in FR} + \text{mol } H_2 \text{ produced in SR}}{\text{mol } CH_4 \text{ feed}} \quad (4.7)$$

$$H_2 \text{ purity in FR (\%)} = \frac{\text{mol } H_2 \text{ produced in FR}}{\text{mol gaseous products in FR (dry basis)}} \times 100 \quad (4.8)$$

$$H_2 \text{ purity in SR (\%)} = \frac{\text{mol } H_2 \text{ produced in SR}}{\text{mol gaseous products in SR (dry basis)}} \times 100 \quad (4.9)$$

$$CH_4 \text{ conversion (\%)} = \frac{\text{mol } CH_4 \text{ in - mol } CH_4 \text{ out}}{\text{mol } CH_4 \text{ in}} \times 100 \quad (4.10)$$

4.2 Model validation

As the integrated SECLR-WS process presents a new concept, experimental data of the proposed process is quite limited. However, the model of the proposed process developed in this study is derived from two basic chemical looping processes: SECLR and CLWS. Thus, the parts of the SECLR-WS process were individually validated. The first part of the SECLR-WS model, which involves the SECLR process, was validated using the experimental data reported by Rydén and Ramos (2012). Pure CH_4 was used as feedstock and chemical looping reforming took place in a fluidized bed reactor. The temperature of the FR was varied in the 600–750 °C range, and the input parameters: S_{FR}/CH_4, NiO/CH_4, and CaO/CH_4 molar ratios were 1.8, 1, and 1, respectively. Table 4.3 shows the resulting H_2 and CO_2 concentrations from the experimental results and simulation data of the SECLR process. It was found that the model predictions were in good agreement with the experimentally obtained H_2 concentrations. The over-estimation of the CO_2 concentration at high temperatures occurred from the incomplete conversion of CH_4 in the experimental process. CH_4 conversion can be improved using higher S_{FR}/CH_4 molar ratios than indicated by the equilibrium conditions (Rydén and Ramos, 2012). The CLWS process was validated using the work done by Edrisi *et al.* (2014) under the same conditions (Table 4.4). It was found that the predictive results of the CLWS model were in good agreement with the value reported in that literature (Table 4.5). From the validation results presented here, the developed model of the SECLR-WS process consisting of the SECLR and CLWS models will be used to analyze the performance of the process.

Table 4.3 Comparison of the simulation results and experimental data (Rydén and Ramos, 2012) of the SECLR process.

Temperature	Concentration (% mol/mol dry basis)					
	Simulation		Experimental		Relative error (%)	
	H_2	CO_2	H_2	CO_2	H_2	CO_2
600	0.9812	0.0058	0.9876	0.0058	0.6596	0.3506
650	0.9388	0.0200	0.9488	0.0216	1.0627	8.0937
700	0.8725	0.0568	0.8308	0.0707	4.7801	24.4665
750	0.7282	0.0988	0.7080	0.1255	2.7759	27.0957

Table 4.4 Operating conditions for validation of the CLWS process.

	Feed stream	
Fuel		
	Component	CH_4 1 kmol s^{-1}
	Temperature	450 ^oC
	Pressure	20 bar
Stream		
	Component	H_2O 6.55 kmol s^{-1}
	Temperature	400 ^oC
	Pressure	22 bar
Air		
	Component	N_2 2.533 kmol $s^{-1}$and O_2 0.673 kmol s^{-1}
	Temperature	470 ^oC

Pressure	20 bar
Reactor	
Fuel reactor temperature	723 ºC
Steam reactor temperature	727 ºC
Air reactor temperature	880 ºC
Pressure	20 bar
Solid circulation	
Component	Fe_2O_3 4 kmol $s^{-1}$and $MgAl_2O_4$ 6 kmol s^{-1}

Table 4.5 Comparison of the simulation results and experimental data (Edrisi *et al.*, 2014) of the CLWS process.

		Molar fraction		
		Simulation	Reference	Absolute error
Gaseous product from fuel reactor				
	CH_4	0.00025	0.0002	0.00005
	CO_2	0.33324	0.3333	$5.06x10^{-05}$
	H_2O	0.66649	0.6665	$1.1x10^{-06}$
Gaseous product from steam reactor				
	H_2O	0.59333	0.5938	0.0004637
	H_2	0.40666	0.4062	0.0004637

CHAPTER V
THERMODYNAMIC ANALYSIS AND OPTIMIZATION

This chapter presents the effect of the operating parameters on the performance of the SECLR-WS process. The effect of key operating parameters such as a temperature of FR, a temperature of SR, steam to methane molar ratio in FR, iron oxide to methane molar ratio, and calcium oxide to methane molar ratio on the process performance in terms of hydrogen yield and purity are analyzed using a thermodynamic approach. Additionally, the optimization is performed to find the suitable operating condition offering maximum yield of H_2 while consumes lowest energy.

5.1 Sensitivity analysis

The sensitivity analysis in simulation is performed to investigate the effect of the operating parameters on the process performance. The key operating parameters in the SECLR-WS process are FR and SR temperature, and Fe_3O_4/CH_4, CaO/CH_4, S_{FR}/CH_4, S_{SR}/CH_4 molar ratios. The performance of the process is expressed in terms of H_2 yield in FR, H_2 yield in SR, total H_2 yield, H_2 purity in FR, H_2 purity in SR, and CH_4 conversion. In addition, the effect of the operating pressure of SR on CO molar concentration in SR is investigated. The low CO concentration in high purity H_2 stream is importance for such application, i.e. LT-PEMFC.

5.1.1 Effect of the steam feed FR to methane molar ratio

Figures 5.1–5.4 show the effect of the S_{FR}/CH_4 molar ratio in the 0-8 range on the H_2 yield in the FR and SR, total H_2 yield, H_2 purity in the FR, and CH_4 conversion, respectively given an FR operating temperature of 500–800 °C, SR temperature of 500 °C, and Fe_3O_4/CH_4, CaO/CH_4, and S_{SR}/CH_4 molar ratios of 1, 1.66, and 2.87 respectively. The results showed that the maximum H_2 yield in the FR decreased when the temperature of the FR was increased. This could be explained by the CaO capturing CO_2 and generating $CaCO_3$ in the carbonation reaction (Eq. (3.3)), which was favored

at low temperatures, and shifting of the equilibrium of the SMR (Eq. (3.1)) and water gas shift (Eq. (3.2)) reactions toward the product side according to the Le Chatelier's principle (Medrano *et al.*, 2018; Shokrollahi Yancheshmeh *et al.*, 2016). Le Chatelier's principle is used to predict changes in equilibrium when conditions such as temperature, concentration, or pressure are changed in chemical equilibrium reactions. The chemical equilibrium will shift to counteract the stress.

Figure 5.1 shows the H_2 yield in the FR and SR as a function of the S_{FR}/CH_4 molar ratio for each tested temperature. The process was composed of three phases. The first phase was the partial oxidation reaction (Eq. (3.4)) of CH_4 by Fe_3O_4 into $Fe_{0.947}O$, water-gas shift (Eq. (3.2)), and SMR (Eq. (3.1)), resulting in more H_2 product in the FR. As S_{FR}/CH_4 kept increasing, the process advanced to the second phase where $Fe_{0.947}O$ was partially re-oxidized to Fe_3O_4 using steam in an enriched H_2O environment because the rates of the forward and backward steam-iron reaction (Eq. (3.6)) were very similar (K. Svoboda *et al.*, 2007). Due to decreasing the amount of $Fe_{0.947}O$, the H_2 yield in the SR was gradually reduced due to the absence of $Fe_{0.947}O$ as a reactant in the steam-iron reaction (Eq. (3.6)). Moreover, it was found that the total H_2 yield decreased as shown in Figure 5.2. Subsequently, when the S_{FR}/CH_4 molar ratio was increased, the slope of the graph in Figure 5.2 advanced to the final phase. The main reaction in the final phase was the SMR reaction (Eq. (3.1)), which produced H_2, due to $Fe_{0.947}O$ completely reacting with steam to form Fe_3O_4.

Figure 5.3 shows the change in H_2 purity with the S_{FR}/CH_4 molar ratio at different temperatures. It was found that when the FR temperature was increased, the maximum H_2 purity in the FR decreased. In addition, at FR temperatures of 500, 600, and 700 °C, when the S_{FR}/CH_4 molar ratio was increased in the first stage, H_2 purity in the FR significantly increased until it reached the point where re-oxidation occurred. At that point, the purity of H_2 in the FR became constant even though the H_2 yield in the FR increased, because the amounts of CH_4 and CO_2 were increased. When the entire amount of $Fe_{0.947}O$ was re-oxidized, increasing the S_{FR}/CH_4 molar ratio had an insignificant effect on the purity of H_2. When the FR temperature was 800 °C, the purity of H_2 increased with increasing the S_{FR}/CH_4 molar ratio.

Figure 5.4 shows the change in CH_4 conversion by varying the S_{FR}/CH_4 molar ratio at different temperatures. It was found that at low temperatures, when the S_{FR}/CH_4 molar ratio was increased, the CH_4 conversion increased in the earliest stage of the process. This was due to the partial (Eq. (3.4)) and complete (Eq. (3.5)) oxidation reactions between CH_4 and Fe_3O_4 and the SMR reaction (Eq. (3.1)) occurring. When the S_{FR}/CH_4 molar ratio further increased, CH_4 conversion decreased due to the re-oxidation of $Fe_{0.947}O$ to Fe_3O_4 by steam, leading to the lack of reactant for the oxidation (Eq. (3.4) and (3.5)) and SMR (Eq. (3.1)) reactions. After the S_{FR}/CH_4 molar ratio increased until $Fe_{0.947}O$ was completely re-oxidized, CH_4 conversion increased due to the SMR reaction (Eq. (3.1)). At high temperatures, CH_4 conversion was very high because the complete oxidation (Eq. (3.5)) and SMR reaction (Eq. (3.1)) were favored (Go *et al.*, 2009). However, at high temperatures, the water-gas shift (Eq. (3.2)) and carbonation (Eq. (3.3)) reactions were not favored leading to high amounts of CO_2 and CO, and low maximum H_2 yield and purity in the FR.

To achieve a high operational efficiency, the S_{FR}/CH_4 molar ratio should be appropriate for obtaining a high H_2 yield (total H_2 yield and H_2 yield in the FR) and high H_2 purity in the FR, while $Fe_{0.947}O$ must not be re-oxidized in the FR. Although increasing the S_{FR}/CH_4 molar ratio can increase the H_2 yield and purity in the FR and the total H_2 yield, the decreased amount of $Fe_{0.947}O$ led to the generation of a lower amount of high-purity H_2 from the SR due to the lack of reactant for the steam-iron reaction (Eq. (3.6)). When the appropriate operating value of 2.2 for the S_{FR}/CH_4 molar ratio in the FR at 610 °C and 1 atm was reached, the H_2 yield in the FR, total H_2 yield, and H_2 purity in the FR of 2.98, 3.8, and 97.01 %, respectively, are achieved.

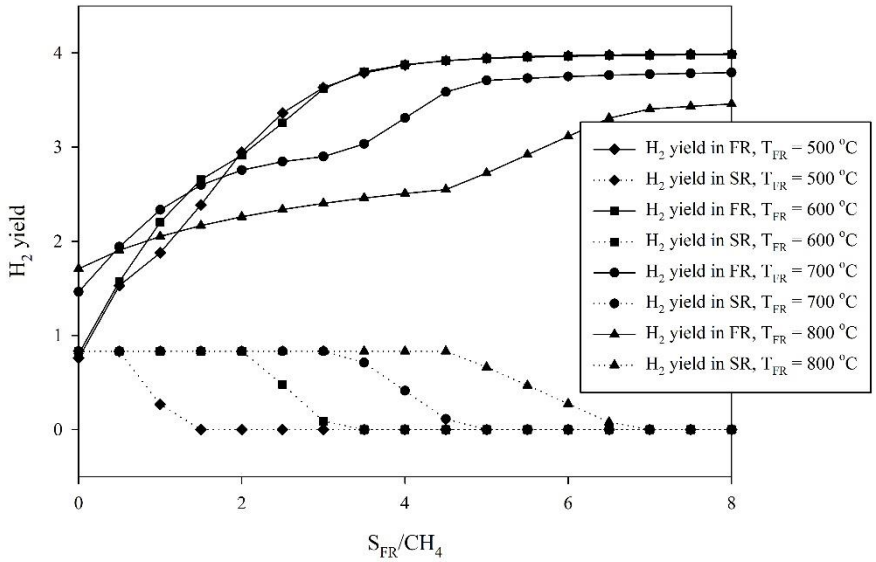

Figure 5.1 The H_2 yield in FR and SR as a function of S_{FR}/CH_4 and T_{FR} at T_{SR} = 500 ^oC, Fe_3O_4/CH_4 = 1, CaO/CH_4 = 1.66, and S_{SR}/CH_4 = 2.87.

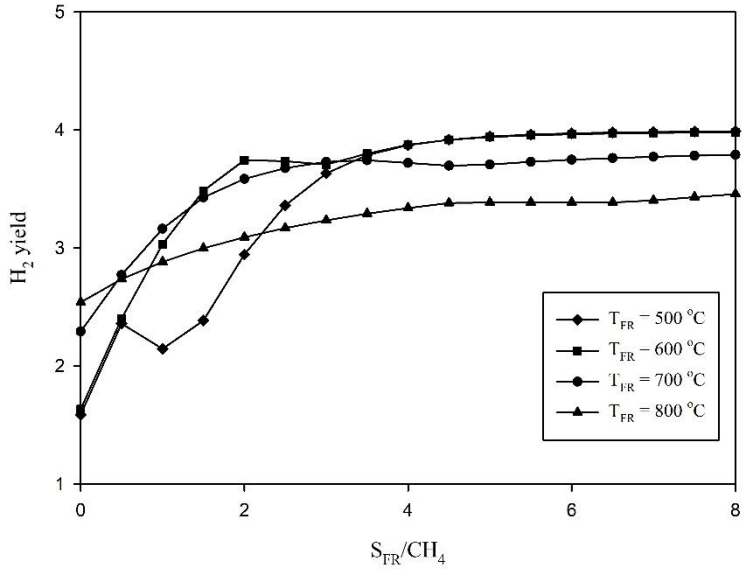

Figure 5.2 The total H_2 yield as a function of S_{FR}/CH_4 and T_{FR} at T_{SR} = 500 ^oC, Fe_3O_4/CH_4 = 1, CaO/CH_4 = 1.66, and S_{SR}/CH_4 = 2.87.

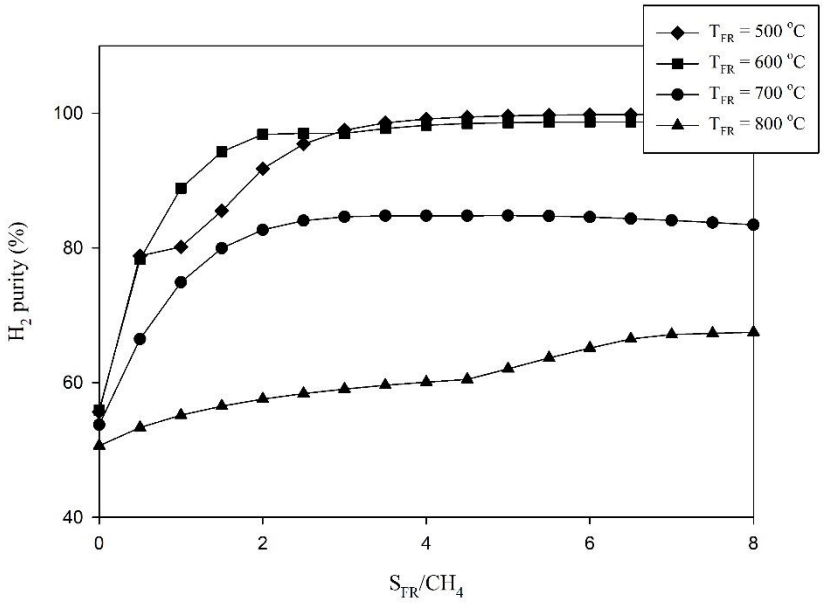

Figure 5.3 The H_2 purity as a function of S_{FR}/CH_4 and T_{FR} at T_{SR} = 500 °C, Fe_3O_4/CH_4 = 1, CaO/CH_4 = 1.66, and S_{SR}/CH_4 = 2.87.

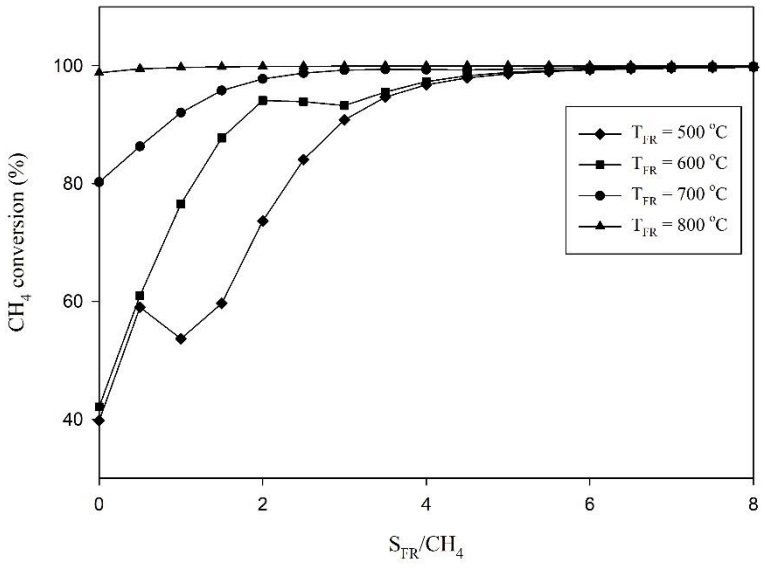

Figure 5.4 The CH_4 conversion as a function of S_{FR}/CH_4 and T_{FR} at T_{SR} = 500 °C, Fe_3O_4/CH_4 = 1, CaO/CH_4 = 1.66, and S_{SR}/CH_4 = 2.87.

5.1.2 Effect of the Fe_3O_4 to methane molar ratio

Figures 5.5–5.8 show the effect of the Fe_3O_4/CH_4 molar ratio in the 0–8 range on the H_2 yield in the FR and SR, total H_2 yield, H_2 purity in the FR, and CH_4 conversion, respectively, for operating FR temperatures in the 500–800 °C range, SR temperature of 500 °C, and S_{FR}/CH_4, CaO/CH_4, and S_{SR}/CH_4 molar ratios of 2.2, 1.66, and 2.87 respectively. The results showed that when the FR temperature was 500 °C, increasing the Fe_3O_4/CH_4 molar ratio did not affect the system. For FR temperatures of 600 °C and higher, increasing the Fe_3O_4/CH_4 molar ratio increased the H_2 yield in the SR but decreased the H_2 yield in the FR as shown in Figure 5.5. This could be explained by the amount of Fe_3O_4 which completely reacted with CH_4 to form $Fe_{0.947}O$ in the complete oxidation reaction (Eq. (3.5)) resulting in increasing CH_4 conversion, as shown in Figure 5.8, and increasing H_2 yield in the SR due to the high amount of $Fe_{0.947}O$, which is a reactant for the steam-iron reaction (Eq. (3.6)). The decreasing of the H_2 yield in the FR was the result of H_2 from the SMR reaction (Eq. (3.1)) reacts with Fe_3O_4 by the reverse steam-iron reaction (Eq. (3.6)). A CH_4 conversion of 100% could not be achieved at low operating temperatures. Although increasing the Fe_3O_4/CH_4 molar ratio resulted in decreasing the H_2 yield in the FR, its effect on the total H_2 yield was the opposite, as shown in Figure 5.6. The total H_2 yield could be increased by increasing the Fe_3O_4/CH_4 molar ratio since more $Fe_{0.947}O$ reacted with steam to produce high-purity H_2 in the SR. In addition, increasing the FR temperature could decrease the H_2 yield in the FR since the carbonation reaction (Eq. (3.3)) was favored at low temperatures as mentioned in section 5.1.1. Although the maximum total H_2 yield of 3.79 could be obtained at a FR temperature of 700 °C and Fe_3O_4/CH_4 molar ratio of 1.75, H_2 purity at that FR temperature, which was 84.77%, was lower than that at a FR temperature of 600 °C, where H_2 purity was maximum: 97.01%, while the H_2 yield in the FR and total H_2 yield were 3.04 and 3.75, respectively, for a Fe_3O_4/CH_4 molar ratio of 0.92.

The purity of H_2 in the FR could be increased by increasing the Fe_3O_4/CH_4 molar ratio for FR temperatures of 600 and 700 °C, and could be decreased by increasing the Fe_3O_4/CH_4 molar ratio when the FR temperature was 800 °C, as shown in Figure 5.7. That was the result of the carbonation reaction (Eq. (3.3)). When the

amount of Fe_3O_4 was increased, CH_4 could react with the excess OC to generate CO and CO_2. At low temperatures, CO_2 could be adsorbed by CaO and CO could react with steam in the water-gas shift reaction (Eq. (3.2)), resulting in lower amounts of CH_4, CO, and CO_2. The suitable Fe_3O_4/CH_4 molar ratio when the FR temperature was 610 °C and the pressure 1 atm was the one allowing to obtain a H_2 yield in the FR, total H_2 yield, and H_2 purity in the FR of 2.98, 3.8, and 97.01%, respectively.

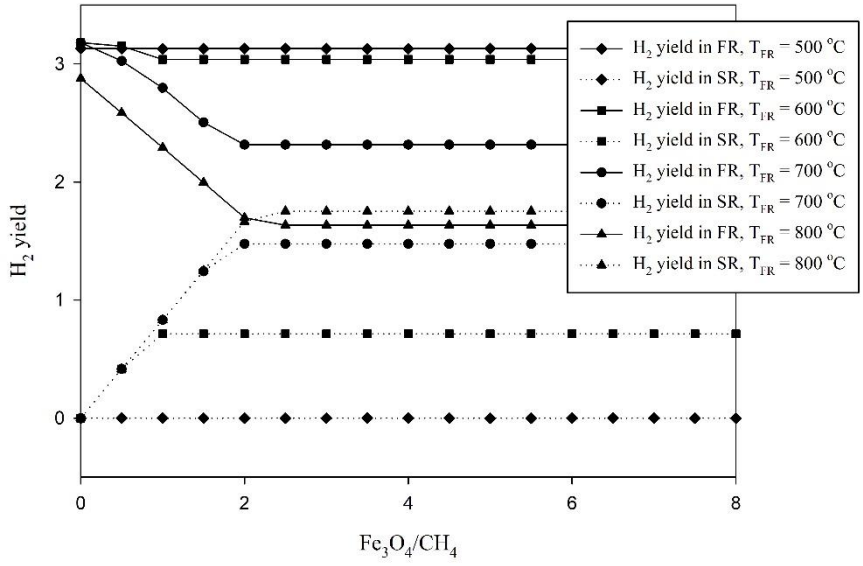

Figure 5.5 The H_2 yield in FR and SR as a function of Fe_3O_4/CH_4 and T_{FR} at T_{SR} = 500 °C, S_{FR}/CH_4 = 2.2, CaO/CH_4 = 1.66, and S_{SR}/CH_4 = 2.87.

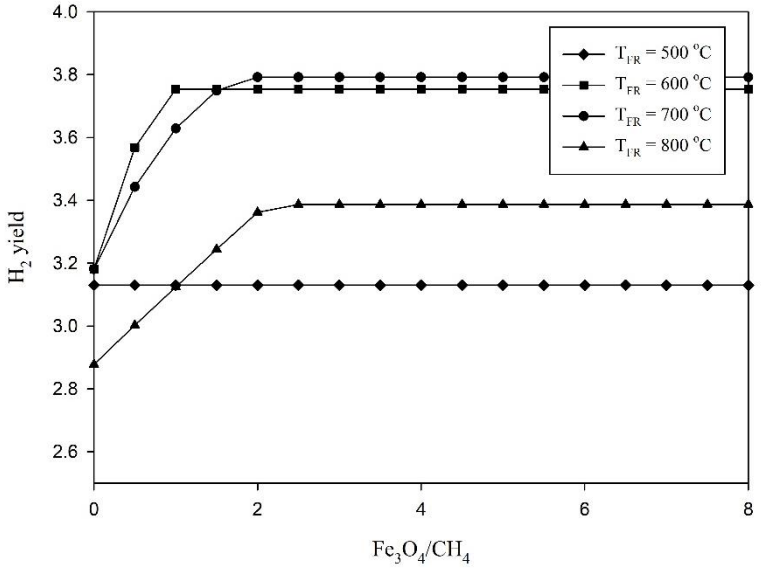

Figure 5.6 The total H_2 yield as a function of Fe_3O_4/CH_4 and T_{FR} at T_{SR} = 500 °C, S_{FR}/CH_4 = 2.2, CaO/CH_4 = 1.66, and S_{SR}/CH_4 = 2.87.

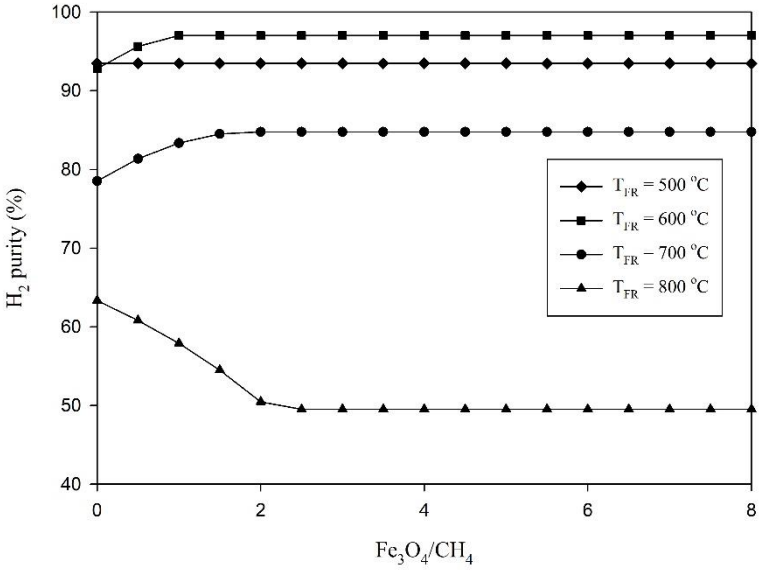

Figure 5.7 The H_2 purity as a function of Fe_3O_4/CH_4 and T_{FR} at T_{SR} = 500 °C, S_{FR}/CH_4 = 2.2, CaO/CH_4 = 1.66, and S_{SR}/CH_4 = 2.87.

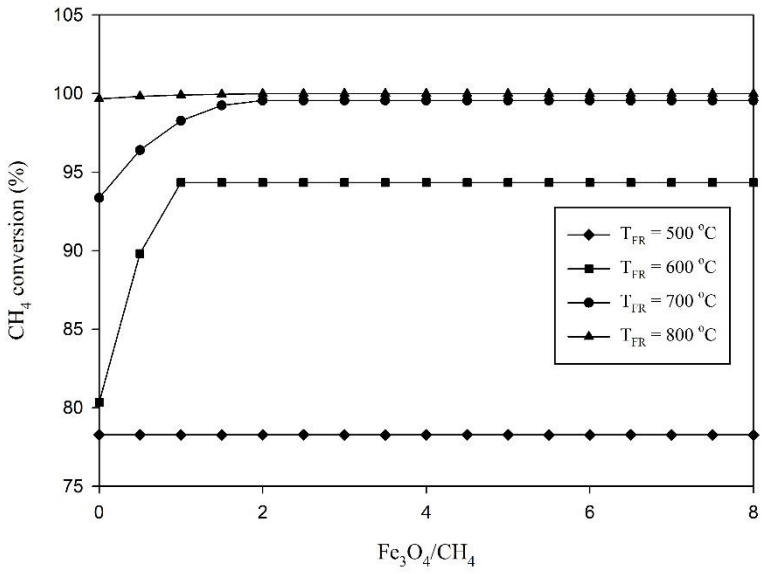

Figure 5.8 The CH_4 conversion as a function of Fe_3O_4/CH_4 and T_{FR} at T_{SR} = 500 °C, S_{FR}/CH_4 = 2.2, CaO/CH_4 = 1.66, and S_{SR}/CH_4 = 2.87.

5.1.3 Effect of the CaO to methane molar ratio

Figures 5.9–5.12 show the effect of the CaO/CH_4 molar ratio in the 0–8 range on the H_2 yield in the FR and SR, total H_2 yield, H_2 purity in FR, and CH_4 conversion, respectively, when the operating FR temperatures were in the 500–800 °C range, the SR temperature was 500 °C, and the S_{FR}/CH_4, Fe_3O_4/CH_4, and S_{SR}/CH_4 molar ratios were 2.2, 1, and 2.87 respectively. The results showed that when the FR temperature was 800 °C, increasing the CaO/CH_4 molar ratio had no effect on the system, as seen in Figures 5.9–5.12. At high FR temperatures, the carbonation reaction (Eq. (3.3)) was not favored; thus CO_2 was not captured by CaO and the system was not affected by adding CaO to it. At the FR temperature is in the range of 500-700 °C, increasing the CaO/CH_4 molar ratio increased the H_2 yield in the FR, as shown in Figure 5.9. By increasing the CaO/CH_4 molar ratio at low temperatures, CO_2 could be captured by CaO via the carbonation reaction (Eq. (3.3)) resulting in enhancing the production of H_2 via the water-gas shift (Eq. (3.2)) and SMR (Eq. (3.1)) reactions. When the FR temperature was increased, the H_2 yield in the FR decreased. However, the maximum total H_2 yield could be obtained when the FR temperature was 600 °C, as shown in Figure 5.10. This

was due to Fe_3O_4 not being able to react with CH_4 to form $Fe_{0.947}O$ by partial (Eq. (3.4)) or complete oxidation (Eq. (3.5)) for a FR temperature of 500 °C and in a steam-enriched environment, since $Fe_{0.947}O$ could react with H_2O to form H_2 at low temperature via the steam-iron reaction (Eq. (6)). The oxidizing and reducing reactivities of iron oxide are average (K. Svoboda *et al.*, 2007). Metal oxides such as manganese oxide (MnO) are very difficult to reduce but oxidizing metallic Mn is an easy process, while NiO can be very easily reduced and oxidizing Ni is very difficult. The oxidizing and reducing reactivities of iron oxide are intermediate between MnO and NiO; therefore iron oxide is sensitive to both oxidizing agents (such as H_2O and CO_2) and reducing agents (such as CH_4, H_2, and CO). Thus, at a FR temperature of 500 °C, $Fe_{0.947}O$ cannot form in the FR, because of the absence of a reactant which could react with steam in the SR to generate high-purity H_2. Therefore, the total H_2 yield was lower at the FR temperature of 500 °C than at 600 °C.

The H_2 purity is found to increase as CaO/CH_4 molar ratio increases when the FR temperature is raised from 500-700 °C, as shown in Figure 5.11. The maximum H_2 purity in the FR, which was 97.01%, while the H_2 yield in the FR and total H_2 yield of 3.04 and 3.75, respectively, could be obtained at the FR temperature of 600 °C and CaO/CH_4 molar ratio of 1.58. Although, the maximum H_2 yield in the FR could be obtained when the FR temperature was 500 °C. At this condition the CH_4 conversion is lower than that at FR temperature of 600 °C, as shown in Figure 5.12, resulting in the highest amount of CH_4 in the gaseous product stream. Even though high CH_4 conversion could be obtained at high FR temperatures (above 600 °C), the H_2 yield in the FR and amount of CO_2 captured were lower than when the FR temperature was 600 °C resulting in the highest amount of CO_2 and lowest H_2 purity in the FR in the gaseous product stream.

The suitable FR operating temperature and CaO/CH_4 molar ratio were determined by considering the highest H_2 yield in the FR and total H_2 yield with the highest H_2 purity in the FR. Capturing CO_2 by CaO in the carbonation reaction (Eq. (3.3)) was favored at low temperature and high CaO/CH_4 molar ratio, but the reaction rate at low temperature was lower than at high temperature, thus requiring large equipment size. The suitable CaO/CH_4 molar ratio when the FR temperature was 610

°C at 1 atm was 1.66. At this condition, H_2 yield in the FR, total H_2 yield, and H_2 purity in the FR of 2.98, 3.8, and 97.01%, respectively, could be obtained.

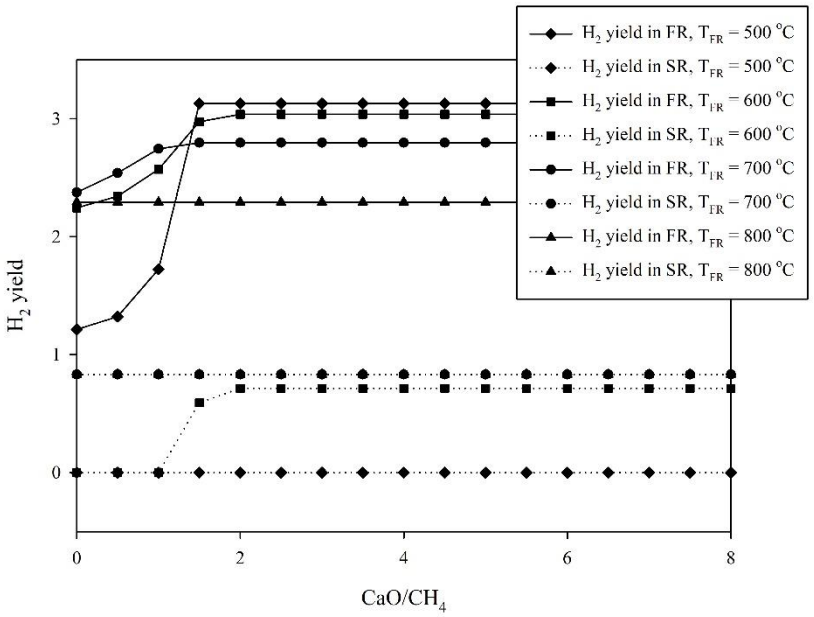

Figure 5.9 The H_2 yield in FR and SR as a function of CaO/CH_4 and T_{FR} at T_{SR} = 500 °C, S_{FR}/CH_4 = 2.2, Fe_3O_4/CH_4 = 1, and S_{SR}/CH_4 = 2.87.

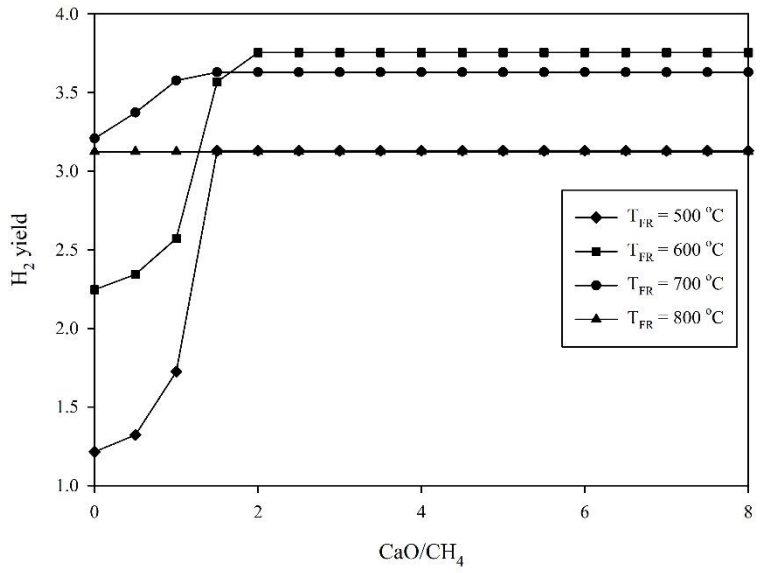

Figure 5.10 The total H_2 yield as a function of CaO/CH_4 and T_{FR} at T_{SR} = 500 °C, S_{FR}/CH_4 = 2.2, Fe_3O_4/CH_4 = 1, and S_{SR}/CH_4 = 2.87.

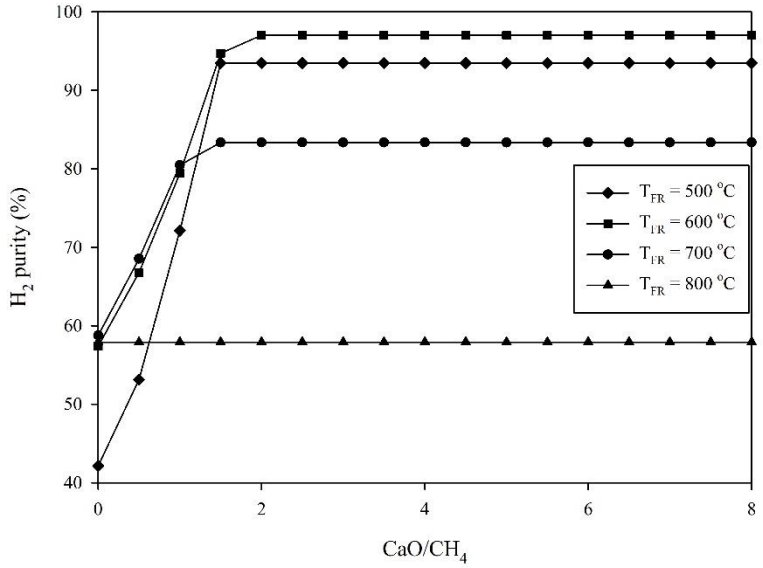

Figure 5.11 The H_2 purity as a function of CaO/CH_4 and T_{FR} at T_{SR} = 500 °C, S_{FR}/CH_4 = 2.2, Fe_3O_4/CH_4 = 1, and S_{SR}/CH_4 = 2.87.

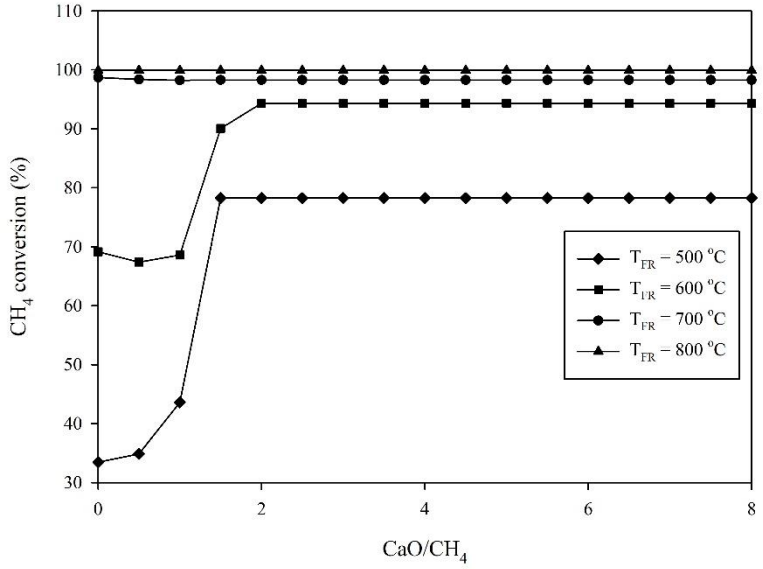

Figure 5.12 The CH_4 conversion as a function of CaO/CH_4 and T_{FR} at T_{SR} = 500 °C, S_{FR}/CH_4 = 2.2, Fe_3O_4/CH_4 = 1, and S_{SR}/CH_4 = 2.87.

5.1.4 Effects of the steam feed SR to methane molar ratio and SR temperature

Figures 5.13–5.16 show the effect of the S_{FR}/CH_4 molar ratio in the 0–8 range on the H_2 yield in the SR, H_2O conversion, H_2 purity in the SR, and CO concentration, respectively, in the 400–800 °C operating SR temperature range, for a FR temperature of 600 °C, and S_{FR}/CH_4, Fe_3O_4/CH_4, and CaO/CH_4 molar ratios of 2.2, 1, and 1.66 respectively. The results showed that increasing the S_{SR}/CH_4 molar ratio increased the H_2 yield in the SR significantly in the earliest stage, then the H_2 yield in the SR only slightly increased, as shown in Figure 5.13. At the SR temperatures of 400, 500, 600, and 700 °C, increasing the S_{SR}/CH_4 molar ratio affected the H_2 yield in the SR in two stages. During the first stage, the rapid increase in the H_2 amount produced by the reaction between $Fe_{0.947}O$ and steam via the steam-iron reaction (Eq. (3.6)) resulted in the highest conversion of H_2O, as shown in Figure 5.14. When $Fe_{0.947}O$ was completely formed from Fe_3O_4, the process advanced to the second stage. In the second stage, steam reacted with CO via the water-gas shift reaction (Eq. (3.2)) resulting in increasing the amount of CO_2 while the H_2 yield in the SR was slightly increased. H_2O conversion gradually decreased. At the SR temperature of 800 °C, increasing the S_{SR}/CH_4 molar ratio affected the H_2 yield in SR in three stages. The first stage was the reaction between $Fe_{0.947}O$ and steam similar to the reaction at low SR temperatures. During the second stage, the water-gas shift (Eq. (3.2)) and calcination (Eq. (3.8)) reactions occurred. The amount of CO_2 was higher at higher temperatures due to the calcination reaction occurring during this stage. Subsequently, the system progressed to the last stage where only the water-gas shift reaction (Eq. (3.2)) occurred. In addition, it was found that increasing the SR temperature decreased the H_2 yield in the SR due to the steam-iron (Eq. (3.6)) and water-gas shift (Eq. (3.2)) reaction being unfavored and resulting in low H_2O conversion.

At the SR temperatures of 400, 500, 600, and 700 °C, H_2 purity in the SR was constant in the earliest stage, and then decreased as the S_{SR}/CH_4 molar ratio increased, as shown in Figure 5.15. In the earliest stage, the composition of the gaseous product was determined by the equilibrium of the gas-solid reactions (Eq. (3.6) – (3.8)); thus, the gaseous composition was constant. As the S_{SR}/CH_4 molar ratio further increased, $Fe_{0.947}O$ was completely converted to Fe_3O_4 and H_2 purity decreased due to the

increasing amount of CO_2 from the water-gas shift (Eq. (3.2)) and calcination (Eq. (3.8)) reactions. When the SR temperature was 800 °C, H_2 purity in the SR was constant in the earliest stage due to the equilibrium of the gas-solid reaction, and then increased via the water-gas shift reaction (Eq. (3.2)) due to the high amount of CO and CO_2 generated in the complete calcination of $CaCO_3$. In addition, it was found that increasing the SR temperature decreased H_2 purity in the SR due to the calcination reaction (Eq. (3.8)) being favored by the high temperature. The H_2 purity and yield in the SR of 99.92% and 0.71, respectively, can be obtained when the SR temperature was 500 °C and S_{SR}/CH_4 molar ratio 2.87.

CO concentration is very important for H_2 used in an application such as LT-PEMFC. Typically, CO concentration in the H_2 feed for LT-PEMFC must be lower than 20 ppm (Bhatia and Wang, 2004). Thus, the effect of CO concentration in high-purity H_2 was studied in this work. The results showed that increasing the S_{SR}/CH_4 molar ratio decreased the CO concentration for all temperature ranges, as shown in Figure 5.16. That occurred because the water-gas shift reaction (Eq. (3.2)) could be performed in the enriching steam environment. In addition, increasing the temperature increased CO concentration due to the calcination of $CaCO_3$. Although low CO concentrations can be achieved at the lowest temperature (i.e., 400 °C) and highest S_{SR}/CH_4 molar ratio (above 15 at T_{SR} = 500 °C), the low reaction rate, large equipment size, and high cost of steam consumption are significant concerns for these operating conditions. Another way to achieve low CO concentrations is to use a high operating pressure. CO concentration is decreased by increasing the pressure, as shown in Figure 5.17. CO concentrations lower than 20 ppm at the SR temperature of 500 °C could be obtained when the pressure was 2 atm and the S_{SR}/CH_4 molar ratio 6.75.

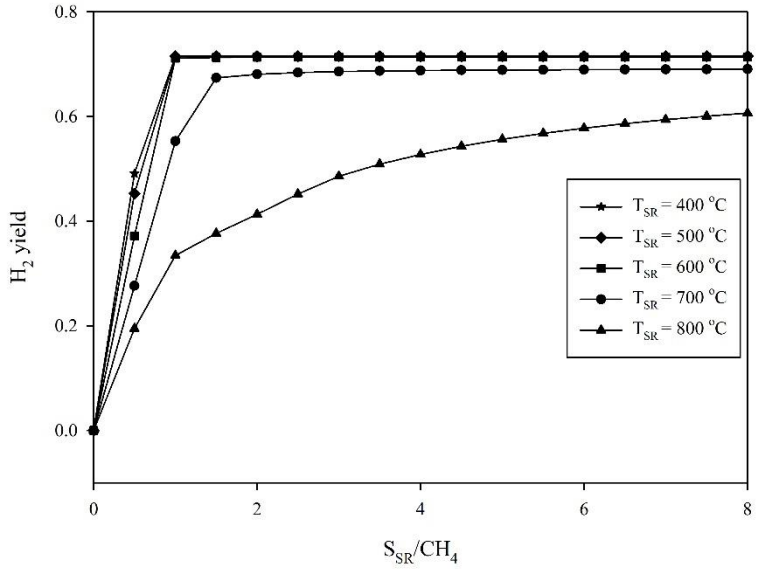

Figure 5.13 The H_2 yield in SR as a function of S_{SR}/CH_4 and T_{SR} at T_{FR} = 600 °C, S_{FR}/CH_4 = 2.2, Fe_3O_4/CH_4 = 1, and CaO/CH_4 = 1.66.

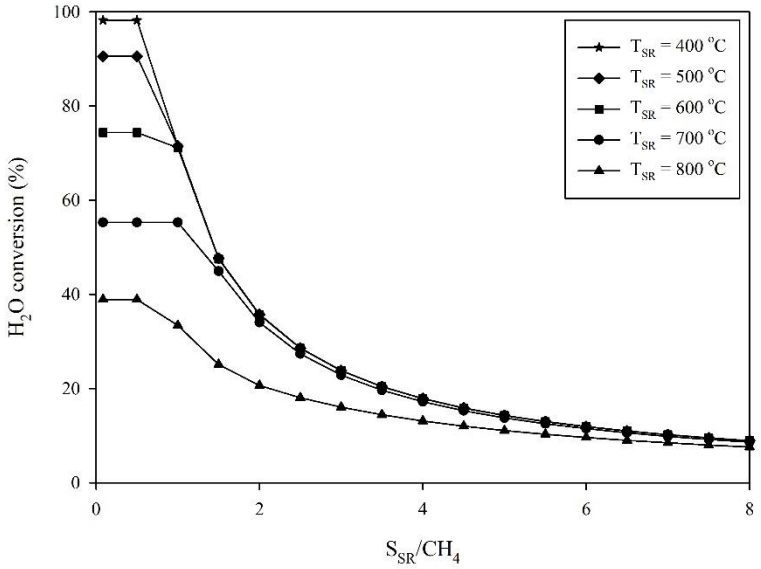

Figure 5.14 The H_2O conversion in SR as a function of S_{SR}/CH_4 and T_{SR} at T_{FR} = 600 °C, S_{FR}/CH_4 = 2.2, Fe_3O_4/CH_4 = 1, and CaO/CH_4 = 1.66.

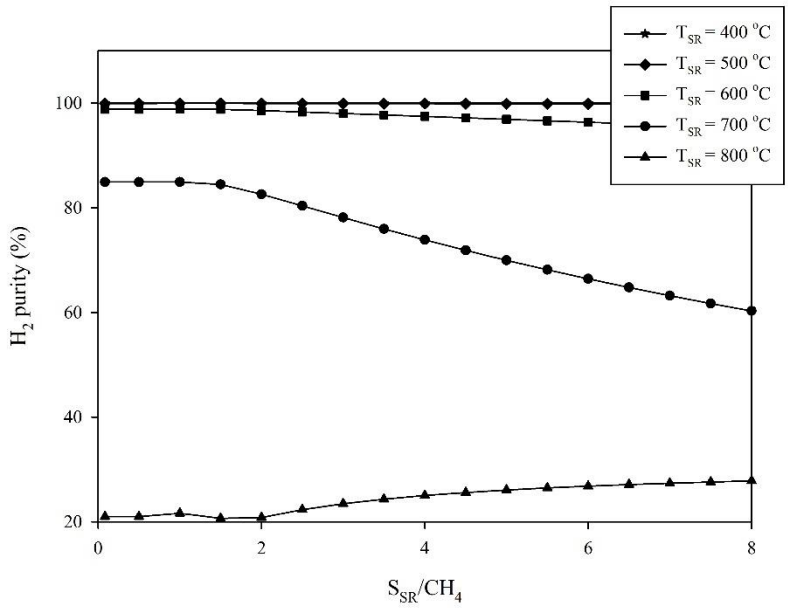

Figure 5.15 The H_2 purity in SR as a function of S_{SR}/CH_4 and T_{SR} at T_{FR} = 600 °C, S_{FR}/CH_4 = 2.2, Fe_3O_4/CH_4 = 1, and CaO/CH_4 = 1.66.

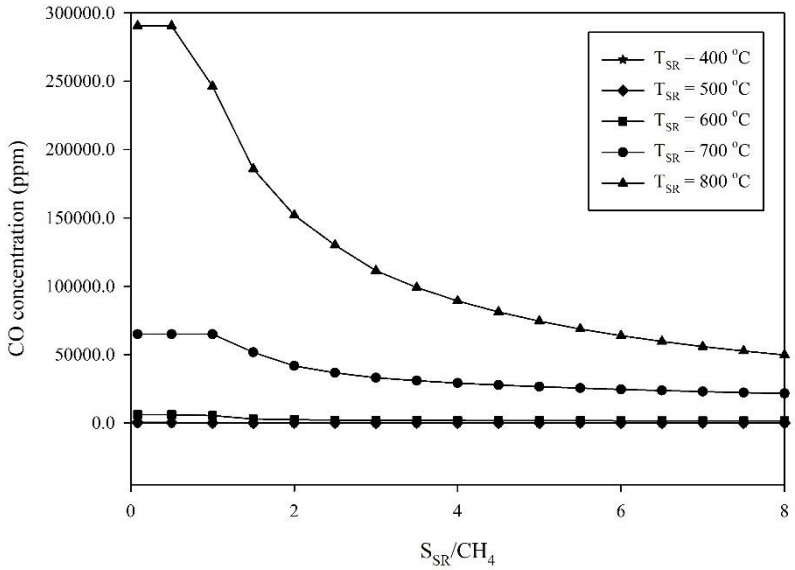

Figure 5.16 The CO molar concentration in SR as a function of S_{SR}/CH_4 and T_{SR} at T_{FR} = 600 °C, S_{FR}/CH_4 = 2.2, Fe_3O_4/CH_4 = 1, and CaO/CH_4 = 1.66.

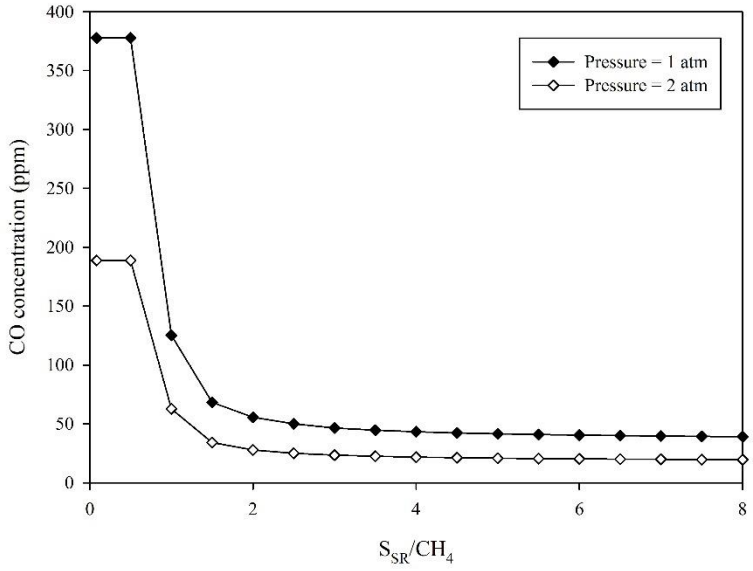

Figure 5.17 The CO molar concentration in SR as a function of S_{SR}/CH_4 and pressure at T_{FR} = 600 ºC, T_{SR} = 500 ºC, S_{FR}/CH_4 = 2.2, Fe_3O_4/CH_4 = 1, and CaO/CH_4 = 1.66.

5.1.5 Effect of the CO_2 molar concentration in biogas feed

Figures 5.18 and 5.19 show the effect of the molar concentration of CO_2 in the 0–90 % range in the biogas feed on H_2 yield and purity in the FR and SR, respectively for the operating SR temperature of 500 °C, FR temperature of 600 °C, and S_{SR}/CH_4, S_{FR}/CH_4, Fe_3O_4/CH_4, and CaO/CH_4 molar ratios of 2.87, 2.2, 1 and 1.66, respectively. The results showed that increasing the $\%CO_2$ had a negative effect on the system. Both H_2 yield and purity were constant when $\%CO_2$ was in the 0–40 % range due to the equilibrium of the gas-solid reaction in the presence of an excess amount of CaO. For the 0–40% range of $\%CO_2$, the CaO/CH_4 molar ratio was fixed at 1.66 while the CaO to carbon (CaO/C) molar ratio was higher than 1; thus, a high amount of CO_2 in the FR could be captured by CaO to promote the water-gas shift (Eq. (3.2)) and SMR (Eq. (3.1)) reactions. By contrast, for the 40–90 % range of $\%CO_2$, the CaO/C molar ratio was less than 1, thus the small amount of CO_2 in the FR could be effectively captured to decrease the H_2 yield and purity in the FR. CH_4 cannot react with Fe_3O_4 to form $Fe_{0.947}O$ in the enriched CO_2 and steam environment due to the limited equilibrium of

the reactions (Eq. (3.6)) and (Eq. (3.7)). Therefore, H_2 yield in the SR was decreased by increasing the $\%CO_2$ in the 40–90% range.

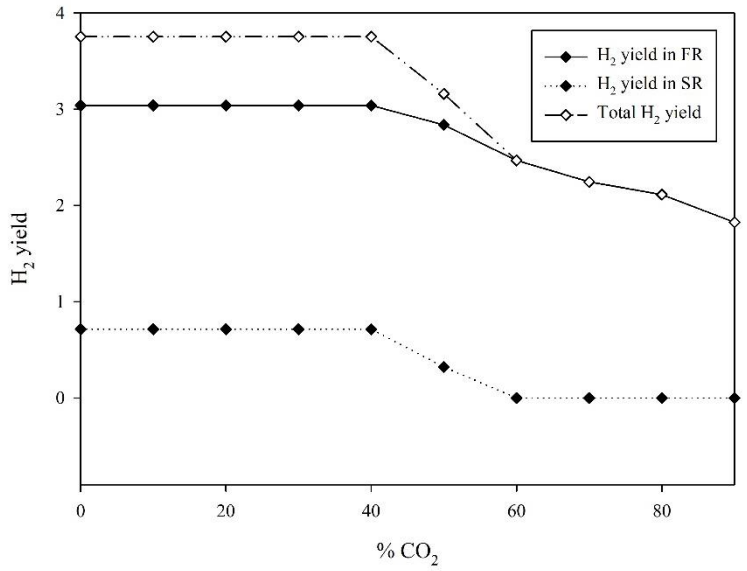

Figure 5.18 The H_2 yield in FR and SR, and the total H_2 yield as a function of $\%CO_2$ at T_{SR} = 500 °C, T_{FR} = 600 °C, S_{FR}/CH_4 = 2.2, Fe_3O_4/CH_4 = 1, CaO/CH_4 = 1.66, and S_{SR}/CH_4 = 2.87.

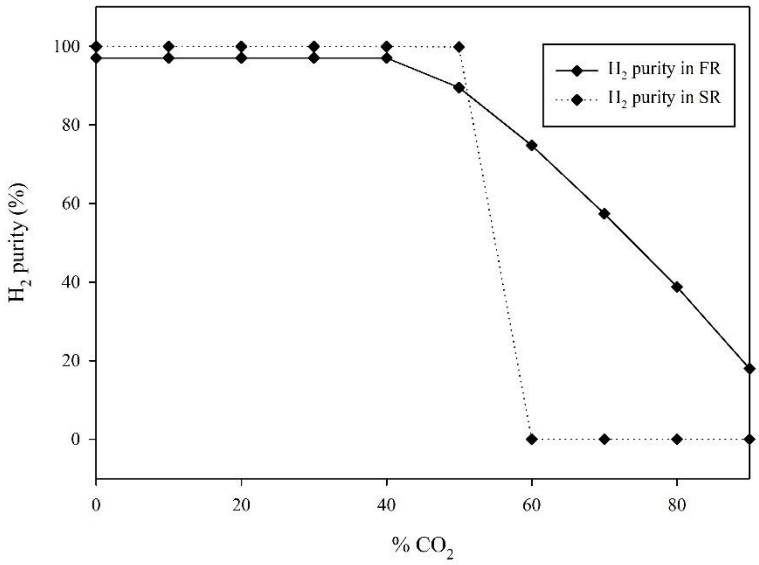

Figure 5.19 The H_2 purity in FR and SR as a function of $\%CO_2$ at T_{SR} = 500 °C, T_{FR} = 600 °C, S_{FR}/CH_4 = 2.2, Fe_3O_4/CH_4 = 1, CaO/CH_4 = 1.66, and S_{SR}/CH_4 = 2.87.

5.1.6 Energy demand

To more understand the SECLR-WS process, the simplified heat calculation is performed. The heat duty for each reactor is calculated by $Q(heat\ duty) = \sum_{out} \dot{n}_i h_i - \sum_{in} \dot{n}_i h_i$, where $\dot{n}_i$ and h_i are molar flow rate and specific molar enthalpy of component *i*. For the net heat duty or total heat demand of reactor is calculated by $Q_{total,reactor} = Q_{FR} + Q_{SR} + Q_{calcinator}$. The negative and positive sign of *Q* is represented the nature of the process in terms of exothermic and endothermic processes, respectively.

Figure 5.20 shows the effect of the S_{FR}/CH_4 and Fe_3O_4/CH_4 molar ratios on the energy demand of the FR for each temperature. It was found that the exothermic conditions in the FR could be obtained at low FR temperatures. At low FR temperatures, the water-gas shift (Eq. (3.2)) and carbonation (Eq. (3.3)) reactions, which are exothermic, were favored; thus, the heat demand in the FR was decreased. The high S_{FR}/CH_4 molar ratio had the tendency to increase heat duty in the FR while the high Fe_3O_4/CH_4 molar ratio had the tendency to decrease heat duty in the FR. Since the high amount of steam can react with CH_4 via the endothermic SMR reaction (Eq. (3.1)) and some amount of heat was used to heat up the steam, the heat demand in the FR was high when the process was operated at high S_{FR}/CH_4 molar ratios. By contrast, when the process was operated at high Fe_3O_4/CH_4 molar ratios, the large amount of the high-temperature circulating solid could supply heat to the FR; thus, the heat demand in the FR was decreased. Figure 5.21 shows the effect of the S_{FR}/CH_4 and Fe_3O_4/CH_4 molar ratios on the total energy demand for each FR temperature. The results showed that increasing the S_{FR}/CH_4 molar ratio increased the total heat demand, while the effect of the Fe_3O_4/CH_4 molar ratio on the total heat demand was insignificant. This was due to the total heat demand mainly depending on the heat duty of the calcinator, which increased when the amount of $CaCO_3$ increased by increasing the S_{FR}/CH_4 molar ratio.

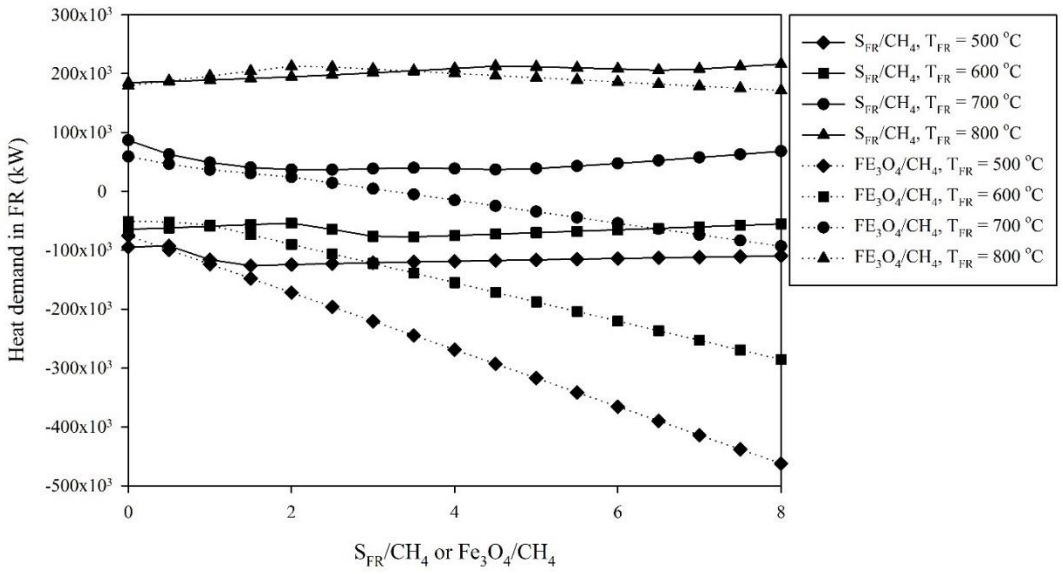

Figure 5.20 The heat demand in FR as a function of S_{FR}/CH_4 molar ratio (Fe_3O_4/CH_4 = 1), Fe_3O_4/CH_4 molar ratio (S_{FR}/CH_4 = 2.2), and T_{FR} at T_{SR} = 500 ºC, CaO/CH_4 = 1.66, and S_{SR}/CH_4 = 2.87.

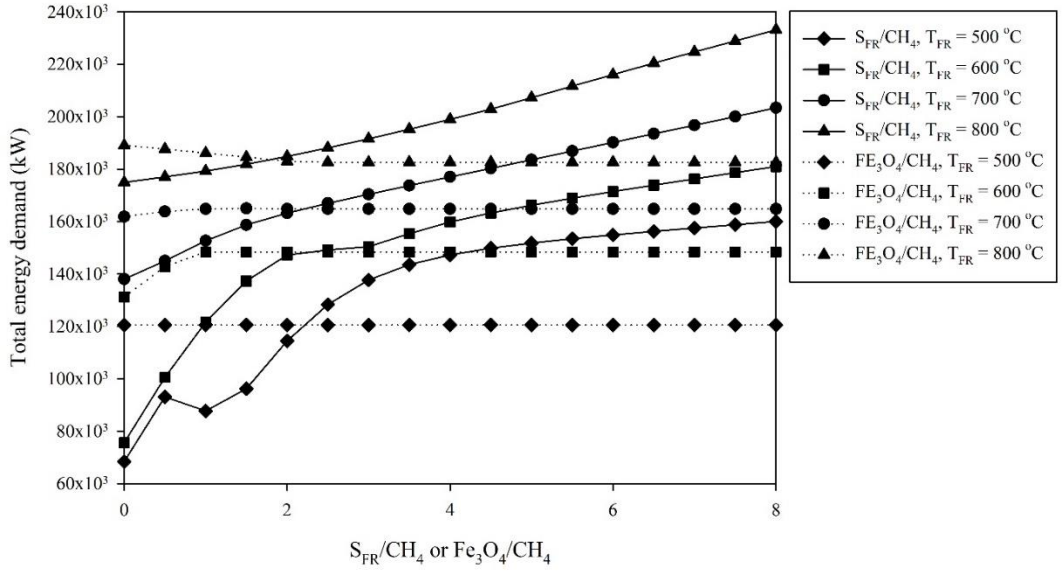

Figure 5.21 The total heat demand as a function of S_{FR}/CH_4 molar ratio (Fe_3O_4/CH_4 = 1), Fe_3O_4/CH_4 molar ratio (S_{FR}/CH_4 = 2.2), and T_{FR} at T_{SR} = 500 ºC, CaO/CH_4 = 1.66, and S_{SR}/CH_4 = 2.87.

5.2 Optimization

After the sensitivity analysis carried out, the optimization of the SECLR-WS process can be performed. The decision variable is chosen by considering the operating parameter that influence on the process performance. The operating parameters, which are manipulated to achieve the objective function, are T_{FR}, S_{FR}/CH_4 molar ratio, S_{SR}/CH_4 molar ratio, CaO/CH_4 molar ratio, and Fe_3O_4/CH_4 molar ratio. The total hydrogen yield and energy demand strongly depends on the T_{FR}, S_{FR}/CH_4 molar ratio, CaO/CH_4 molar ratio, and Fe_3O_4/CH_4 molar ratio, while the S_{SR}/CH_4 molar ratio is strongly impact on the CO concentration of high purity hydrogen product stream. The SR temperature is fixed at 500 ^oC due to the appropriated of kinetic and thermodynamic conversion (Cormos, 2010; Zeng *et al.*, 2012). While the calcinator temperature is fixed at 860 ^oC which is the condition that $CaCO_3$ can completely converted to CaO. The 1 kmol/sec of biogas, which compose 60 mol% of CH_4 and 40 mol% of CO_2 is a considered feedstock. All inlet streams are heated from 25 ^oC to 400 ^oC before entering the reactor. The system is operated at atmospheric pressure. The flowsheet for formulated optimization problems is shown in Figure 5.22. The optimization problem was formulated separately in three cases. In the first case (CASEI), the objective function is set by aiming at maximization of the total hydrogen production (or total hydrogen yield) represented in Eq. (4.7). In the second and third case (CASEII and CASEIII, respectively), the objective functions aim to maximize thermal efficiency (η_{th}) of the system following Eq. (3.20). The lower heating value of H_2 and CH_4 are 244 and 802.34 MJ/kmol, respectively (Perry and Green, 2008). The total heat demand (Q_{total}) in this case can be specified by Eq. (5.2):

$$Q_{total} = Q_{FR} + Q_{SR} + Q_{CAL} + Q_{H1} + Q_{H2} + Q_{H3} \tag{5.2}$$

where Q_{FR}, Q_{SR}, and Q_{CAL} are the heat duty of FR, SR, and CAL, respectively. Q_{H1}, Q_{H2}, and Q_{H3} are the heat duty of HEATER1, HEATER2, and HEATER3, respectively.

The constraints, which are applied in all case, are the hydrogen purity of H_2-rich syngas and high purity hydrogen stream are greater than or equal to 97 % and 99.9 %, respectively, which are the maximum value from the sensitivity analysis. Additionally,

in the third case, the production rate in high purity hydrogen is greater than 0.4 kmol/sec, which it is applied as a constraint, based on about 50 MW stationary electricity production by 50 % performance of PEMFC for parasitic energy in the process (pump and compressor). The power of generated can be estimated by Eq. (5.2):

$$P_e = \eta_{el} \times (LHV_{H_2} \times \dot{N}_{H_2, high\ purity\ H_2\ stream}) \tag{5.2}$$

where P_e is electric power. η_{el} is electric efficiency of fuel cell and $\dot{N}_{H_2, high\ purity\ H_2\ stream}$ is the molar flow rate of high purity H_2 stream.

The summary of objective function and constraint in all optimization case are shown in Table 5.1. The optimization problem of a system can be solved by using provided default method in Aspen Plus, sequential quadratic programming (SQP). SQP is an iterative method for the solution of constrained nonlinear optimization problems. The advantage of the SQP is the ability to handle the of any degree of non-linearity also non-linearity in constraints (Poku *et al.*, 2004).

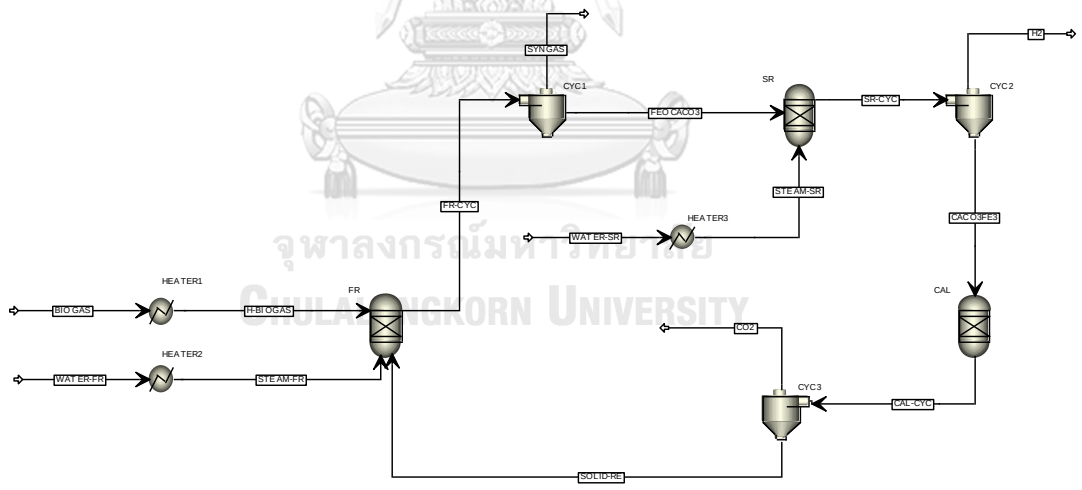

Figure 5.22 Simulation flowsheet of SECLR-WS process for optimization problem.

Table 5.1 Objective function and constraint in optimization problem

Parameter	CASEI	CASEII	CASEIII
Objective function	Maximum total H_2 yield	Maximum thermal efficiency (η_{th})	Maximum thermal efficiency (η_{th})
Constraint 1. H_2 purity in syngas stream ≥ 97 %	√	√	√
Constraint 2. H_2 purity in high purity H_2 stream ≥ 99.9 %	√	√	√
Constraint 3. H_2 flow rate in high purity H_2 stream ≥ 0.4 kmol sec^{-1}			√

The optimization results are shown in Table 5.2. The optimization in CASEI, which uses the maximum total H_2 yield as objective function, shows the highest total yield value of 3.90, without needing to enter steam into FR, while it is necessary to feed steam into the SR in large quantities, with the S_{SR}/CH_4 molar ratio of 8.73 at optimum operating conditions. The operation of this condition can produce hydrogen from both FR and SR, according to the constraints that hydrogen purity of H_2-rich syngas and high purity H_2 stream must be greater than 97 % and 99.9 %, respectively. However, the large amount of steam supplied to the SR will cause the large amount of energy consumed to generating steam. In addition, the high amount of iron oxide is required. For CASEI, the high value of Fe_3O_4/CH_4 molar ratio of 3.34 must be needed. A large amount of iron oxide feed will affect the size of the reactor, which may be large as well. Compared to CASEI and CASEII, the CASEII uses the maximum thermal efficiency as objective function. The objective function in CASEII considers the heat required in the process. In CASEII, at the optimal operating conditions, the total H_2 yield was less than in CASEI, the total H_2 yield in CASEII is 3.73. The S_{FR}/CH_4 molar ratio at optimal condition of CASEII is 3.19 which higher than the S_{SR}/CH_4 molar ratio, which is 0.01. It can be seen that, in CASEII, the system can be operated according to the objective

function by feeding large quantities of steam to the FR and feeding steam into the SR in small quantities, which is different from CASEI. Because the high amount of steam entering the SR to achieve high production rate of H_2 affects the amount of energy required in the system. The energy required in the system is high when the high amount of steam feed to SR. Thus, to achieve the high thermal efficiency, the H_2 should be mainly produced from FR. Therefore, the CASEI has lower thermal efficiency than CASEII. The thermal efficiency of CASEI is 59.89 % while CASEII is 72.27 %. The Fe_3O_4/CH_4 molar ratio in CASEII is 0.07, which is lower than in CASEI because the system requires to minimize the complete oxidation reaction (Eq. (3.5)), which decrease the hydrogen product.

By comparing CASEI and CASEII, it was found that if the thermal efficiency of the system is high, the production rate of H_2 in high purity H_2 stream must be low. If the high amount of high purity H_2 is required, the thermal efficiency must be low. The appropriate objective function of the process is maximized thermal efficiency, because of the hydrogen production between two grades (H_2-rich syngas and high purity H_2 stream) is flexibility. The amount of hydrogen product in two streams can be adjusted by manipulating the three operating parameters, S_{FR}/CH_4, S_{SR}/CH_4, and Fe_3O_4/CH_4 molar ratios. When the large quantity of high purity H_2 are needed, the maximum thermal efficiency can be achieved by decreasing the S_{FR}/CH_4 molar ratio, and increasing the S_{SR}/CH_4 and Fe_3O_4/CH_4 molar ratio, as shown in CASEIII. In CASEIII, the objective function is to maximize the thermal efficiency by considering additional constraint which the production rate of high purity H_2 must be greater than 0.4 kmol/sec (which is equivalent to H_2 yield in SR of 0.66). The amount of high purity hydrogen of 0.4 kmol/sec can be used in PEMFC for electric production of about 50 MW, when the PEMFC has 50 % electric efficiency. When comparing CASEII and CASEIII, it was found that the S_{SR}/CH_4 and Fe_3O_4/CH_4 molar ratios of CASEIII is higher than CASEII, and the S_{FR}/CH_4 molar ratio of CASEIII is lower than CASEII.

Table 5.2 Simulation results of SECLR-WS process

Parameters	CASEI	CASEII	CASEIII
Total H_2 yield	3.90	3.73	3.77
η_{th} (%)	59.89	72.27	68.42
H_2 yield in FR	1.41	3.72	3.11
H_2 yield in SR	2.49	0.01	0.66
T_{FR} (^oC)	611.8	605.7	606.8
S_{FR}/CH_4 molar ratio	0	3.19	2.35
S_{SR}/CH_4 molar ratio	8.73	0.04	2.33
Fe_3O_4/CH_4 molar ratio	3.34	0.07	0.92
CaO/CH_4 molar ratio	2.17	2.15	1.94

CHAPTER VI
COMPARISON OF PERFORMANCE ON THE NOVEL CHEMICAL LOOPING PROCESS FOR HYDROGEN PRODUCTION

Comparison of sorption-enhanced chemical looping reforming and water splitting process with sorption-enhanced chemical looping reforming process and chemical looping water splitting process is presented in this chapter. The SECLR-WS process is a integrated of SECLR and CLWS process. The SECLR and CLWS processes offer different qualities and quantities of hydrogen. The SECLR can produce the H_2-rich syngas with 98 % H_2 purity and hydrogen yield of 3.3 mol H_2/mol CH_4, while the CLWS can produce the high H_2 purity with 99.9 % H_2 purity and hydrogen yield of 2.68 mol H_2/mol CH_4. However, both SECLR and CLWS processes can capture 99% CO_2. The performance of the systems in terms of hydrogen production and hydrogen purity is considered. In addition, the description of SECLR and CLWS process is given in this chapter.

6.1 Detail of the sorption-enhanced chemical looping reforming (SECLR) process

Process simulation flowsheet of the SECLR process, which is simulated based on Rydén and Ramos (2012) work, is shown in Figure 6.1. In this study, for the comparison of SECLR-WS and SECLR process, the SECLR process was simulated by Aspen Plus program using the Redlich-Kwong-Soave equation of state with Boston-Mathias modification (ESRKS) for calculation of thermodynamic properties. The SECLR process for hydrogen production from natural gas uses the NiO as an oxygen carrier and CaO as a CO_2 adsorbent. This process composes of three reactors, which are FR, calcinator (CAL), and AR. Firstly, the natural gas (C-CH4), which is assumed to compose only CH_4, and water (WATER-FR) are fed to the HEATER1 and HEATER2, respectively, for increase the temperature of natural gas and water from 25 ^oC to 321 ^oC before they are fed to FR. The NiO and CaO in S-FR stream was fed to

FR. In the FR, CH_4 reacts with H_2O and NiO by the steam-methane reforming reaction and partial oxidation of CH_4, respectively. The generated CO_2 from the reaction between CH_4 and NiO is captured by CaO, thus the water-gas shift reaction is promoted. After reacting, the NiO and CaO are transformed to Ni and $CaCO_3$. Then, the mixer of gaseous product and solid from the FR (FR-CYC) are fed to the CYC1 for separating gas and solid. The main product of the FR is H_2-rich syngas (SYNGAS) stream. The solid from FR (S-CAL1) is fed to CAL in which the calcination is taken places to regenerate CaO. Then, the mixture of CO_2 gas and solid from CAL (CAL-CYC) is fed to the CYC2 for separating gas and solid. The main gaseous product from the CAL is CO_2 (CO2). The mixture of solids from CAL (Ni, NiO, and CaO) is split into two streams. The first stream (S-FR) is recycled to the FR to produce the hydrogen. Another solid stream (S-AR) is fed to the AR to regenerate the NiO by the oxidation reaction. The air (AIR) is fed to the HEATER3 to increase the temperature from 25 ^oC to 576 ^oC before entering the AR. The Ni is re-oxidized by O_2 in the air stream. The mixer of gaseous and solids from the AR is fed to CYC3 for separating gaseous and solid. The gas product from AR is the depleted air or N_2 (N2). The solid from the AR (S-CAL2) is fed back to CAL for a complete loop. This process can be operated under autothermal condition at 1 atm due to the highly exothermic reaction in AR can supply heat in the whole system. The purpose of the splitting SOLID stream from the CAL to FR and AR is to solve the heat balance of the process.

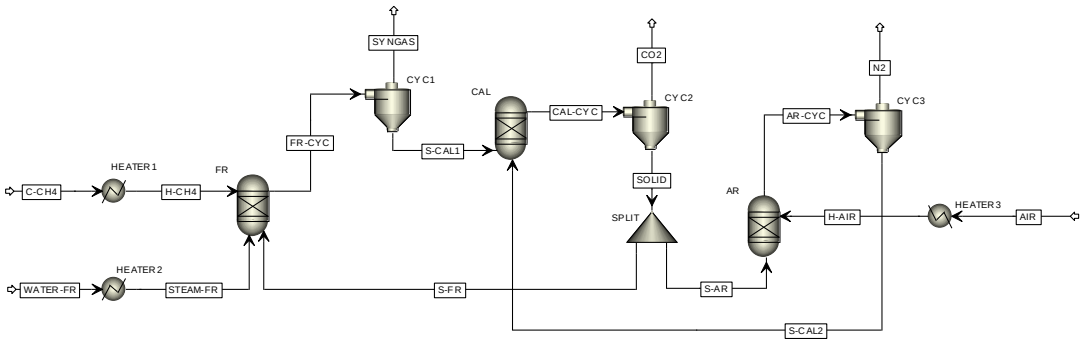

Figure 6.1 Process simulation flowsheet of SECLR process for comparison with SECLR-WS process.

6.2 Detail of the chemical looping water splitting (CLWS) process

Process simulation flowsheet of the SECLR process, which is simulated based on Edrisi *et al.* (2014) work, is shown in Figure 6.2. In this study, for the comparison of SECLR-WS and CLWS process, the CLWS process was simulated by Aspen Plus program using the Redlich-Kwong-Soave equation of state with Boston-Mathias modification (ESRKS) for calculation of thermodynamic properties. The CLWS process for hydrogen production from natural gas uses the three form of iron oxide as an oxygen carrier and $MgAl_2O_4$ as an inert supporting material. This process composes of three reactors, which are FR, SR, and AR. Firstly, the natural gas (C-CH4), which is assumed to compose only CH_4 is fed to the HEATER1 for heating the temperature of natural gas from 25 ^oC to 450 ^oC before entering to FR. The Fe_2O_3 in FE2O3 stream is fed to FR. In the FR, CH_4 reacts with Fe_2O_3 by complete oxidation of CH_4. The main gaseous product from the FR is CO_2 and H_2O (CO2+H2O). After reacting, the Fe_2O_3 is transformed to $Fe_{0.947}O$. Then, the mixer of gaseous product and solid from the FR (FR-CYC) are fed to the CYC1 for separating gas and solid. The solid from FR (FEO) is fed to the SR which the steam-iron reaction takes place to generate the pure H_2 product stream (H2). The water for feed to the SR (WATER-SR) is heated by HEATER2 from 25 ^oC to 400 ^oC. After the $Fe_{0.947}O$ react with the stream, the $Fe_{0.947}O$ is transformed to Fe_3O_4. Then, the mixture of gaseous and solid from SR (SR-CYC) is fed to the CYC2 for separating gas and solid. The solid from SR (FE3O4) is fed to the AR for regenerate by the oxidation reaction. The air (AIR) is fed to the HEATER3 for heating the temperature from 25 ^oC to 470 ^oC before entering the AR. The Fe_3O_4 is fully oxidized to Fe_2O_3 by O_2 in the air stream. The mixer of gaseous and solids from the AR is fed to CYC3 for separating gaseous and solid. The gas product from AR is the depleted air or N_2 (N2). The solid from the AR (FE2O3) is fed back to FR for a complete loop. This process can be operated under autothermal condition due to the highly exothermic reaction in AR can supply heat for the whole system.

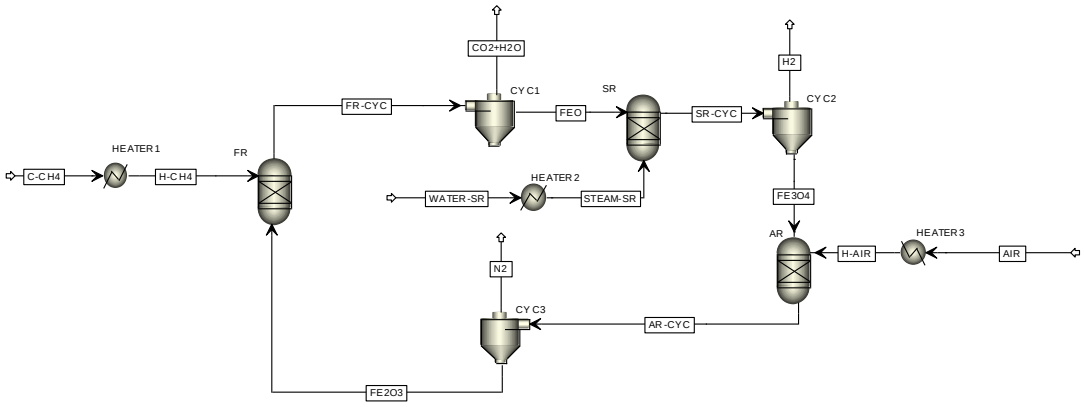

Figure 6.2 Process simulation flowsheet of CLWS process for comparison with SECLR-WS process.

6.3 Details of combined sorption-enhanced chemical looping reforming and water splitting (SECLR-WS) process

For the process performance comparison, the simulation of the SECLR-WS process for the production of hydrogen from natural gas was simulated by Aspen Plus program, as shown in Figure 6.3. The Redlich-Kwong-Soave equation of state with Boston-Mathias modification (ESRKS) is used for calculation of thermodynamic properties. The SECLR-WS process for hydrogen production from natural gas uses the two forms of the iron oxide as an oxygen carrier and CaO as a CO_2 adsorbent. This process composes of three reactors, which are FR, SR, and calcinator (CAL). Firstly, the natural gas (C-CH4), which is assumed to compose only CH_4, and water (WATER-FR) are fed to the HEATER1 and HEATER2, respectively, for heating the temperature of natural gas and water from 25 ^oC to 400 ^oC before entering to FR. The Fe_3O_4 and CaO in SOLID-RE stream was fed to FR. In the FR, CH_4 reacts with H_2O and Fe_3O_4 by the steam-methane reforming reaction and partial oxidation of CH_4, respectively. The generated CO_2 from the reaction between CH_4 and Fe_3O_4 was captured by CaO, thus the equilibrium of water-gas shift reaction is shifted to the product side. After reacting, the Fe_3O_4 and CaO are transformed to $Fe_{0.947}O$ and $CaCO_3$. Then, the mixer of gaseous product and solid from the FR (FR-CYC) are fed to the CYC1 for separating gas and solid. The main product in the process, which obtained from the FR, is H_2-rich

syngas in SYNGAS stream. The solid from FR (FEOCACO3) is fed to the SR which the steam-iron reaction is taken place to generate the high purity H_2 stream (H2). The water fed to the SR (WATER-SR) is heated by HEATER3 from 25 ºC to 400 ºC. After the $Fe_{0.947}O$ react with the stream, the $Fe_{0.947}O$ is transformed to Fe_3O_4. Then, the mixture of gaseous and solid from SR (SR-CYC) is fed to the CYC2 for separating gas and solid. The solid from SR (CACO3FE3) is fed to the CAL which the calcination is taken places to regenerate CaO. Then, the mixture of CO_2 gas and solid from CAL (CAL-CYC) is fed to the CYC3 for separating gas and solid. The main gaseous product from the CAL is CO_2 (CO2). Then, the solid stream from CAL (SOLID-RE) is recycled to the FR for complete process loop. This process is operated under isothermal and isobaric condition. The pressure of all process streams and all reactor is maintained at 1 atm.

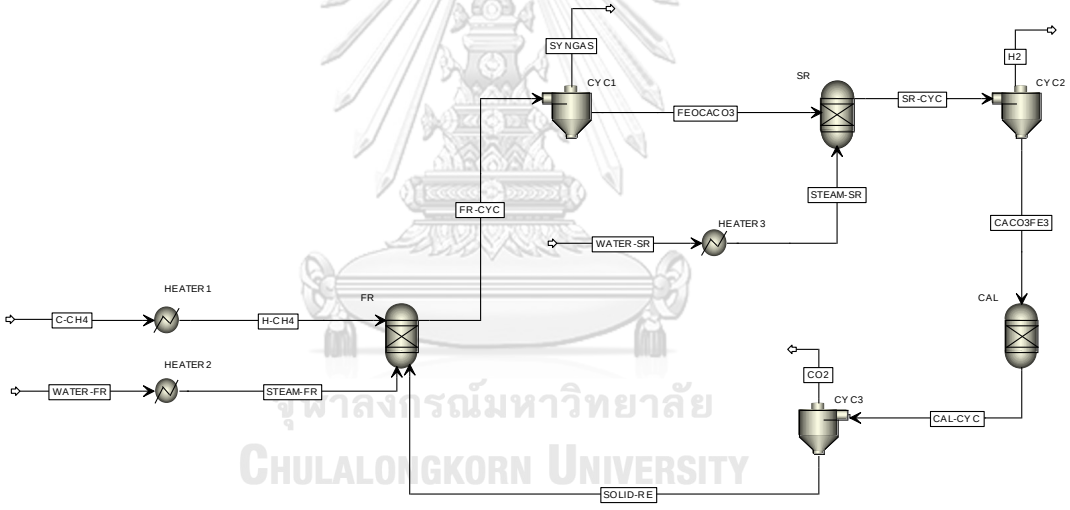

Figure 6.3 Process simulation flowsheet of SECLR-WS process for comparison with SECLR and CLWS process.

6.4 Hydrogen purity and thermal efficiency comparison of SECLR-WS with SECLR and CLWS process

Comparison of the hydrogen production efficiency of the SECLR-WS process with the SECLR and CLWS processes is shown in this section. In this study, the optimal operating condition of the SECLR and CLWS are based on the Rydén and

Ramos (2012) and Edrisi *et al.* (2014) work, respectively. The SECLR and CLWS can be operated in autothermal conditions while the SECLR-WS process operates under isothermal conditions by using external heating and cooling. The pressure of SECLR, SECLR-WS, and CLWS process are 1 atm. For the SECLR-WS process, the appropriate operating conditions are simulated in three cases, case 1 (CASE I-com). The objective is to produce the highest amount of hydrogen (maximum H_2 yield). Case 2 (CASEII-com) uses the objective function that aim to produce H_2 at maximum thermal efficiency (η_{th}). The last case (CASE III-com) uses the same objective equation as case 2 but the additional constraint, which is the flow rate of high purity H_2 stream must be greater than 0.4 kmol/sec, is applied. The operating conditions of all three processes are shown in Table 6.1, and the optimum operating conditions are shown in Table 6.2.

Table 6.1 Operating condition of all three processes.

Condition	SECLR	CLWS	SECLR-WS		
			CASEI-com	CASEII-com	CASEIII-com
Nominal feed stream condition					
CH4					
CH_4 flow rate (kmol sec^{-1})	1	1	1	1	1
Temperature (^oC)	25	25	25	25	25
Pressure (atm)	1	1	1	1	1
WATER-FR					
H_2O flow rate (kmol sec^{-1})	2.2	-	7.18	3.25	2.76
Temperature (^oC)	25	-	25	25	25
Pressure (atm)	1	-	1	1	1
WATER-SR					
H_2O flow rate (kmol sec^{-1})	-	6.55	4.62	0.049	1.39
Temperature (^oC)	-	25	25	25	25
Pressure (atm)	-	1	1	1	1

AIR (21 mol% O_2 79 mol% N_2)					
Air flow rate (kmol sec^{-1})	2.53	3.20	-	-	-
Temperature (^oC)	25	25	-	-	-
Pressure (atm)	1	1	-	-	-
Reactor temperature feed (^oC)					
H-CH4	321	450	400	400	400
STEAM-FR	321	-	400	400	400
STEAM-SR	-	400	400	400	400
H-AIR	576	470	-	-	-
Reactor condition					
FR					
Temperature (^oC)	580.8	722.5	500	609.1	610.8
Pressure (atm)	1	1	1	1	1
SR					
Temperature (^oC)	-	726.0	500	500	500
Pressure (atm)	-	1	1	1	1
AR					
Temperature (^oC)	1010.2	875.9	-	-	-
Pressure (atm)	1	1	-	-	-
CAL					
Temperature (^oC)	884.6	-	860	860	860
Pressure (atm)	1	-	1	1	1

Table 6.2 Simulation results for comparison of SECLR-WS with SECLR and CLWS process.

Parameters	**SECLR**	**CLWS**	**SECLR-WS**		
			CASEI-com	**CASEII-com**	**CASEIII-com**
SYNGAS stream					
H_2 yield	2.8115	-	3.9848	3.7324	3.3768
H_2 purity (drybasis)	98.46	-	99.85	97.01	97.00

H2 stream					
H_2 yield	-	2.6643	0	0.0133	0.4001
H_2 purity (drybasis)	-	99.99	0	99.92	99.93
Total H_2 yield	2.8115	2.6643	3.9848	3.7457	3.7769
Heat duty in reactor (kW)					
FR	0	0	-147487.4	-11609.3	10435.4
SR	-	0	17648.5	-45464.8	-63606.6
AR	0	0	-	-	-
CAL	0	-	383644.8	286734.5	286200.4
Heat duty in heater (kW)					
HEATER1	12888.5	20094.4	17190.6	17190.6	17190.6
HEATER2	119318.2	374286.5	410383.7	185718.2	158125.4
HEATER3	42599.1	43007.9	264207.8	2826.3	79954.9
Total heat demand	174805.9	434367.8	945588.1	435395.5	488300.2
η_{th} **(%)**	70.20	52.43	55.62	73.84	71.40

Figure 6.4 shows the total H_2 yield and thermal efficiency of different H_2 production processes, the H_2 yield results show that the SECLR-WS process operated by CASEI-com offer the highest hydrogen yield of 3.9848. In addition, the SECLR-WS process can produce higher amount of H_2 than SECLR and CLWS processes. Because the SECLR-WS process can produce hydrogen from both FR and SR. H_2 in FR can be produced by steam-methane reforming and partial oxidation of methane in a CaO environment, so the water-gas shift reaction can be occurred and the reaction is shifted forward. While H_2 in the SR is produced by the steam-iron reaction. Theoretically, the total hydrogen yield of the SECLR-WS is 4, which more than those of the SECLR and CLWS process. The highest hydrogen produced in CASEI-com is from feeding large amount of steam into FR, and the steam feed into the SR is not needed. Due to the large amount of steam entering FR at low temperatures, the water-gas shift reaction is improved. However, Fe_3O_4 cannot be converted to $Fe_{0.947}O$ in FR due to the enriched steam environment, resulting in the inability to produce high purity hydrogen in SR. In terms of hydrogen purity, the SECLR and CLWS processes produce pure hydrogen at 98.46 % and 99.99 %, respectively. The CLWS process produces

highly purified hydrogen with no CO contaminated. H_2 produced from the CLWS process can be used in all types of fuel cell systems. And for the SECLR-WS process, CASEI-com can only produce H_2 in the H_2-rich syngas stream with 99.85 % purity of H_2, while CASEII-com and CASEIII-com can be produced the H_2-rich syngas with H_2 purity approximately 97.0 %. The CASEII-com and CASEIII-com can also produce the high purity H_2 with H_2 purity of 99.9 %. Although in the CASEI-com, H_2 produced from H_2-rich syngas streams is high H_2 purity. However, it also has high CO concentration, which makes it unsuitable for some fuel cell systems. In addition, comparing with SECLR and CLWS, large amounts of steam must be fed into the FR to obtain high H_2 purity. If the high purity H_2 from the SECLR-WS process is needed, it can be obtained by adjusting the operating condition to produces high purity H_2. H_2 produced from SR is purified close to the CLWS process and has a low CO concentration while H_2 produced from FR is purified close to the SECLR process.

In terms of thermal efficiency (η_{th}), the lowest thermal efficiency of 52.43 % found at CLWS process. The highest thermal efficiency process is the SECLR-WS process at CASEII-com with 73.84 % thermal efficiency. The SECLR process has a thermal efficiency of 70.20 %. The low thermal efficiency of the CLWS process is due to the extremely high heat of 374286.5 kW required to evaporate the steam to high temperature before entering the SR. Since the CLWS process is needed high amount of heat while the production of hydrogen is low, so the CLWS process is low thermal efficiency. The SECLR and SECLR-WS processes need to be operated under low pressure conditions to avoid the deactivation of the adsorbent. If the process operated at high pressure, the regenerate step of adsorbent must be occurred at high temperature (Antzara *et al.*, 2015). For the SECLR-WS process in the CASEI-com case, despite high hydrogen production about 1.5 times higher than the CLWS process but still has low thermal efficiency. Due to the large amount of steam entering the FR reactor, the heat required for steam is very high. As a result, thermal efficiency was only 55.62 %, which is close to the CLWS process. Although the SECLR and CLWS processes can be operated at autothermal condition, but the SECLR-WS, in the case of CASEII-com and CASEIII-com, can achieve higher energy efficiency than the SECLR and CLWS process. Since the SECLR-WS process in that CASEII-com and CASEIII-com produce

more H_2 than SECLR and CLWS, resulting in higher thermal efficiency. In addition, the autothermal operation requires high solid circulation rate to carry heat from the exothermic reactor to another endothermic reactor. In the SECLR and CLWS processes, there are solids in the system of 2172.3 kg/sec and 1543.8 kg/sec, respectively, while the SECLR-WS in the CASEIII-com has solids only 319.2 kg/sec. Moreover, increasing the production of high purity H_2 stream in the SECLR-WS from CASEII-com to CASEIII-com resulted in only a slight reduction in thermal efficiency. By increasing the production of high purity H_2 stream of 0.39 kmol/sec, thermal efficiency is reduced by only 2.43 %.

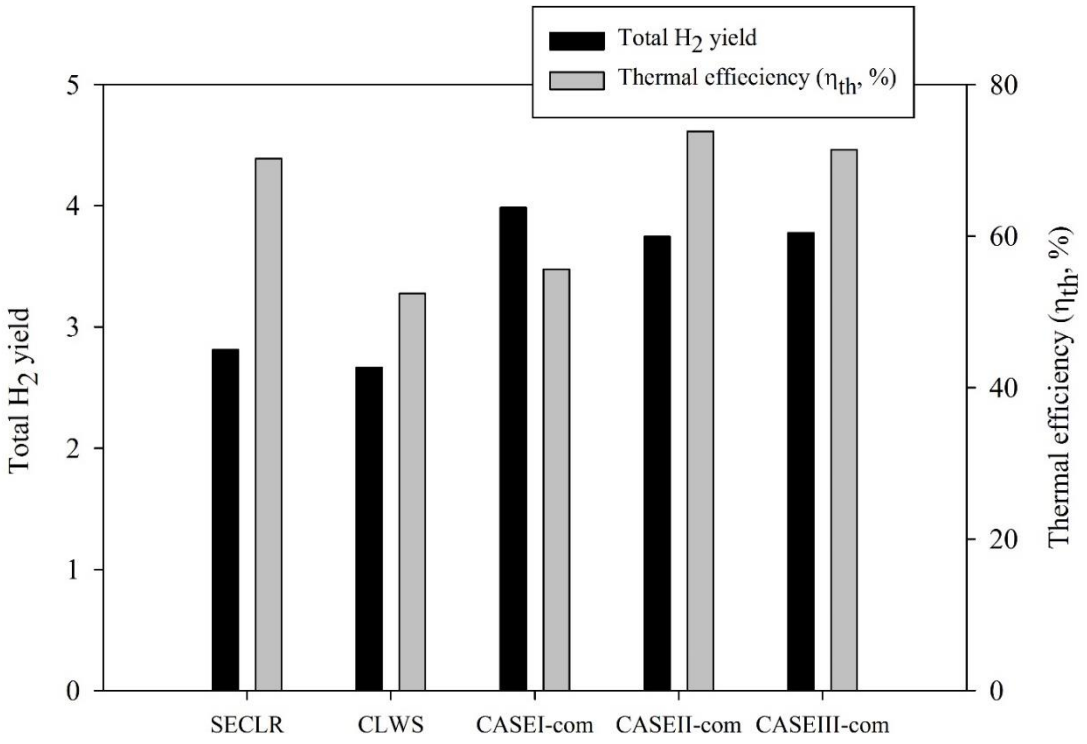

Figure 6.4 Total H_2 yield and thermal efficiency of SECLR, CLWS and SECLR-WS process.

CHAPTER VII
HEAT EXCHANGER NETWORK DESIGN

The sorption-enhanced chemical looping reforming and water splitting process, SECLR-WS, was analyzed from the thermodynamical point of view in Chapter 5. In addition, the optimal conditions based on different objective functions was discussed. In this chapter, the heat exchanger network design was performed based on a pinch analysis to improve the thermal efficiency of the SECLR-WS process. The aim is to maximize a heat recovery in the process, resulting in a minimum requirement of cold and hot utilities.

7.1 Data extraction

The first step for performed the pinch analysis is indicating the hot and cold process streams in the interested. In this study, the operating condition for heat exchanger network design is the optimal operating condition in CASE III, as shown in Table 7.1. The process simulation flowsheet of SECLR-WS shown in Figure 7.1. In heat exchanger network design, the biogas and water are supplied at a temperature of 25 ^{o}C and atmospheric pressure. The biogas and water were heated by HEATER1, HEATER2, and HEATER3 from 25 ^{o}C to 400 ^{o}C before entering the reactor. The streams STEAM-FR and STEAM-SR are considered in a single stream due to the reducing number of unnecessary streams. The gaseous products from FR, SR, and CAL were cooled to 150 ^{o}C. The process streams data from mass and energy balance by simulation using Aspen Plus simulator shown in Table 7.2.

Table 7.1 Optimal operating condition of SECLR-WS process for heat exchanger network design.

Parameters	Operating condition
Biogas feed (kmol sec^{-1})	1.00
T_{FR} (^oC)	606.8
T_{SR} (^oC)	500.0
T_{CAL} (^oC)	860.0
S_{FR}/CH_4 molar ratio	2.35
S_{SR}/CH_4 molar ratio	2.33
Fe_3O_4/CH_4 molar ratio	0.92
CaO/CH_4 molar ratio	1.94

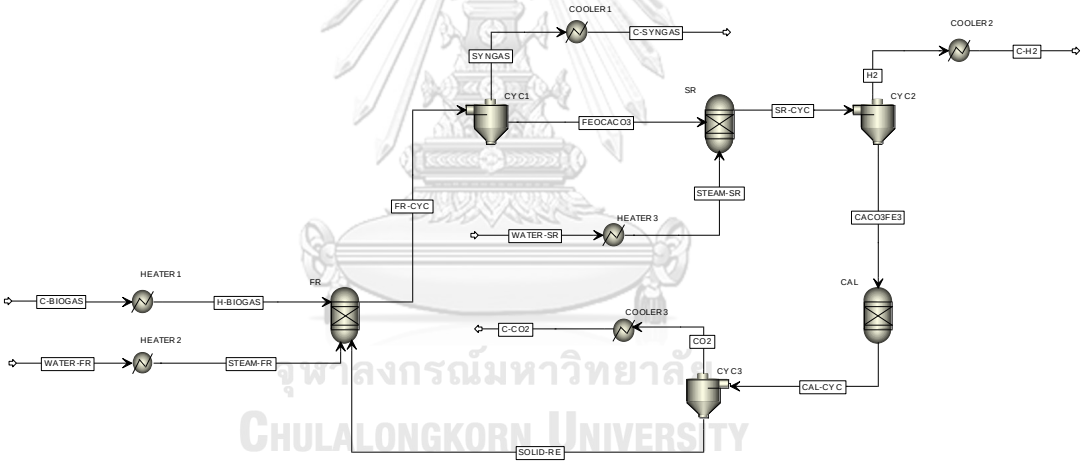

Figure 7.1 Simulation flowsheet of SECLR-WS process for heat exchanger network design.

Table 7.2 Process streams data of SECLR-WS process for heat exchanger network design.

Stream name	Type	Supply temperature (T_s, ^oC)	Target temperature (T_t, ^oC)	Stream heat load (kW)	Heat capacity flow rate (CP, kW/^oC)
BIOGAS	Cold	25	400	16912.5	45.1
WATER	Cold	25	400	160910.8	152.3
SYNGAS	Hot	606.8	150	-37987.3	31.8
H2	Hot	500	150	-16873.3	34.4
CO2	Hot	860	150	-33644.0	50.2

7.2 Energy target calculation

Once the data of the process streams have been obtained. The next step is to calculate the minimum target energy or the maximum heat recovery. The minimum target energy from pinch analysis can be calculated using a graphical method or problem table algorithm. In this study, the minimum target energy was calculated by problem table algorithm. The details of the graphical method and problem table algorithms were discussed in section 3.5. In this study, the preselection of ΔT_{min} is 125 ^oC, and the shifted temperature of process streams data is shown in Table 7.3.

Table 7.3 The data of SECLR-WS process stream with shifted temperature.

Stream name	Type	CP (kW/^oC)	Actual temperature		Shifted temperature	
			T_s (^oC)	T_t (^oC)	S_s (^oC)	S_t (^oC)
1. BIOGAS	Cold	45.1	25	400	87.5	462.5
2. WATER	Cold	152.3	25	400	87.5	462.5
3. SYNGAS	Hot	31.8	606.8	150	544.3	87.5
4. H2	Hot	34.4	500	150	437.5	87.5
5. CO2	Hot	50.2	860	150	797.5	87.5

The results of minimum energy target by problem table algorithm is shown in cascade heat calculation in Table 7.4. The results show that only hot utility of 89318.6 kW requires in the process and the pinch point is not found. This problem, only one type of utility requires and no pinch point, is called threshold problem in the type of non-utility end.

Figure 7.2 shows the hot and cold composite curve in the SECLR-WS process. When fixing the hot composite curve and move the cold curve to the left, so that the ΔT_{min} decreases. But the minimum target energy does not change. The only hot utility requires of 89318.6 kW still constant, and the heat exchange for the hot stream to cold stream still sufficient (not need cold utility). While moving the cold composite curve to the right to increase the ΔT_{min} over 125 °C, the minimum target energy is increased, as shown in Figure 7.3. The point of ΔT_{min} that change in minimum target energy is called ΔT_{min} threshold and the problem in that case is called the threshold problem.

Table 7.4 Cascade calculation for minimum energy target of SECLR-WS process.

Shifted temperature (^oC)	Streams flow	Interval number	$S_i - S_{i+1}$ (^oC)	$\sum CP_H - \sum CP_C$ (kW/^oC)	ΔH_i (kW)	Start with zero hot utility (kW)	Start with minimum hot utility (kW)
$S_1 = 797.5$	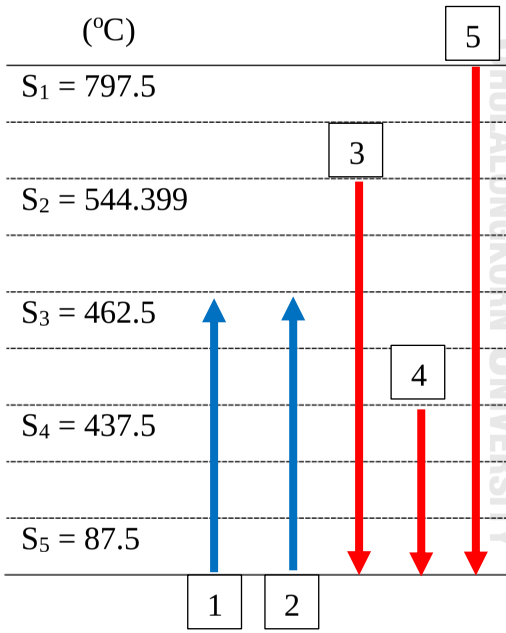					0	89318.658
		1	253.1	+47.38599945	11993.44		
$S_2 = 544.399$						11993.44	101312.1026
		2	81.899	+130.5277206	10690.09		
$S_3 = 462.5$						22683.53	112002.1928
		3	25	-343.6681408	-8591.70		
$S_4 = 437.5$						14091.83	103410.4893
		4	350	-295.4585407	-103410.4		
$S_5 = 87.5$						-89318.658	0

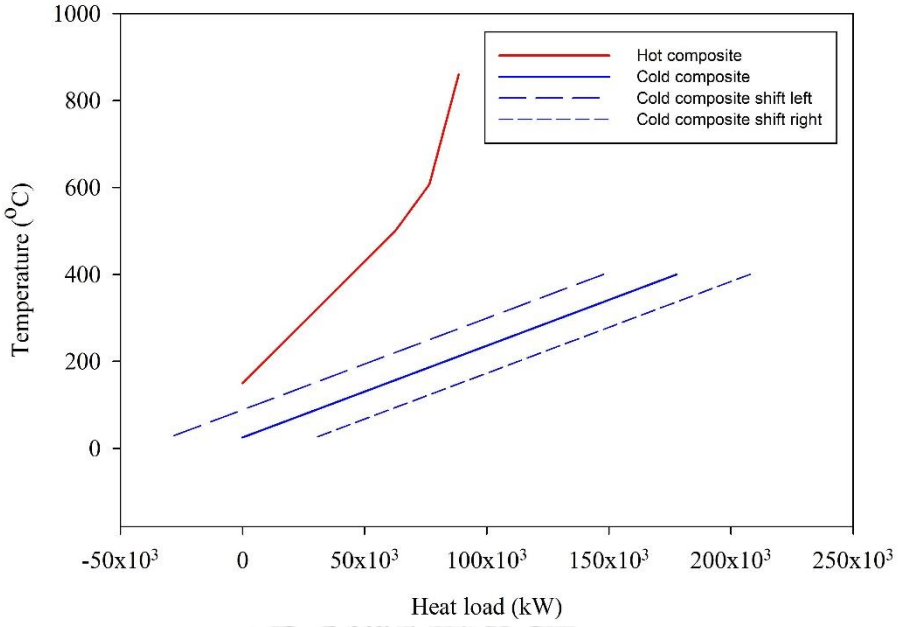

Figure 7.2 Hot and cold composite curve of SECLR-WS process.

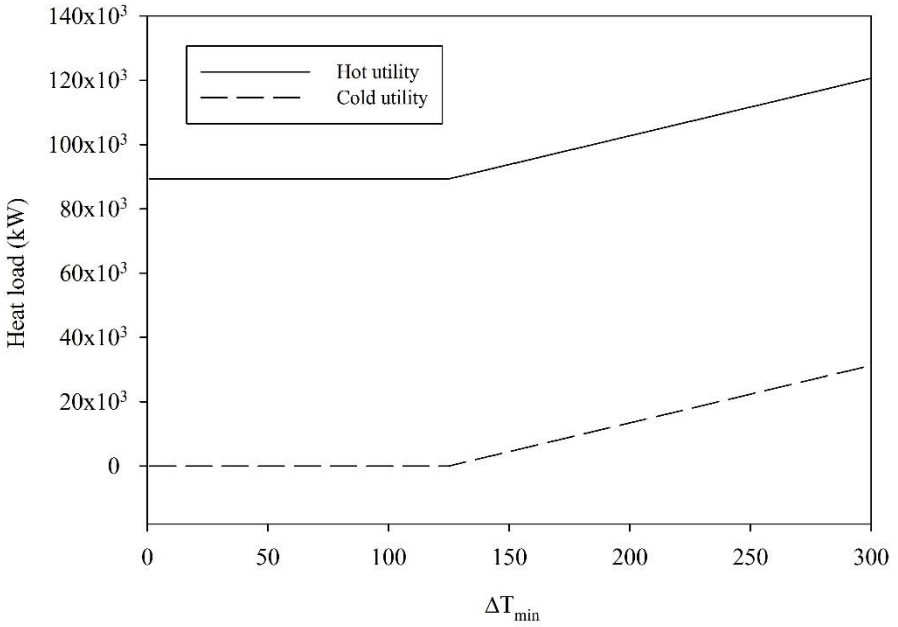

Figure 7.3 Hot and cold utility as a function of ΔT_{min} of SECLR-WS process.

A threshold problem occurs when increasing of the ΔT_{min}, in the first stage, only the hot or cold utility are requiring, which is constant as shown in Figure 7.3. This problem does not has the pinch point temperature when the ΔT_{min} below ΔT_{min} min threshold, as shown in Figure 7.2. When the ΔT_{min} is increased greater than the ΔT_{min} threshold, the process will require more hot utility and cold utility, and also the pinch point temperature appears. For the design of the heat exchange network at ΔT_{min} less than ΔT_{min} threshold is very flexible. The design usually takes into account the placement of a heater unit or cooler unit to allow for better control. It is necessary to use a hot utility and cold utility according to minimum energy target from target calculation (Kemp, 2011).

The appropriate ΔT_{min} for heat exchanger network design is chosen by the minimum of total cost for the process. In general, increasing the ΔT_{min} increases the energy cost but decreases the capital cost of the heat exchanger. Because of the high ΔT_{min} is high driving force resulting to the low heat exchanger size. While decreasing of the ΔT_{min} is the opposite effect. The low value of ΔT_{min} reduces the energy cost, but increases the capital cost instead, as shown in Figure 7.4. In case of threshold problem in the type of non-utility end, the minimum total cost can be obtained in two cases, which are obtained at ΔT_{min} threshold and at greater than ΔT_{min} threshold, as shown in Figure 7.5. Since at ΔT_{min} lower than ΔT_{min} threshold, increasing ΔT_{min} does not change the minimum target energy, while the capital cost continuously decreases. Therefore, the minimum total cost cannot be obtained at ΔT_{min} lower ΔT_{min} threshold (Smith, 2016). However, at ΔT_{min} greater than ΔT_{min} threshold, both cold and hot utility are required, and the number of heat exchanger unit is increased. Thus, the optimal ΔT_{min} usually is at ΔT_{min} threshold (Dimian *et al.*, 2014). In this study, the ΔT_{min} for heat exchanger network design is setting at 125 ^{o}C, which is ΔT_{min} threshold for the SECLR-WS process.

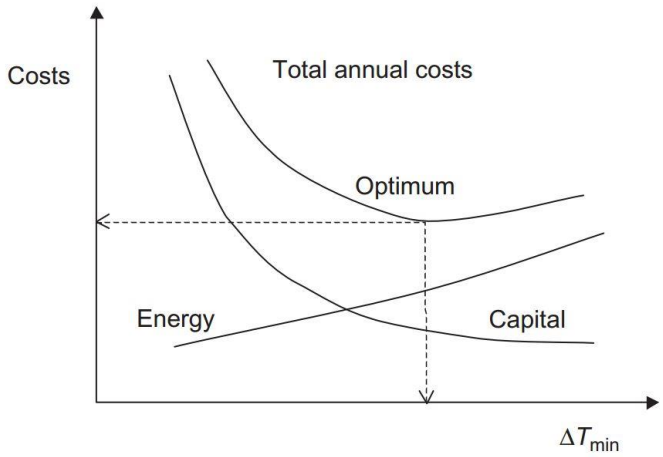

Figure 7.4 Energy and capital cost as a function of ΔT_{min} (Dimian *et al.*, 2014).

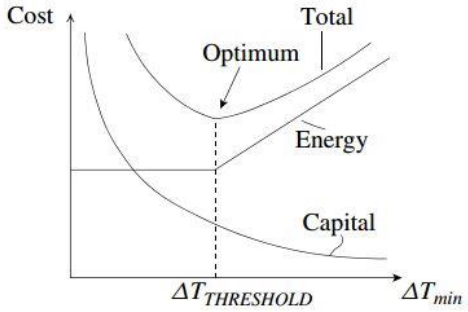

(a) The capital - energy trade-off can lead to an optimum at threshold ΔT_{min}

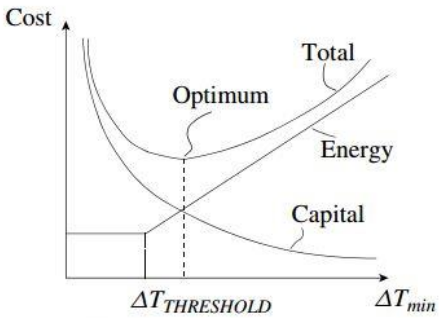

(b) The capital - energy trade-off can lead to an optimum above $\Delta T_{THRESHOLD}$

Figure 7.5 Optimum ΔT_{min} of threshold problem (Smith, 2016).

7.3 Heat exchanger network design

When ΔT_{min} is determined and the minimum target energy for the process is calculated. The next step is to be designing the heat exchanger network by matching appropriated the heat exchanger of cold and hot streams in the process. In the first step, the minimum number of heat exchangers that will be used in the process will be calculated by Eq. (7.1):

$$N_U = (S_{above} + S_{u,above} - 1) + (S_{below} + S_{u,below} - 1) \quad (7.1)$$

where N_U is the minimum heat exchanger unit. S_{above} and S_{below} are the number of streams above and below the pinch temperature. $S_{u,above}$ and $S_{u,below}$ are the number of utility above and below the pinch temperature.

The heat exchanger network of SECLR-WS process is designed at above the pinch temperature (or ΔT_{min} threshold), because the pinch analysis shows that the process is threshold problem in the type of non-utility end with the only hot utility is required. From the data in Table 7.2, the three hot streams and two cold streams are exits and only the hot utility is required, thus the minimum number heat exchanger unit for SECLR-WS process is 5.

For the design of heat exchanger network, normally, the design starts from the pinch point temperature using the grid diagram. For the SECLR-WS process, which is a threshold problem, the design at lower than or equal ΔT_{min} threshold is started from the ΔT_{min} threshold and pinch design rules are also applied to this case. The criterion for the above the pinch design is the matching hot and cold streams must be satisfied the heat capacity flow rate criterion, which is the heat capacity flow rate of the hot stream must be less than cold streams. If the heat capacity flow rate of all hot streams greater than cold streams, or the number of the hot streams is greater than the cold streams, the streams splitting is required. Due to the design of above the pinch point temperature, according to the pinch design rules, the cold utility cannot be used at the above pinch point temperature. Thus, if the number of the hot streams is greater than the cold streams, some hot streams remain in this matching and the cold utility is required, which it breaks the pinch design rule. The splitting stream is done by splitting the streams flow rate, resulting in the heat capacity flow rate is decreased with the ratio

of flow rate decreased. The method to design the heat exchanger network is shown in Figure 7.6.

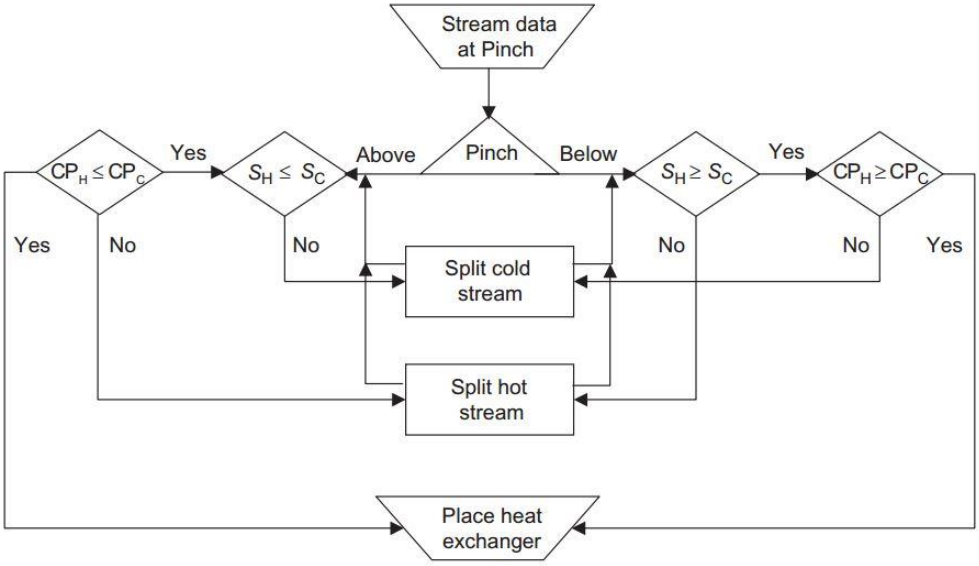

Figure 7.6 Heat exchanger network design procedure at pinch point temperature (Dimian *et al.*, 2014).

The grid diagram for the heat exchanger network design for the SECLR-WS process at ΔT_{min} of 125 ^{o}C is shown in Figure 7.7. The hot SYNGAS stream and cold WATER stream are split into two and three streams, respectively. The first SYNGAS stream exchange with cold BIOGAS stream in the first heat exchanger with 16912.5 kW heat load. The second heat exchanger is used to exchange the heat load of 33644.0 kW between CO2 stream and first WATER stream. The third and fourth heat exchanger are used to exchange the heat load of 21083.4 kW and 16873.3 kW between the second SYNGAS stream and the second WATER stream, and the H2 stream and the last WATER stream, respectively. The last heat exchanger is used to heat the last WATER stream from the temperature of 84.6 ^{o}C to the target temperature of 400 ^{o}C by the external hot utility of 89318.6 kW. From the matching of hot and cold streams in the SECLR-WS process as describe above, the 5 heat exchanger units are required, which corresponded to the minimum unit calculation, and the only hot utility of 89318.6 kW is used in this process, which it is corresponded to the minimum target energy from

problem table algorithm. The flowsheet diagram of SECLR-WS process with completing of heat integration is shown in Figure 7.8. The heat exchanger network design of SECLR-WS process increases the thermal efficiency (η_{th}) of the process from 68.42 to 76.83 %.

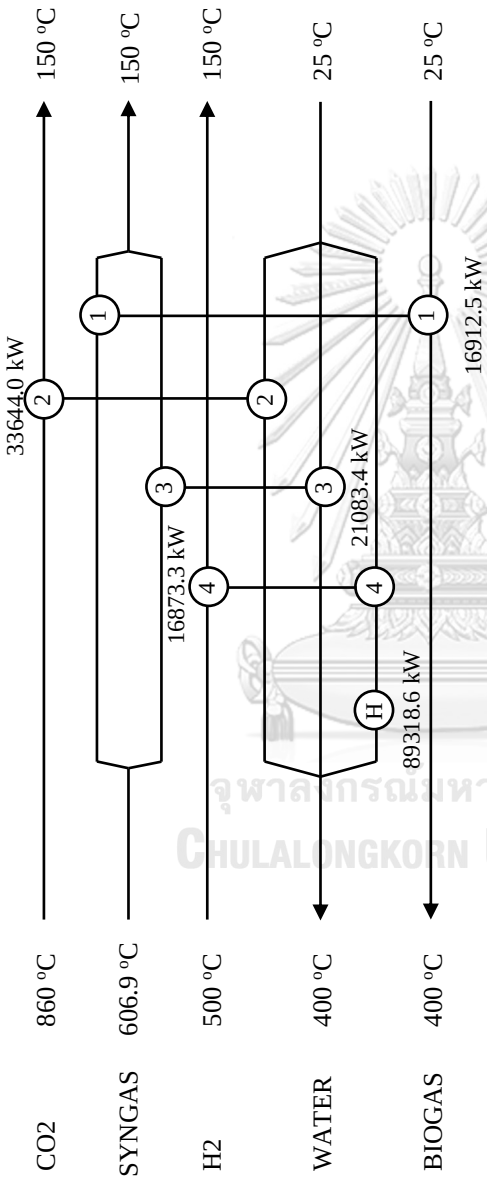

Figure 7.7 Grid diagram for heat exchanger network design of SECLR-WS process.

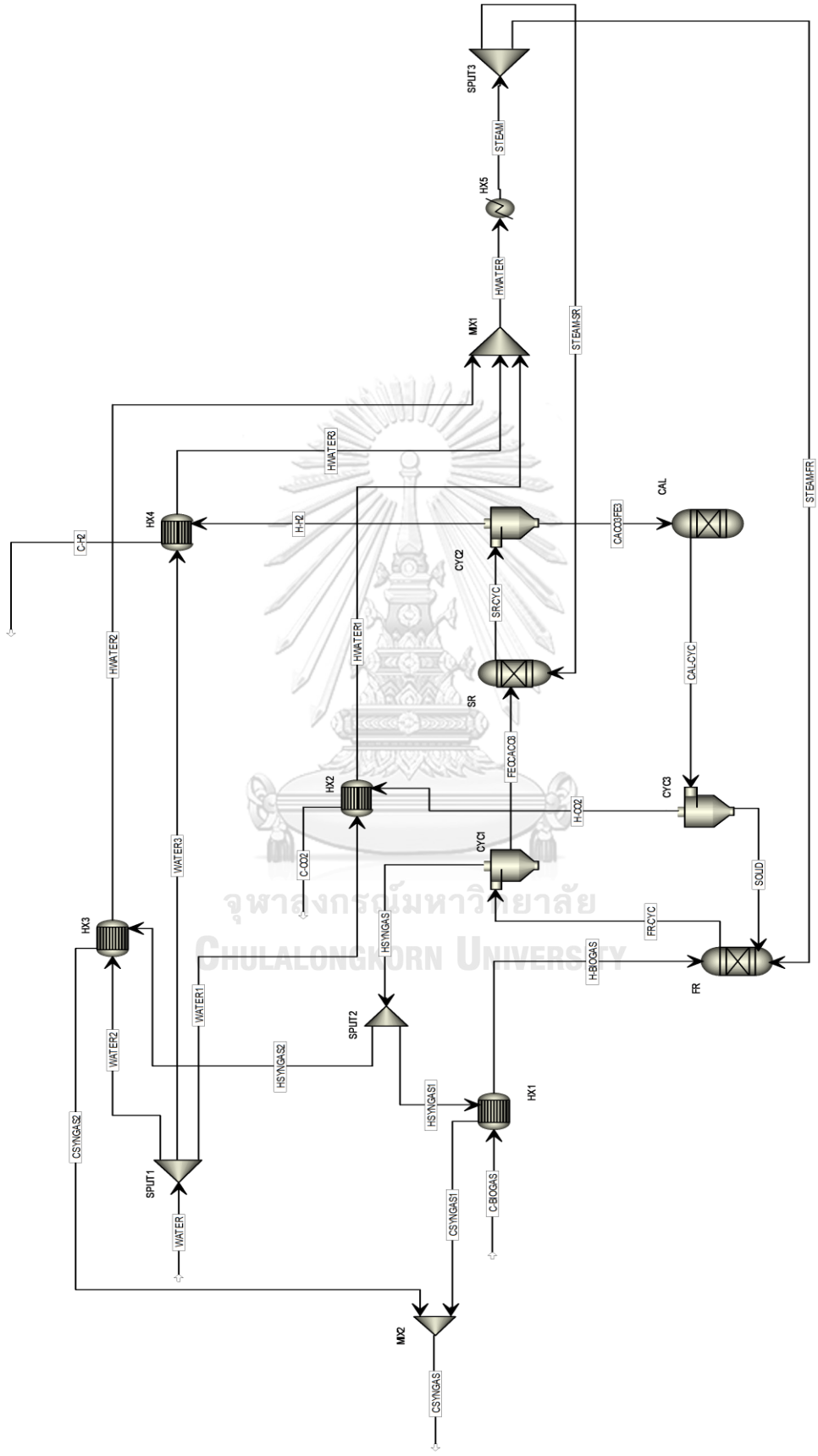

Figure 7.8 Simulation flowsheet of SECLR-WS process with heat exchanger network design.

CHAPTER VIII
ENERGY AND EXERGY ANALYSIS

Previously, the SECLR-WS process is improved by using the optimization method to find the optimal operating condition by adjusting the key operating parameters from the sensitivity analysis, and then the heat exchanger network design is applied to improve the heat recovery in the optimal SECLR-WS process using the pinch analysis. However, the optimization and heat integration of the SECLR-WS process is based on the consideration of only the quantity of energy. Thus, to assess the quality of energy, the energy and exergy analysis are presented in this chapter. Exergy is the maximum useful work which obtained from the system. The exergy analysis is a useful tool to determine the part of inefficiency energy usage in the process. The loss of the potential of work has occurred from the irreversibility of the process which the exergy analysis can be accounted. The energy and exergy analysis of the SECLR-WS process at the optimal operating condition (CASE III) is performed. Moreover, the effect of key operating parameters on the energy (or thermal) and exergy efficiency are also presented in this chapter.

8.1 Energy and exergy analysis of the optimal SECLR-WS process

The SECLR-WS process in case energy and exergy analysis is the optimal operating condition in CASE III, as shown in Table 6.1, and the process flowsheet with heat exchanger network design, as shown in Figure 6.8. For the energy and exergy analysis of the overall process, the energy (η_{th}) and exergy (η_{ex}) efficiencies are determined by Eq. (3.20) and (3.29), respectively. The exergy efficiency of each unit ($\eta_{ex,i}$) can calculate by Eq. (3.30). The considered units for exergy analysis of each unit are reactor (FR, SR, and CAL), heat exchanger and heater (HX1, HX2, HX3, HX4, and HX5), and mixing point or mixer (MIX1 and MIX2), due to the heat transfer and the change of state (change of temperature input and output streams, and also the change of composition of input and output streams) to the units created the exergy destruction

and entropy of the stream. But the perfect cyclone for gas and solid separation (CYC1, CYC2, and CYC3) and the ideal splitter for divided streams (SPLIT1 and SPLIT2) are not considered for the exergy analysis of each unit due to the zero entropy change of the unit leading to the zero exergy destruction of the units.

Table 8.1 shows the energy (or thermal) and exergy efficiency, and the total exergy destruction of the SECLR-WS process at the optimal operating condition. The energy efficiency of 76.83 % and the exergy efficiency of 72.30 % with 75152.8 kW exergy destruction can be obtained when one kmol/sec of biogas is used to produces 2.2675 kmol/sec of total H_2 product (or total H_2 yield of 3.779). Figure 8.1 shows the portion of exergy destruction. The results show that the main exergy destruction is occurred in FR and SR which are 34.23 and 22.27% of the total exergy destruction, respectively, because these units are the reactor which many reactions occur, resulting in high irreversibility and loss of exergy. The high value of exergy destruction can be explained by three reasons. The main reason, for the FR, is this unit uses the methane as a reactant, which high chemical exergy, to produce H_2-rich syngas, which low chemical exergy. The summation of heat from the reaction in FR is exothermic, thus the byproduct of the reactor is heat which is useless and the exergy of this heat is zero when this reactor is operated in the environment state. For the SR, although the chemical exergy of water, which is the reactant, is low and the chemical exergy of H_2, which is the product, is high, the main by-product from this reactor is heat which is useless thus the exergy destruction in this unit is high. The second reason is the mixing of gaseous in product stream decrease the exergy of the product stream. The last reason can be explained by the difference of the temperature feed to the reactor and the temperature of product stream. For the FR, the feed composes of 3 streams, which are H-BIOGAS, STEAM-FR, and SOLID, with temperature of 400, 400, and 860 ^{o}C, respectively, while the temperature of product stream (FR-CYC) is 606.9 ^{o}C, leading to the less total physical exergy of the product stream compare with feed stream. For the exergy destruction of other reactors, CAL, the exergy destruction of the CAL is lower than FR and SR, although, the chemical reaction takes place in these units. Although, the calcinator is the endothermic unit, however, the exergy destruction in this unit is lower than FR and SR. Since the chemical exergy of feed stream to CAL, which

is $CaCO_3$, is low but the product gas and solid from CAL, which are CO_2 and CaO, have high amount of chemical exergy, thus the exergy destruction in CAL is small when compared with FR and SR.

The third order of the exergy destruction occurs in the heater (HX5) which is 18.04 % of the total exergy because this unit consumes the high amount of energy at high temperature. The HX5 is consumed 89318.6 kW of heat to evaporate the saturated water to high-temperature steam at 400 ^{o}C. The high amount of heat with high quality is used as input exergy but the output is the physical exergy of steam at 400 ^{o}C, which is much less than the exergy input. Therefore, the high exergy occurs in HX5. The fourth of exergy destruction is the HX2. The high exergy destruction in HX2 is due to the highest temperature difference in this heat exchanger (the log mean temperature difference in this heat exchanger is 257.12 ^{o}C), thus, the exergy destruction in the heat exchanger unit is high. The next order of the exergy destruction is HX3 and HX4. The low exergy destruction in HX3 is due to the low-temperature difference when compare with HX2, while the low exergy destruction in HX4 is due to the high amount of steam can be created in this heat exchanger leading to the high amount of output physical exergy. The lowest of the exergy destruction of the heat exchanger occurs in HX1 because the low temperature difference and phase change does not occur in this heat exchanger.

The last exergy destruction part in the process is MIX1 and MIX2. The exergy destruction of MIX1 is greater than MIX2 because of the temperature difference in MIX1 is higher than MIX2. The only lesson for the destruction of exergy in the mixer unit in SECLR-WS process is the temperature and phase change of inlet and outlet streams (due to the composition of the mixing streams is same). Considering the MIX1, the purpose of MIX1 is using to combine the three streams of water (HWATER1, HWATER2, and HWATER3) in one stream (HWATER). The temperature of HWATER1, HWATER2, and HWATER3 are 400, 400, and 100 ^{o}C, respectively, while the temperature of HWATER is 100 ^{o}C. The temperature of inlet streams is high while the temperature of outlet stream is low leading to high input physical exergy and low output physical exergy, thus the exergy destruction in MIX1 is high. On the other hand, MIX2 is the combination of two cold syngas streams (CSYNGAS1 and CSYNGAS2)

into single cold syngas stream (CSYNGAS). The temperature of CYNGAS1, CSYNGAS2, and CSYNGAS are the same all, thus the exergy destruction in this unit is low.

The exergy efficiency of each process unit is shown in Figure 8.2. The group of high exergy efficiency in this process is reactor unit, while the group of low exergy efficiency in this process is heat exchanger unit. Because, in this process, the temperature difference of the all heat exchanger is high, this lead to the low exergy efficiency in the all heat exchanger unit. In contrast, the reactor units in this process are high exergy efficiency. Although, the reactor units are highly exergy destruction because the occurring of the reaction leading to high irreversibility. But, in these units, the exergy in is very high when compared with the exergy destruction due to the high amount of chemical exergy of feed streams (biogas for FR and $Fe_{0.947}O$ for SR) and high amount of input heat exergy (for CAL). The exergy efficiency of the process can be increased by decreasing the high exergy destruction in FR and SR. The one option to decrease the exergy destruction in FR and SR is the heat of exothermic reactor must be supplied to the heater. In this way, the exergy destruction of the exothermic reactor (FR and SR) can be decreased by considering the heater and reactor in a single unit, and the exergy efficiency can be improved. The exergy efficiency of the heat exchanger can be improved by using the different level of utility to decreases the temperature different in each heat exchanger unit.

Table 8.1 Energy and exergy efficiency of the optimal SECLR-WS process.

Parameters	Value
η_{th} (%)	76.83
η_{ex} (%)	72.30
Ex_d (kW)	75152.8

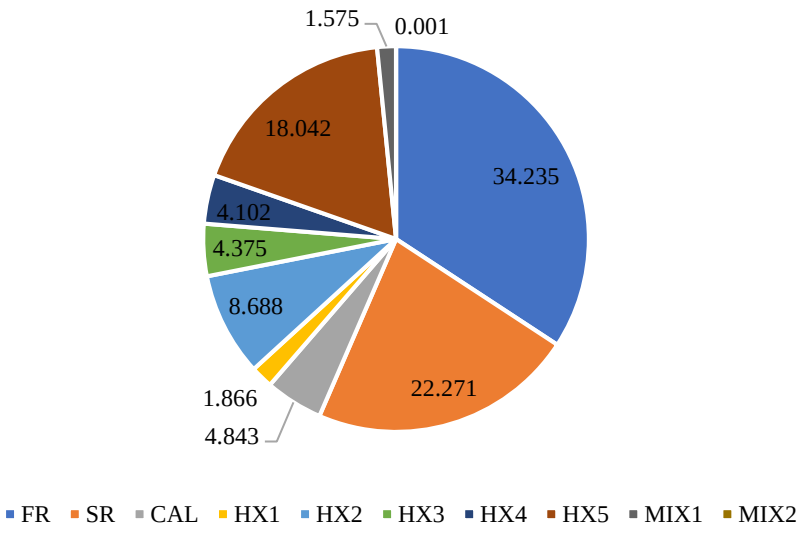

Figure 8.1 Portion of the exergy destruction of each process units.

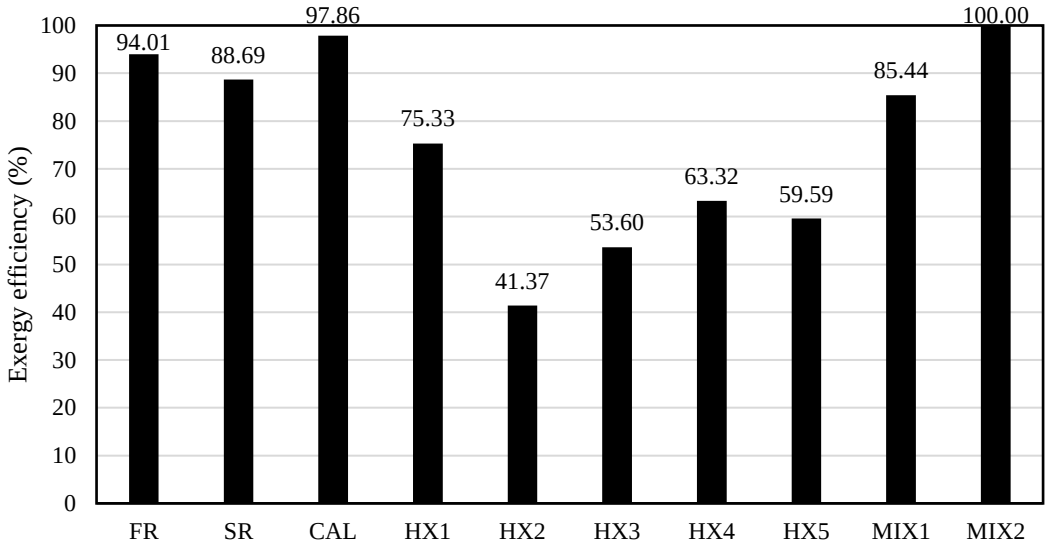

Figure 8.2 Exergy efficiency of each process units.

8.2 Effect of key operating parameters on energy and exergy efficiency

The effect of key operating parameters on the energy and exergy efficiency of the SECLR-WS process is presented in this section. The considering key operating parameters, which affect to the energy and exergy efficiency of the process, are T_{FR},

and Fe_3O_4/CH_4, CaO/CH_4, S_{FR}/CH_4, and S_{SR}/CH_4 molar ratios. In addition, the exergy efficiency of each process units is investigated.

8.2.1 Effect of FR temperature on energy and exergy efficiency

Figure 8.3 shows the effect of T_{FR} on the energy and exergy efficiency of the SECLR-WS process. The results show that the FR temperature affects the energy and exergy efficiency of the process in the same way. When the FR temperature is lower than 600 ^oC, increasing the FR temperature increase the energy and exergy efficiency of the process due to the increase in the amount of total H_2 product. At low FR temperature (500 ^oC), Fe_3O_4 cannot convert to $Fe_{0.947}O$ in FR, leading to the lack of reactant to produce the H_2 from SR, thus the total H_2 is low. Moreover, the lack of reactant in SR resulting in the operation mode in SR is endothermic instead of exothermic, thus the energy and exergy efficiency of the process is low. When the FR temperature is higher than 600 ^oC, increasing the FR temperature can decrease the energy and exergy efficiency of the process due to the decreasing of the amount of total H_2 product and the changing operation mode of FR from exothermic to endothermic. When the FR is operated at high temperature, the H_2 from the FR is decreased due to the unfavored of carbonation reaction (Eq. (3.3)). In addition, some amount of heat is used to heat up the feed streams to high-temperature operation of the FR, leading to the operation mode of FR change to the endothermic mode which decreases the energy and exergy efficiency of the SECLR-WS process. The maximum energy and exergy efficiency of 76.26 and 71.67 % can be obtained at T_{FR} = 600 ^oC. The exergy efficiency of the process is higher than the energy efficiency of the process at T_{FR} = 800 ^oC because of the heat transfer terms. As mention in section 3.6, in this study, the heat source to supply the process is not consideration, thus, when the unit operates by consuming the heat of Qs at Ts, the heat source assuming supply the heat at level of Ts and the input exergy by heat transfer to the unit is $(1-T_0/T_S)Q_S$, which is less than the heat transfer Q_S, resulting in the exergy efficiency is higher than the energy efficiency in some condition. If the heat supply to the unit is from the combustion of fuel such as biogas, the input exergy by heat transfer does not appear and this term appears in the input

chemical exergy to the system resulting in the low exergy efficiency when compared to the case in this study.

Figure 8.4–8.6 show the effect of T_{FR} on the exergy efficiency of reactor, heat exchanger and heater, and mixer unit, respectively, in the SECLR-WS process. The change in FR temperature affects the exergy efficiency of each reactor unit differently. Increasing the FR temperature can increase the exergy efficiency in FR but decrease the exergy efficiency in SR and is not significant changes the exergy efficiency in CAL. Increasing the exergy efficiency in FR as a result of the high temperature of the gas product stream. Thus, the total output exergy of the FR is increased, while the total input exergy of the FR is a little changed, resulting in decreasing of the exergy destruction, as shown in Figure 8.7, and increasing of the exergy efficiency. In contrast, when the FR temperature is increased, the solid from FR is high physical exergy, and then the total input exergy of the SR is increased and the exergy destruction in SR is increased leading to the decreasing of exergy efficiency in SR.

The effect of T_{FR} on the exergy efficiency of the heat exchanger and heater is shown in Figure 8.5. Increasing the FR temperature can be improved the exergy efficiency of HX1 and HX3 due to the increasing temperature of the product gaseous from FR can be used to heat the biogas feed and water feed stream. The sharply increasing of the exergy efficiency in HX5 when the FR temperature is increased from 700 to 800 ^{o}C is the result from the low-temperature steam produced from the HX5 leading to low energy quality is used and the exergy destruction in this unit is low. The low temperature of the steam is the cause of the hot gas streams from CAL cannot obtain due to the CO_2 cannot capture in high-temperature FR, thus the water cannot receive heat from the CO2 stream. The decreasing of exergy efficiency in HX4 result from the increasing of H_2 product in high purity H_2 stream leading to low physical exergy of the gas product stream from the SR (because of the mass of H_2 is lower than H_2O) and decreasing of the exergy in of the HX4. The 100 % efficiency of HX2 at FR temperature of 800 ^{o}C is resulted from the zero-flow of CO_2 due to the carbonation reaction (Eq. (3.3)) cannot occur in the FR, leading to the change of exergy in this unit. The last part for the energy analysis of each unit is mixer unit. Increasing the FR

temperature decrease the exergy efficiency in MIX1 due to the large of the different temperature of inlet and outlet stream in this unit. A part of syngas from the FR is used to heat up the water. Therefore, when the FR temperature is increased, the temperature of the gas product from FR and the hot water from HX3 are increased, leading to the increasing of a temperature difference in MIX1.

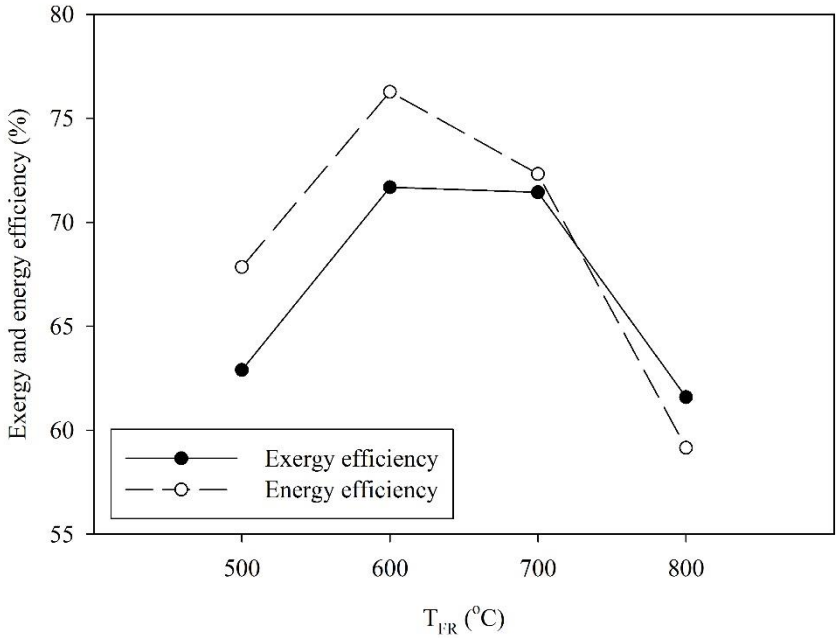

Figure 8.3 The exergy and energy efficiency of the SECLR-WS process as a function of T_{FR}.

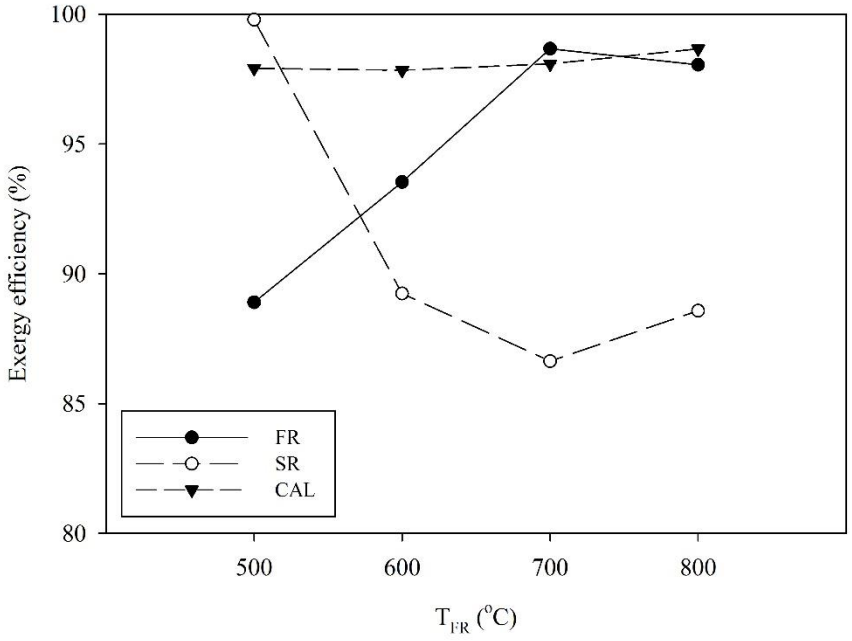

Figure 8.4 The exergy efficiency of the reactor unit as a function of T_{FR}.

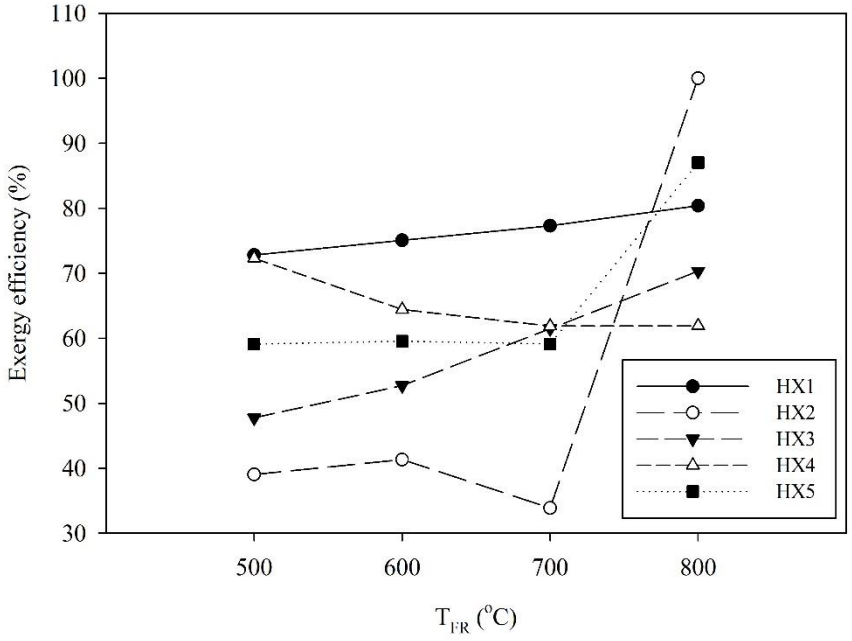

Figure 8.5 The exergy efficiency of the heat exchanger unit as a function of T_{FR}.

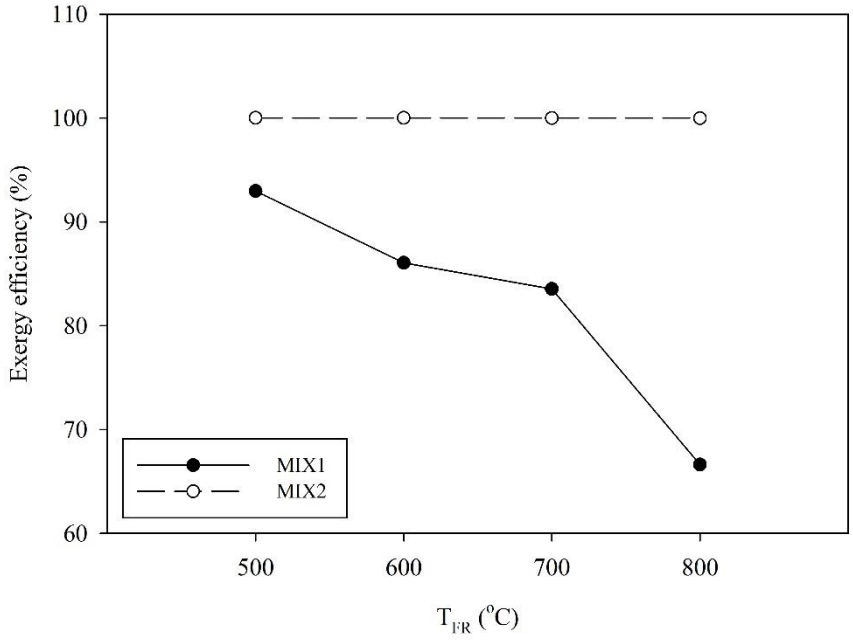

Figure 8.6 The exergy efficiency of the mixer unit as a function of T_{FR}.

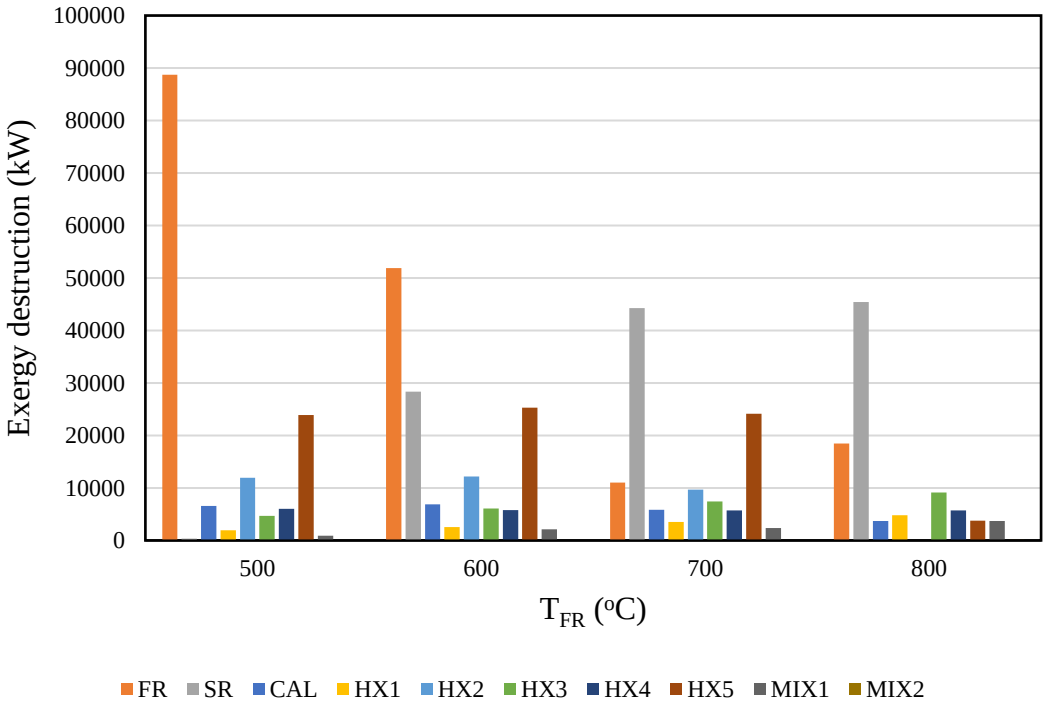

Figure 8.7 The exergy destruction of process unit as a function of T_{FR}.

8.2.2 Effect of Fe_3O_4/CH_4 molar ratio on energy and exergy efficiency

Figure 8.8 shows the effect of Fe_3O_4/CH_4 molar ratio on the energy and exergy efficiency of the SECLR-WS process. The results show that the energy efficiency of the process is increased when the Fe_3O_4/CH_4 molar ratio is increased from 0.1 to 1, and constant at the Fe_3O_4/CH_4 molar ratio of 1 to 3. While the exergy efficiency of the process is increased when the Fe_3O_4/CH_4 molar ratio is increased from 0.1 to 1 and is decreased at the Fe_3O_4/CH_4 molar ratio of 1 to 3. The increasing of the energy efficiency of the process in the range of the Fe_3O_4/CH_4 molar ratio of 0.1 to 1 is the result from the increase of the total H_2 product while the net energy demand of the reactor is constant in this range. When the Fe_3O_4/CH_4 molar ratio is increased in the range of 1 to 3, the total hydrogen product and the net energy demand of reactor are constant, thus the energy efficiency is constant in this range of the Fe_3O_4/CH_4 molar ratio. In term of the exergy efficiency of the process, increasing of the exergy efficiency of the process in the range of 0.1 to 1 of the Fe_3O_4/CH_4 molar ratio is due to the increase of total H_2 product. The decreasing of exergy efficiency at the high Fe_3O_4/CH_4 molar ratio (higher than 1) is due to the increase of energy demand in CAL while the total H_2 product is constant. Since, when the Fe_3O_4/CH_4 molar ratio is increased, the amount of solid to the CAL is increased, leading to the high needed of the energy to heat the high amount of solid from feed temperature (500 ^oC) to reactor temperature (860 ^oC).

Figure 8.9–8.11 show the effect of the Fe_3O_4/CH_4 molar ratio on the exergy efficiency of reactor unit, heat exchanger and heater unit, and the mixer unit, respectively, in the SECLR-WS process. For the FR reactor, in the range of the Fe_3O_4/CH_4 molar ratio of 1 to 3, increasing the Fe_3O_4/CH_4 molar ratio decrease the exergy efficiency of the FR, due to the increase of the high amount of solid circulation with high temperature to FR leading to the increase of the waste heat generated from the FR. Thus, the exergy destruction in the FR is increased, as shown in Figure 8.12, and the exergy efficiency of the FR is decreased in the range of the Fe_3O_4/CH_4 molar ratio of 1 to 3. For the range of the Fe_3O_4/CH_4 molar ratio of 0.1 to 1, some amount of heat from the exothermic reaction is used to supply to the endothermic reaction in FR, thus the waste heat generated from FR is small increased in this range of Fe_3O_4/CH_4 molar ratio, leading to the insignificant change of the exergy efficiency. The sharply

decreasing of exergy efficiency of the SR reactor at the Fe_3O_4/CH_4 molar ratio of 0.1 to 1 is the result of the exothermic reaction in SR leading to the high amount of waste heat generated. In the range of the Fe_3O_4/CH_4 molar ratio of 0.1 to 1, the Fe_3O_4 is totally converted to $Fe_{0.947}O$ in FR, thus increasing the Fe_3O_4/CH_4 molar ratio in this range increases amount of reactant feed to the SR and the high amount of waste heat generated from the exothermic steam-iron (Eq. (3.6)) reaction. But in the range of the Fe_3O_4/CH_4 molar ratio of 1 to 3, the exergy efficiency of the SR is almost constant, due to the constant amount of $Fe_{0.947}O$ feed to SR. Noting that, although, the amount of Fe_3O_4 is increased in this range of Fe_3O_4/CH_4 molar ratio, but the amount of Fe_3O_4 which convert to $Fe_{0.947}O$ is limited due to the gas-solid equilibrium reaction in the FR.

The effect of the Fe_3O_4/CH_4 molar ratio on the exergy efficiency of the heat exchanger and heater is shown in Figure 8.10. The results show that increasing of the Fe_3O_4/CH_4 molar ratio is an insignificant change of the exergy efficiency in these units. The small increase of the exergy efficiency in HX1, HX2, and HX3 is the result from the increasing of mass flow rate of gas product streams from the FR and CAL, leading to the increase of the amount of the input exergy of the HX1, HX2, and HX3. The decreasing of the exergy efficiency of the HX4 when the Fe_3O_4/CH_4 molar ratio is increased in the range of 0.1 to 1 is due to the decreasing of the input physical exergy of the HX4 from the increasing of H_2 gas in product streams from the SR. The last part which is affected by the Fe_3O_4/CH_4 molar ratio is the MIX1. The exergy efficiency of the MIX1 is decreased by increasing the Fe_3O_4/CH_4 molar ratio in the range of 0.1 to 1, due to the increase of temperature of the HWATER1 and HWATER2 streams, which exchange heat with H-CO2 and HSYNGAS2 stream, respectively.

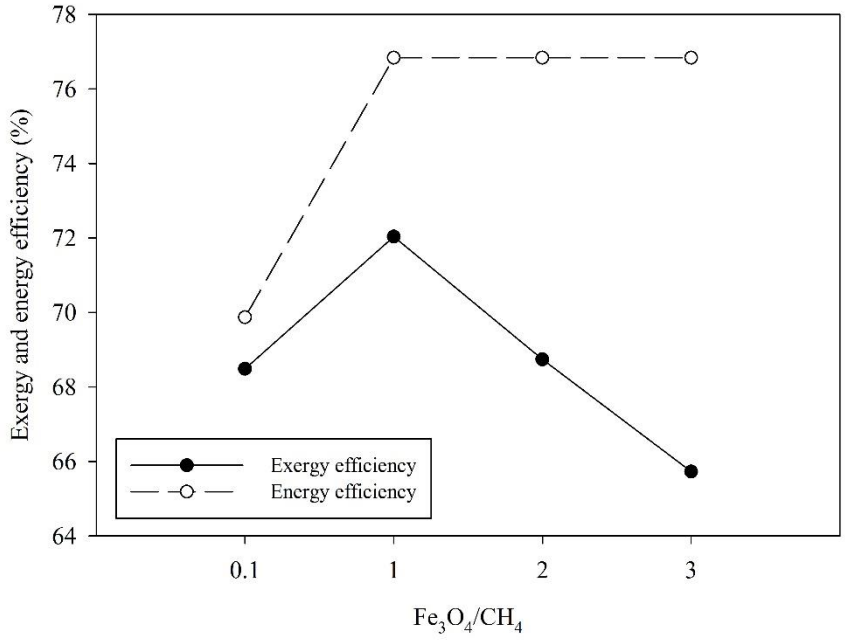

Figure 8.8 The exergy and energy efficiency of the SECLR-WS process as a function of Fe_3O_4/CH_4 molar ratio.

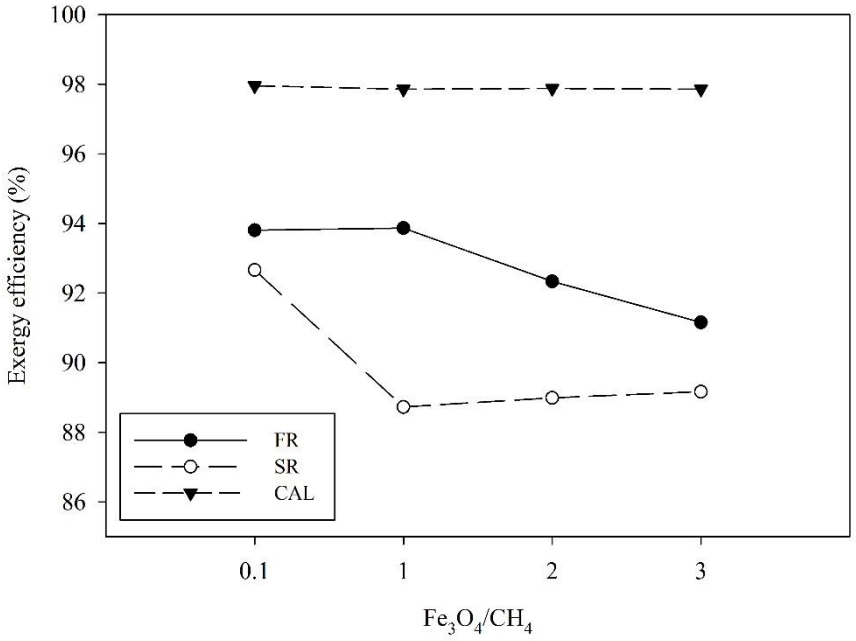

Figure 8.9 The exergy efficiency of the reactor unit as a function of Fe_3O_4/CH_4 molar ratio.

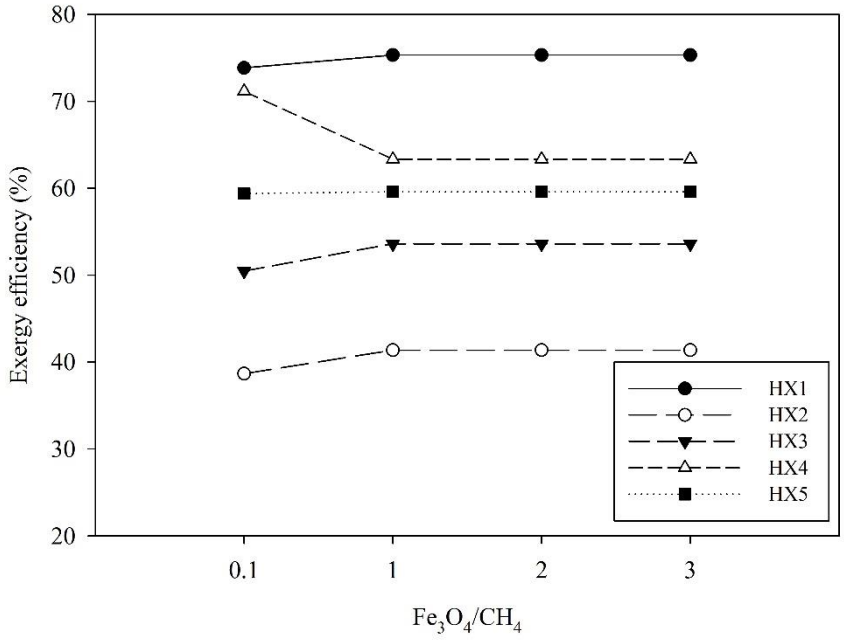

Figure 8.10 The exergy efficiency of the heat exchanger unit as a function of Fe_3O_4/CH_4 molar ratio.

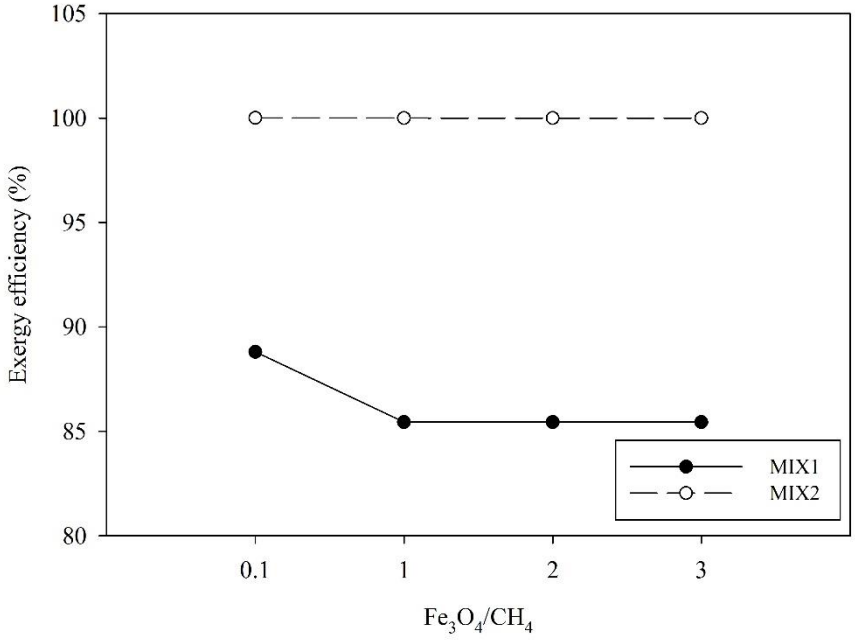

Figure 8.11 The exergy efficiency of the mixer unit as a function of Fe_3O_4/CH_4 molar ratio.

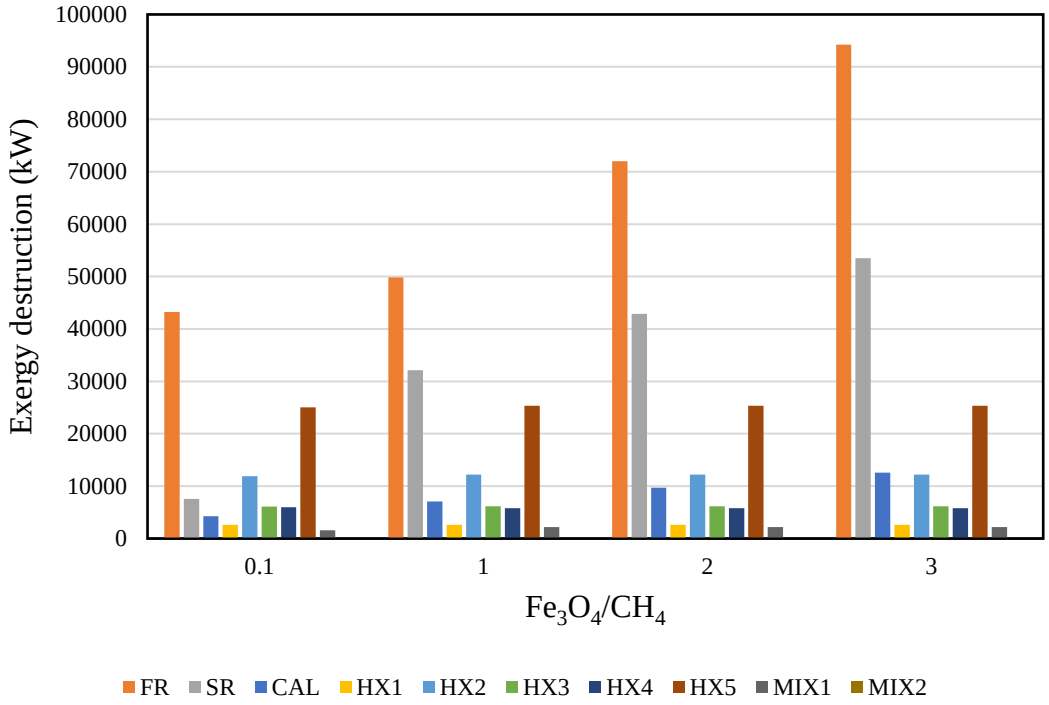

Figure 8.12 The exergy destruction of process unit as a function of Fe_3O_4/CH_4 molar ratio.

8.2.3 Effect of CaO/CH_4 molar ratio on energy and exergy efficiency

Figure 8.13 shows the effect of the CaO/CH_4 molar ratio on the energy and exergy efficiency of the SECLR-WS process. The results show that the energy and exergy efficiency of the process is increased when the CaO/CH_4 molar ratio is increased. When increasing the CaO/CH_4 molar ratio, the total H_2 product is increased due to the high amount of CO_2 can be adsorbed and the equilibrium of water-gas shift (Eq. (3.2)) and steam-methane reforming (Eq. (3.1)) reactions is shifted toward. Thus, the energy and exergy efficiency are increased, when the CaO/CH_4 molar ratio is increased.

In contrast with the exergy efficiency of the process, the exergy efficiency of the reactors, which are FR and SR, is decreased when the CaO/CH_4 molar ratio is increased, as shown in Figure 8.14. For the FR, increasing the CaO/CH_4 molar ratio can increase the amount of CaO feed the FR, leading to the high input chemical exergy. While the output chemical exergy of the product stream from the FR is almost constant

due to the increase of the conversion of CH_4 and CO, which are high chemical exergy, to H_2, which is low chemical exergy, in the FR, leading to increasing of exergy destruction, as shown in Figure 8.17. When added the high amount of CaO to the FR, the high amount of CO_2 captured can be achieved and the water-gas shift (Eq. (3.2)) and steam-methane reforming (Eq. (3.1)) reaction can be improved. For the SR, the decreasing of exergy efficiency in range of CaO/CH_4 molar ratio of 0.1 to 1 is the result from the increasing of exergy of steam and solid streams feed to SR. When increasing the CaO/CH_4 molar ratio in range of 0.1 to 1, Fe_3O_4 cannot convert to $Fe_{0.947}O$ due to the high amount of CO_2 in the FR reactor, thus, nothing reaction can be occurred in SR due to the lack of reactant and high amount of solid with high temperature of 606.9 ^oC is fed to SR, which operate at 500 ^oC. In addition, increasing amount of CaO increases amount of CO_2 gas product from the CAL and high amount of heat from CO_2 stream can be exchanged with a water stream to generate high-temperature stream feed to the SR. For all that reason, the input exergy of the SR is high but the output exergy of the SR is low, thus the exergy destruction of SR is high when the CaO/CH_4 molar ratio is increased in the range of 0.1 to 1. When increasing the CaO/CH_4 molar ratio in the range of 1 to 2, the exergy efficiency of the SR is decreased due to the steam-iron reaction (Eq. (3.6)) is occurred, leading to the high waste heat is generated and high exergy destruction occurs in this range of CaO/CH_4 molar ratio. But in the range of CaO/CH_4 molar ratio of 2 to 3, increasing the CaO/CH_4 molar ratio slightly increase the exergy efficiency of SR due to the high amount of CaO feed to SR, leading to the high input chemical exergy of the SR, while the exergy destruction is slightly increased by the high amount of solid feed with high temperature increase the exergy destruction due to the waste heat is generated. Thus, the exergy efficiency of the SR is increased by increasing CaO/CH_4 molar ratio in range of 2 to 3.

Figure 8.15 shows the effect of the CaO/CH_4 molar ratio on the exergy efficiency of the heat exchanger and heater unit in the SECLR-WS process. The results show that the exergy efficiency of all heat exchanger except HX2 is decreased when the CaO/CH_4 molar ratio is increased. For the HX2, increasing the CaO/CH_4 molar ratio increase the exergy efficiency of the HX2 due to the high amount of CO_2 gas inlet streams increase physical exergy of this stream. Although, increasing of CaO/CH_4

molar ratio increase the temperature difference in HX2 leading to high exergy destruction, as shown in Figure 8.17, but the high value of exergy destruction is compensated by the high value of the physical exergy of CO_2 stream. Thus, the exergy efficiency of the HX2 is increased although the exergy destruction of HX2 is increased. The highest exergy destruction in the group of heat exchanger occurs in the heater (HX5). Increasing of CaO/CH_4 molar ratio can decrease the exergy efficiency of the HX5 due to the high quality of heat is used to heat up the steam. The results of the effect of the CaO/CH_4 molar ratio on the exergy efficiency of mixer unit are shown in Figure 8.16. Increasing the CaO/CH_4 molar ratio slightly affect the exergy efficiency of the MIX1. When the CaO/CH_4 molar ratio is increased in the range of 0.1 to 1, the exergy efficiency of MIX1 is increased because of the temperature difference of streams is decreased leading to the decreasing of exergy destruction of this unit.

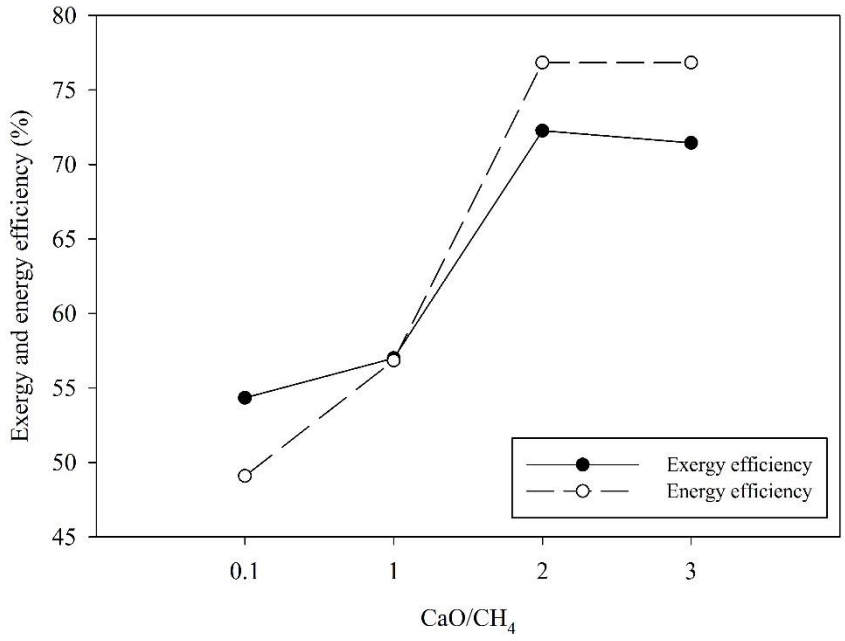

Figure 8.13 The exergy and energy efficiency of the SECLR-WS process as a function of CaO/CH_4 molar ratio.

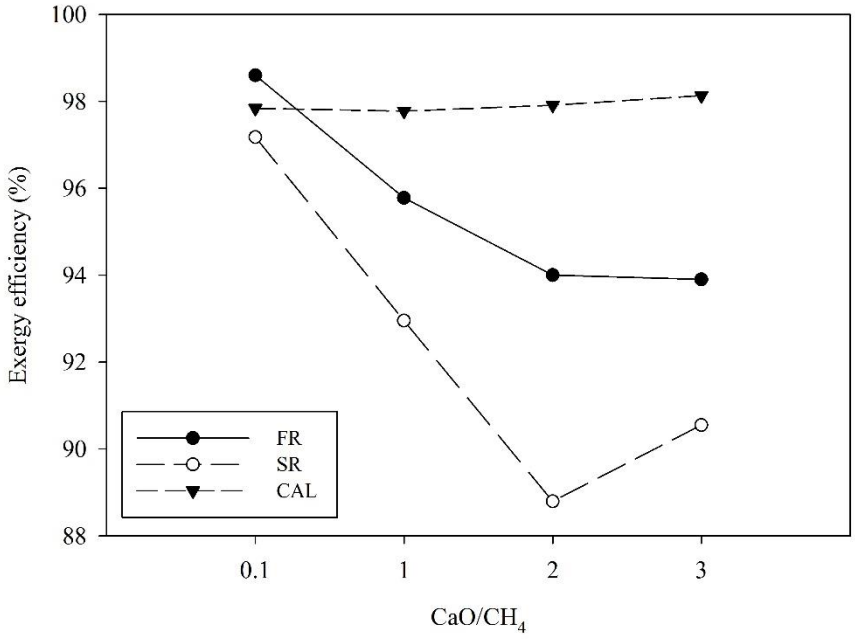

Figure 8.14 The exergy efficiency of the reactor unit as a function of CaO/CH_4 molar ratio.

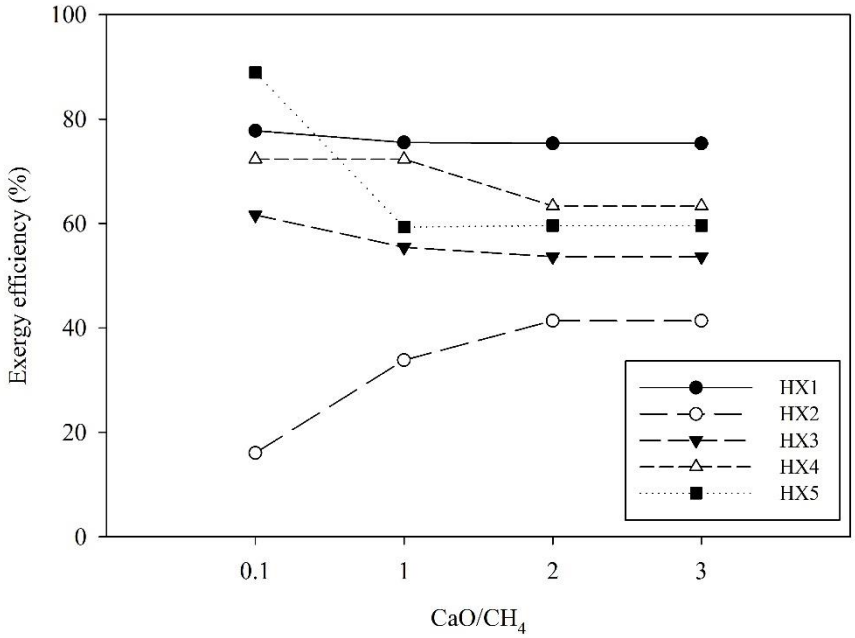

Figure 8.15 The exergy efficiency of the heat exchanger unit as a function of CaO/CH_4 molar ratio.

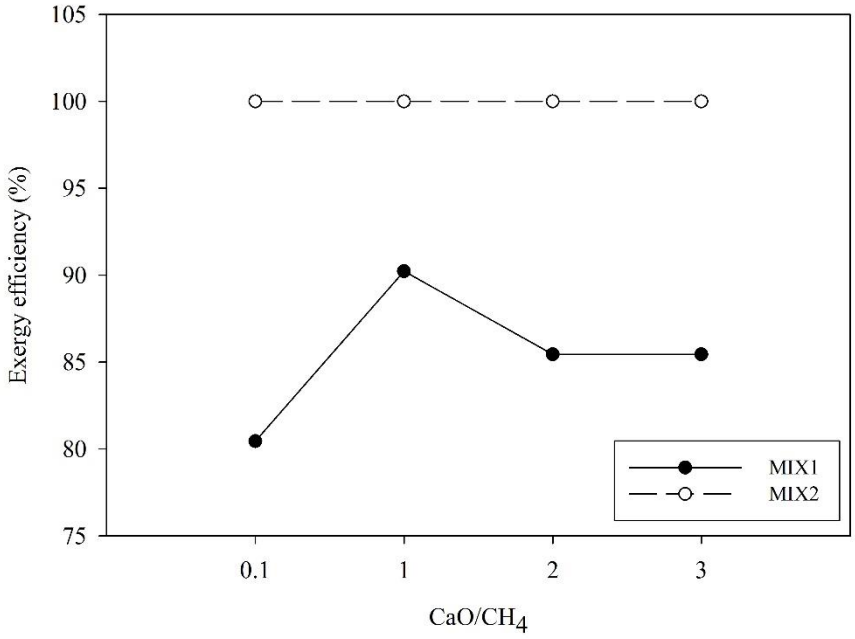

Figure 8.16 The exergy efficiency of the mixer unit as a function of CaO/CH_4 molar ratio.

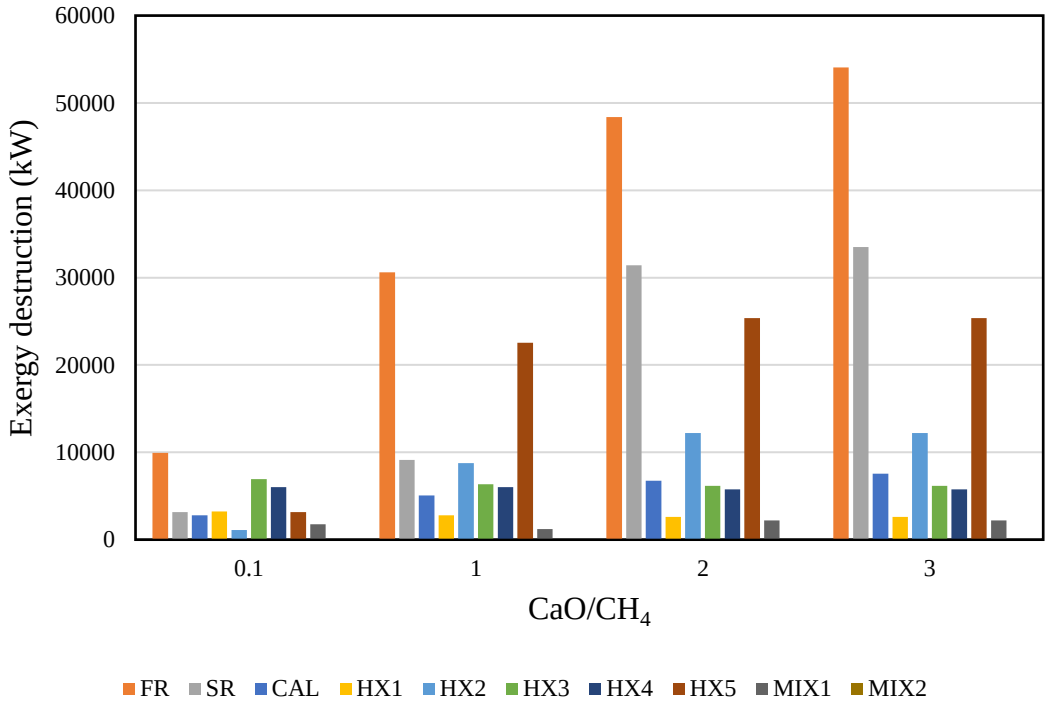

Figure 8.17 The exergy destruction of process unit as a function of CaO/CH_4 molar ratio.

8.2.4 Effect of S_{FR}/CH_4 molar ratio on energy and exergy efficiency

Figure 8.18 shows the effect of the S_{FR}/CH_4 molar ratio on the energy and exergy efficiency of the SECLR-WS process. The results show that the energy and exergy efficiencies are increased when the S_{FR}/CH_4 molar ratio is increased. The reason for this result is the increasing of S_{FR}/CH_4 molar ratio increase the total H_2 product, leading to the increasing of energy and exergy efficiency. The energy efficiency is slightly decreased in the range of S_{FR}/CH_4 molar ratio of 2 to 3 as a result of the high amount of steam in FR increases the amount of $CaCO_3$ leading to the increase of heat demand in CAL, while the total H_2 product is almost constant.

Figure 8.19–8.21 show the effect of S_{FR}/CH_4 molar ratio on the exergy efficiency of reactor unit, heat exchanger and heater unit, and the mixer unit, respectively, in the SECLR-WS process. The results show that increasing the S_{FR}/CH_4 molar ratio slightly affect the exergy efficiency of the FR and CAL. For the FR, the input exergy and output exergy of the FR slightly changes. Although, increasing the S_{FR}/CH_4 molar ratio increase amount of steam feed to FR, but when amount the steam is high, the temperature of the steam is low, and the input exergy of the FR is almost constant. The output exergy of the FR is almost constant same as the input exergy of the FR because of compensating between chemical exergy of gas and solid in the product stream. Increasing the S_{FR}/CH_4 molar ratio can increase the chemical exergy in gas phase due to the high amount of H_2 can be produced, but it decreases the chemical exergy in solid phase due to the decreasing of CaO. For the SR, the exergy efficiency of the SR is increased by increasing the S_{FR}/CH_4 molar ratio. The main reason for this result is the temperature of steam fed to the SR is high at low S_{FR}/CH_4 molar ratio. The high- temperature feed streams resulting in the high waste heat of the SR is generated and the exergy destruction is high, as shown in Figure 8.22.

The effect of S_{FR}/CH_4 molar ratio on the exergy efficiency of the heat exchanger and heater is shown in Figure 8.20. The results show that increasing the S_{FR}/CH_4 molar ratio can increase the exergy efficiency of the HX1 and HX3 and decrease the exergy efficiency of the HX2 and HX5. Increasing the exergy efficiency of the HX1 and HX3 is due to increasing the mass flow rate of SYNGAS stream when the S_{FR}/CH_4 molar ratio is increased, leading to the increase of the input physical exergy of the HX1 and

HX3. For the HX2, increasing the S_{FR}/CH_4 molar ratio increase the temperature difference leading to the increase of the exergy destruction, as shown in Figure 8.22. Although, the physical exergy of CO2 stream can be increased by increasing the S_{FR}/CH_4 molar ratio, the value of the input exergy of HX2 is less increased when compared with the increasing of the exergy destruction. The reason for decreasing the exergy efficiency of HX5 in the S_{FR}/CH_4 molar ratio range of 0.1 to 2 is the decreasing of the temperature of the steam generated from the heater by increasing of the amount of water feed. When the S_{FR}/CH_4 molar ratio is increased from 0.1 to 2, the temperature of steam in STEAM stream is decreased from 1293.8 to 504.4 ^oC leading to the decreasing of physical exergy of STEAM stream and the exergy destruction is increased. Although, decreasing the temperature of STEAM will result in the decreasing of input exergy by heat transfer to the heater. But the decreasing of the exergy of heat input of the heater is an exponential function in terms of $(1-T_0/T)$, thus decreasing of the temperature at high value decrease the exergy by heat transfer in the small value. On the other hand, when the S_{FR}/CH_4 molar ratio increase from 2 to 3, the temperature of STEAM stream decrease from 504.4 to 233.3 ^oC, leading to the decreasing of the exergy by heat transfer into the heater in high value and the exergy destruction of heater is decreased, as shown in Figure 8.22. Thus, the exergy efficiency of the HX5 is increased by increasing the S_{FR}/CH_4 molar ratio in the range of 2 to 3. In addition, increasing of S_{FR}/CH_4 molar ratio can improve the exergy efficiency of the MIX1, as shown in Figure 8.21. This is the result of the decreasing of the temperature difference when S_{FR}/CH_4 molar ratio is increased.

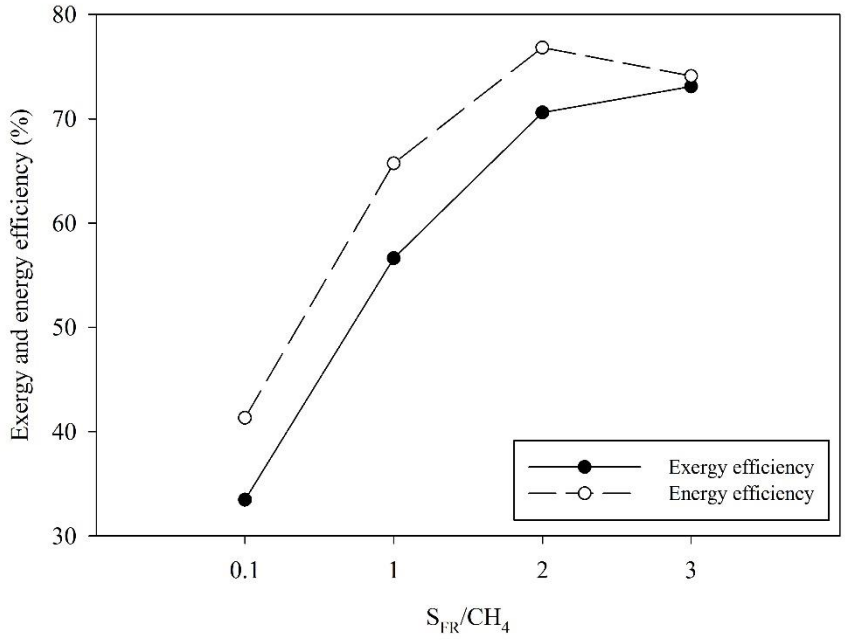

Figure 8.18 The exergy and energy efficiency of the SECLR-WS process as a function of S_{FR}/CH_4 molar ratio.

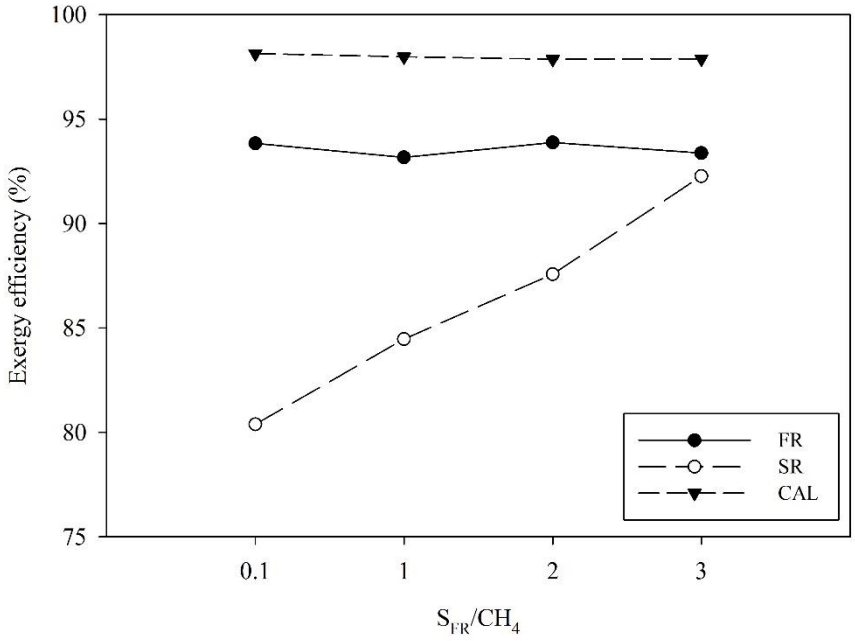

Figure 8.19 The exergy efficiency of the reactor unit as a function of S_{FR}/CH_4 molar ratio.

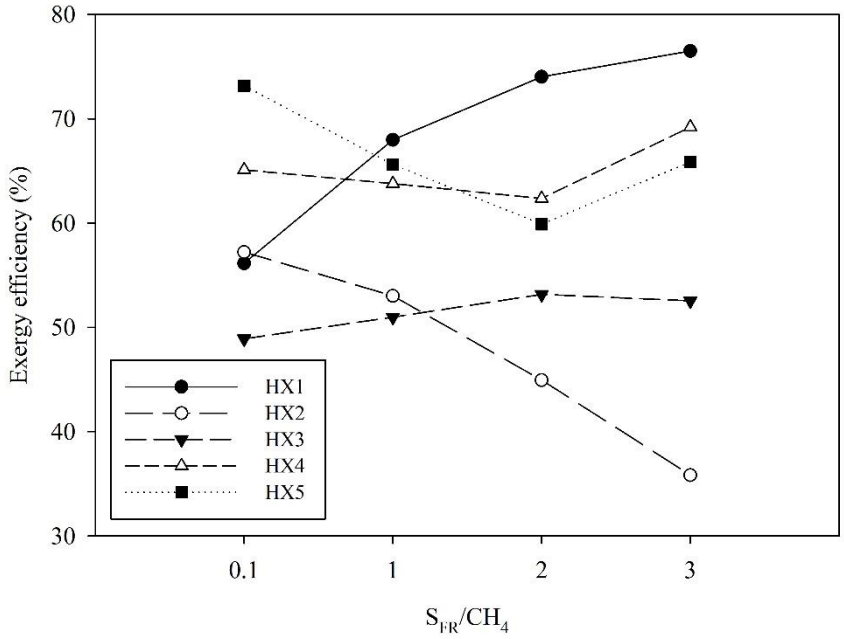

Figure 8.20 The exergy efficiency of the heat exchanger unit as a function of S_{FR}/CH_4 molar ratio.

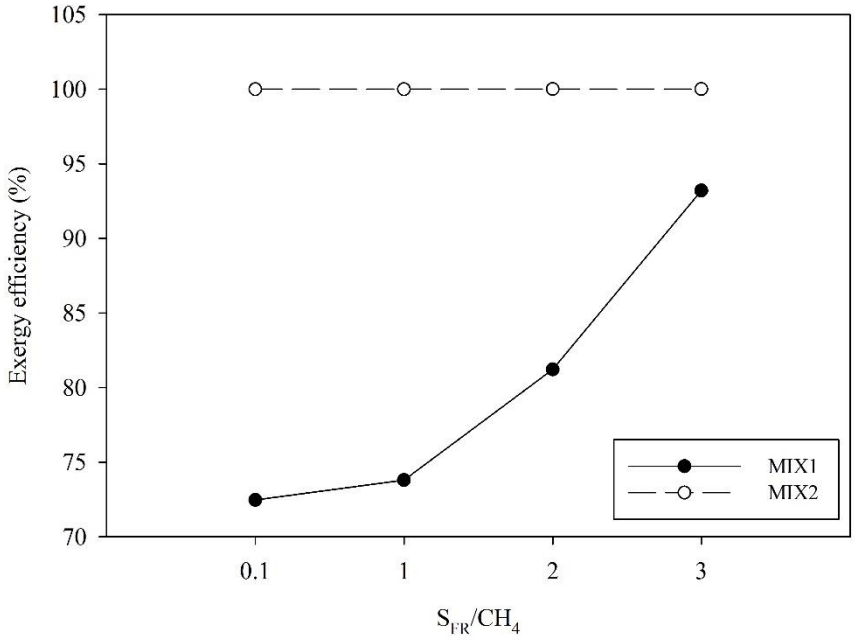

Figure 8.21 The exergy efficiency of the mixer unit as a function of S_{FR}/CH_4 molar ratio.

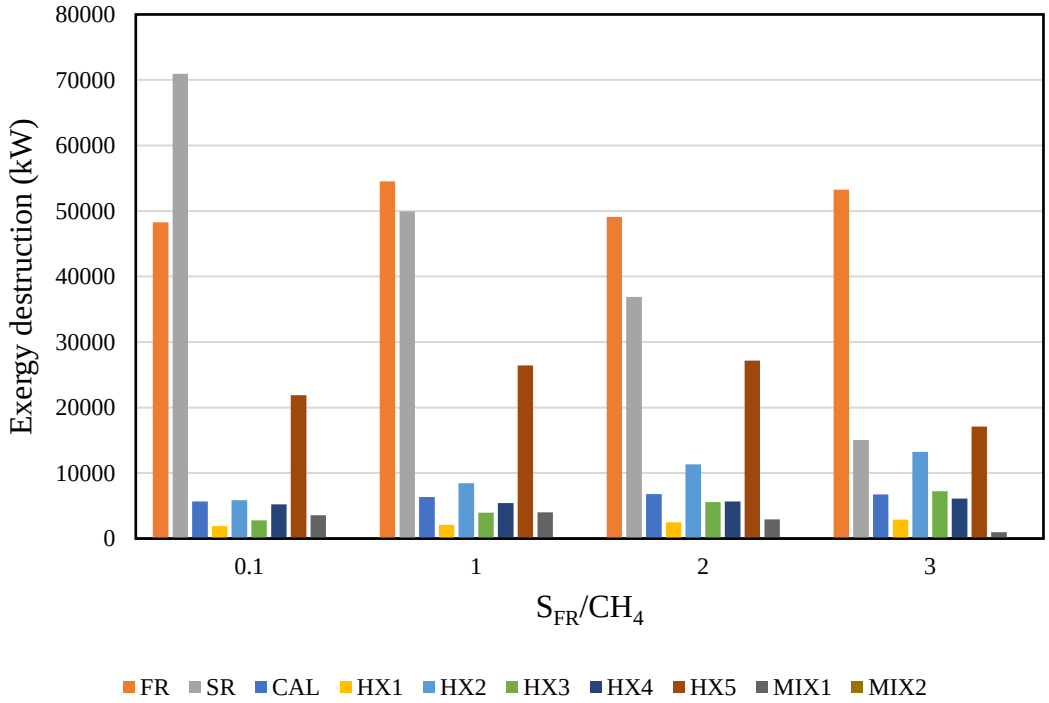

Figure 8.22 The exergy destruction of process unit as a function of S_{FR}/CH_4 molar ratio.

8.2.5 Effect of S_{SR}/CH_4 molar ratio on energy and exergy efficiency

Figure 8.23 shows the effect of S_{SR}/CH_4 molar ratio on the energy and exergy efficiency of the SECLR-WS process. The results show that the energy and exergy efficiency is increased when the S_{SR}/CH_4 molar ratio is increased in the range of 0.1 to 1. But in the range of the S_{SR}/CH_4 molar ratio of 1 to 3, increasing the S_{SR}/CH_4 molar ratio increases the exergy efficiency and decreases the energy efficiency. Because, when the S_{SR}/CH_4 molar ratio is increased in the range of 0.1 to 1, the H_2 production is increased leading to the increase of the energy and exergy efficiency of the process. While, when the S_{SR}/CH_4 molar ratio is increased in the range of 1 to 3, the H_2 production is constant and the amount of water feed is increased, leading to the low temperature of steam feed to the FR and SR. When low temperature of steam feed to the FR and SR, the heat of exothermic from the FR and SR are decreased while the heat of endothermic from CAL and heater is constant, thus the energy efficiency of the process is decreased by increasing of the net energy input to the process. On the other

hand, if the heat of exothermic from the FR and SR are decreased, it means that the waste heat generated from the reactor is decreased. Therefore, the exergy efficiency of the process is increased by increasing the S_{SR}/CH_4 molar ratio in the range of 1 to 3.

Figure 8.24–8.27 show the effect of the S_{SR}/CH_4 molar ratio on the exergy efficiency of reactor unit, heat exchanger and heater unit, and the mixer unit, respectively, in the SECLR-WS process. The results show that increasing the S_{SR}/CH_4 molar ratio increases the exergy efficiency in FR. Increasing the S_{SR}/CH_4 molar ratio not affect to the exergy output of the FR, but the exergy input of the FR is decreased due to the temperature of steam feed to the FR is decreased. Thus, the exergy destruction of FR is decreased, and the exergy efficiency of the FR is increased when the S_{SR}/CH_4 molar ratio is increased, as shown in Figure 8.27. For the SR, the exergy efficiency of the SR is decreased when the S_{SR}/CH_4 molar ratio is increased in the range of 0.1 to 1. This is the result of the increase of the steam, leading to the increase of the exothermic steam-iron reaction (Eq. (3.6)). Thus, the high waste heat is generated in the SR when the S_{SR}/CH_4 molar ratio is increased in the range of 0.1 to 1, and the exergy efficiency of the SR is decreased. The increasing of the exergy efficiency of the SR in the range of the S_{SR}/CH_4 molar ratio of 1 to 3 is the same reason for the increase of the exergy efficiency in FR. The exergy efficiency of the SR is increased due to the low temperature of steam feed to the SR while the heat from exothermic reaction is constant, leading to the low input exergy of the SR and low generated waste heat.

The effect of the S_{SR}/CH_4 molar ratio on the exergy efficiency of the heat exchanger and heater is shown in Figure 8.25. The results show that increasing the S_{SR}/CH_4 molar ratio can increase the exergy efficiency of the HX4 and decrease the exergy efficiency of the HX2 and HX3. Increasing the exergy efficiency of the HX4 is the result of the increasing of S_{SR}/CH_4 molar ratio, leading to the high amount of mass flow rate of stream H2 with a high amount of physical exergy. Thus, increasing of the S_{SR}/CH_4 molar ratio can be increases the exergy efficiency of HX4 by increasing of the input physical exergy of the HX4. In contrast, increasing the S_{SR}/CH_4 molar ratio decrease the exergy efficiency of the HX2 and HX3 due to the increasing of the temperature difference, leading to the increasing of the exergy destruction in HX2 and HX3, as shown in Figure 8.27, and decreasing of the exergy efficiency of HX2 and

HX3. Moreover, increasing the S_{SR}/CH_4 molar ratio can be improve the exergy efficiency of the MIX1, as shown in Figure 8.26. The reason for this result is the same as by increasing the S_{FR}/CH_4 molar ratio, when the S_{SR}/CH_4 molar ratio is increased, the temperature difference is decreased, leading to decreasing the exergy destruction of the MIX1.

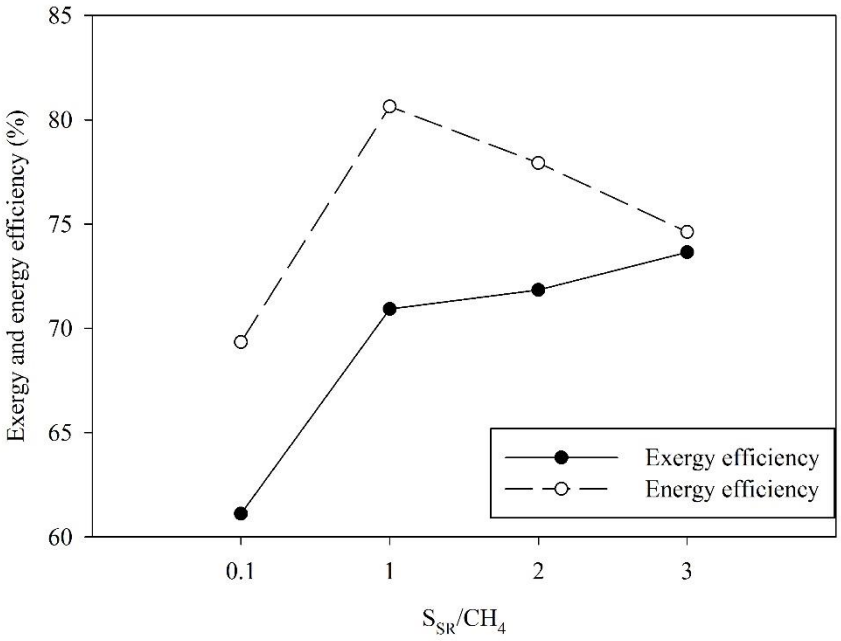

Figure 8.23 The exergy and energy efficiency of the SECLR-WS process as a function of S_{SR}/CH_4 molar ratio.

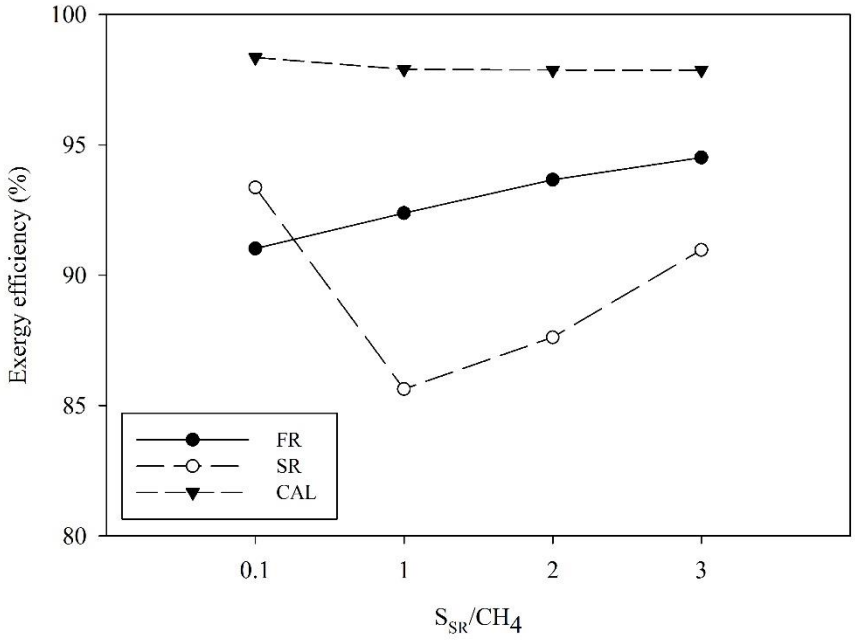

Figure 8.24 The exergy efficiency of the reactor unit as a function of S_{SR}/CH_4 molar ratio.

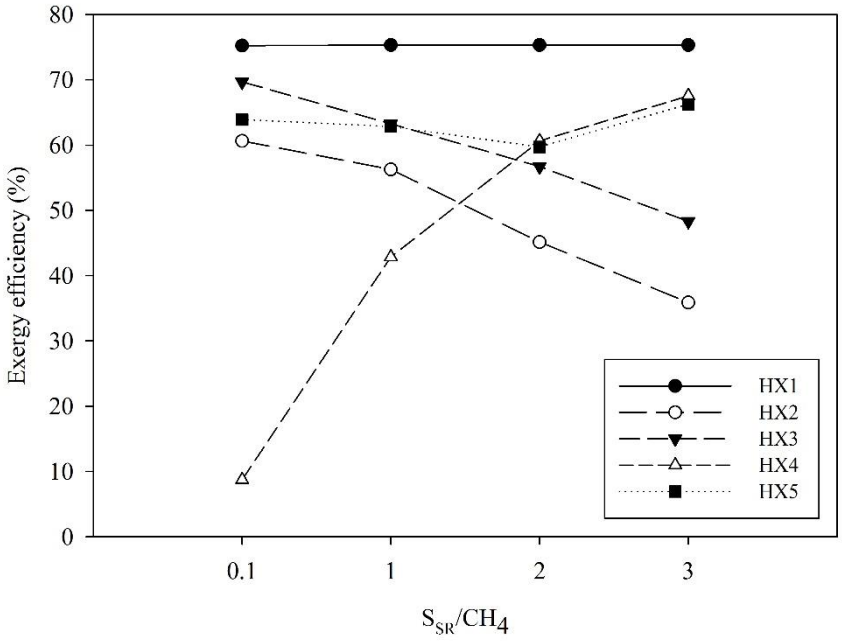

Figure 8.25 The exergy efficiency of the heat exchanger unit as a function of S_{SR}/CH_4 molar ratio.

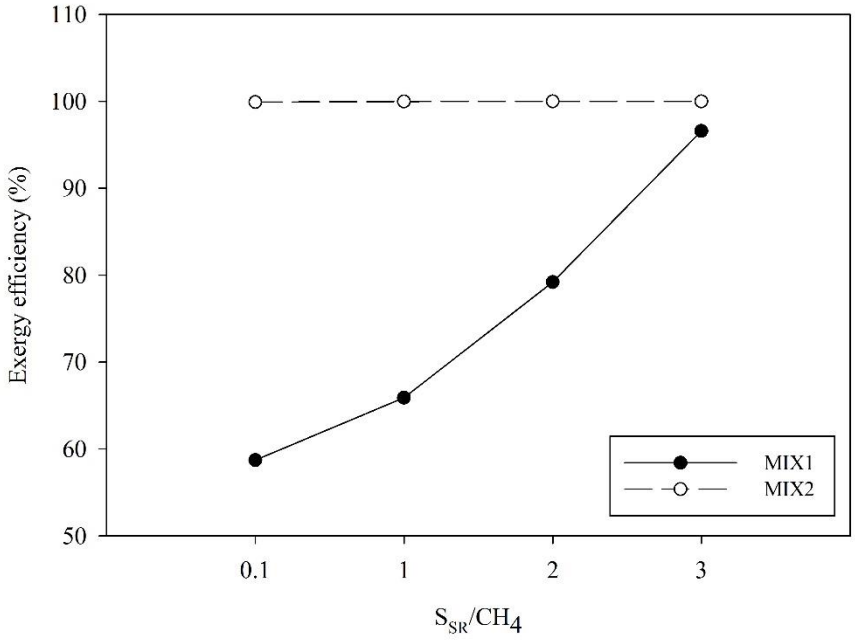

Figure 8.26 The exergy efficiency of the mixer unit as a function of S_{SR}/CH_4 molar ratio.

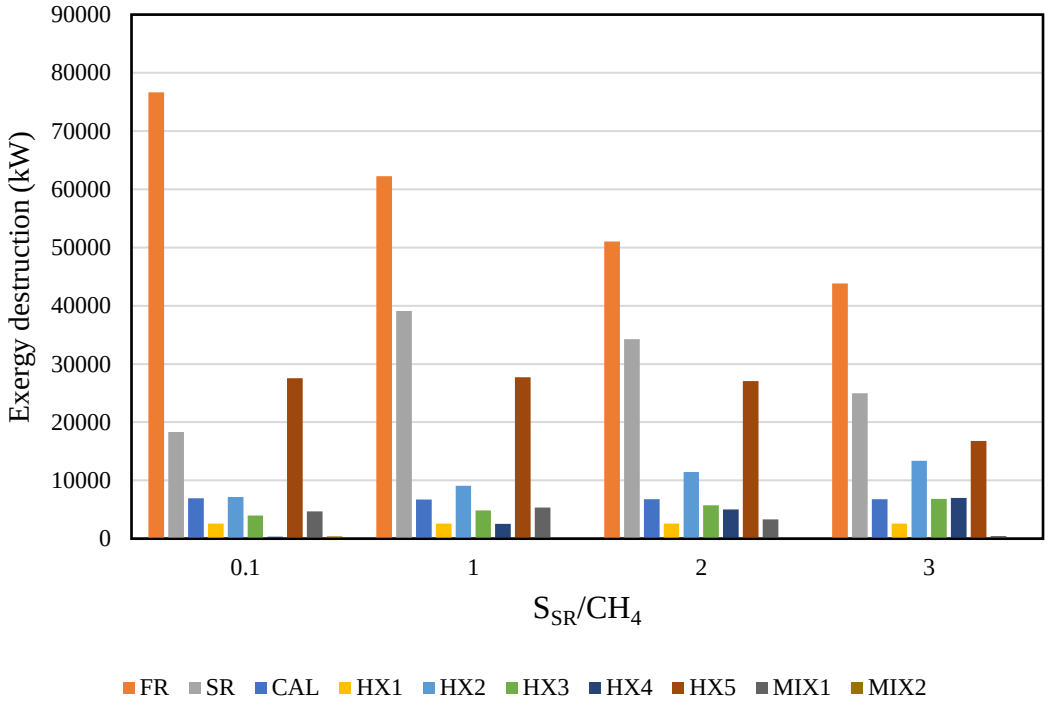

Figure 8.27 The exergy destruction of process unit as a function of S_{SR}/CH_4 molar ratio.

CHAPTER IX
CONCLUSION AND RECOMMENDATIONS

The novel integrated process of sorption-enhanced chemical looping reforming and water splitting (SECLR-WS) process for H_2 production was studied in this research. Biogas as a renewable fuel was considered as feedstock. The effects of primary operating parameters on the process performance in terms of the H_2 yield and purity are investigated using a thermodynamic approach under steady-state condition. The optimal operating conditions with two different objective functions i.e., maximize H_2 production and maximize thermal efficiency, were determined, and the optimal SECLR-WS process was compared to the SECLR and the CLWS process in terms of hydrogen yield and purity, and thermal efficiency of the process. Moreover, the pinch analysis was used to design the heat exchanger network of the SECLR-WS process to achieve the maximum heat recovery at the optimal operating conditions, and the exergy analysis of SECLR-WS was performed to determine the inefficient part in the process. The summary results of the study and the recommendation of future works are presented in this chapter.

9.1 Conclusion

The combined SECLR-WS process was studied using a thermodynamic approach. The simulation of the process was performed using an Aspen Plus simulator and a minimization of Gibbs free energy method. From the parametric analysis, it was found that H_2 purities in the H_2-rich syngas and high-purity H_2 stream of 97.01 and 99.93%, respectively, with a high total H_2 yield of 3.8 can be obtained when T_{FR} = 610 °C, T_{SR} = 500 °C, and the S_{FR}/CH_4, CaO/CH_4, Fe_3O_4/CH_4, and S_{SR}/CH_4 molar ratios were 2.2, 1.66, 1, and 2.87, respectively. At low FR temperatures (less than 800 °C), increasing of S_{FR}/CH_4 and CaO/CH_4 molar ratios could improve the H_2 yield in the FR, total H_2 yield, and H_2 purity in the FR due to the sorption-enhanced reforming. The high value of the Fe_3O_4/CH_4 molar ratio had an inverse effect on the H_2 yield in the FR due to the oxidation of CH_4 and H_2. Moreover, increasing of Fe_3O_4/CH_4 molar ratio

could improve the heat demand in the FR. The high CO_2 concentration in the feed stream had a negative effect on H_2 yield and purity due to the excess amount of CO_2, which could not be completely captured by CaO. In addition, higher the SR operating pressures were more suitable than low pressures because a low CO concentration in the high-purity H_2 stream could be achieved at high pressures when using small S_{SR}/CH_4 molar ratios. The advantages of these operating conditions were the small equipment size, and low amount of steam needed. A CO concentration of 20 ppm could be obtained when T_{SR} was 500 °C and the S_{SR}/CH_4 molar ratio was approximately 6.75.

After the sensitivity analysis was performed, the optimization of the SECLR-WS process was conducted. Two objective functions, which maximize the total H_2 yield and maximize the thermal efficiency of the process, were used to optimize the SECLR-WS process in three cases. From the optimization, the results showed that the maximum total H_2 yield of 3.9081 was obtained without the steam feed to FR in CASEI. The SECLR-WS process can operated in high thermal efficiency while produces the two grades of the H_2 product. The flexibility of two grades H_2 production could be done by adjusting the three operating parameters i.e., S_{FR}/CH_4, S_{SR}/CH_4, and Fe_3O_4/CH_4 molar ratios. When the large quantities of high purity H_2 was needed, the maximum thermal efficiency could be achieved by decreasing the S_{FR}/CH_4 molar ratio and increasing the S_{SR}/CH_4 and Fe_3O_4/CH_4 molar ratios. The H_2 yield in FR of 3.1126 and in SR of 0.6666 with the high thermal efficiency of 68.42 % were obtained at the optimal operating condition in CASEIII, which were T_{FR} of 606.8 ^oC, S_{FR}/CH_4, S_{SR}/CH_4, Fe_3O_4/CH_4, and CaO/CH_4 molar ratio of 2.35, 2.33, 0.92, and 1.94, respectively.

The comparison of the combined SECLR-WS process with the two sub processes, which were the SECLR and CLWS processes in terms of the H_2 yield and purity, and the thermal efficiency of the process was presented. The feed used in the comparison study was 1 kmol/sec of natural gas was assumed to be pure of CH_4. The results showed that the SECLR and CLWS processes could operated at the autothermal condition. The highest total H_2 of 3.9848 could be obtained in the SECLR-WS process at the optimal CASEI-com. The lowest thermal efficiency of 52.49 % occured in the CLWS process, because the high purity H_2 could be produced at high pressure system and high amount of steam. While the highest thermal efficiency of 73.84 % occured in

the SECLR-WS process at the optimal CASEII-com. Although the SECLR and CLWS process can be operated at the autothermal condition, the total amount of produced H_2 was low. Thus, when compared with the SECLR and CLWS processes, the SECLR-WS process could be offered the high total H_2 yield and thermal energy efficiency. In addition, the SECLR-WS process could produce the two grades of H_2 product. The H_2 yield in H_2-rich syngas stream and high purity H_2 stream of 3.3768 and 0.4001, respectively, could be obtained with high thermal efficiency of 71.40 % at the optimal operating condition in CASEIII-com which was at T_{FR} of 610.8 ^oC, S_{FR}/CH_4, S_{SR}/CH_4, Fe_3O_4/CH_4, and CaO/CH_4 molar ratio of 2.76, 1.39, 1.13, and 1, respectively.

The performance of the optimal SECLR-WS process was improved by performing the heat integration scheme. The purpose of this study was to improve the thermal efficiency of the SECLR-WS process, which was operated at the optimal operating condition CASEIII, for H_2 production from biogas. The results from pinch analysis indicated that the process was the threshold problem in the type of non-utility end. The only 89318.6 kW of hot utility was the minimum utility required in the process at the ΔT_{min} of 125 ^oC. The heat exchanger network design was performed by selecting the optimal ΔT_{min} of 125 ^oC, which was the ΔT_{min} threshold. The heat exchanger network in the optimal SECLR-WS process consisted of the five heat exchangers. From the heat integration, the thermal efficiency of the optimal SECLR-WS process was increased from 68.42 % to 76.83 %.

To access the reliable performance of the optimal SECLR-WS process with heat integration, the energy and exergy analyses are performed, and the effect of key operating parameters on the energy and exergy efficiency of the process was investigated. The results showed that, in the optimal SECLR-WS process, the highest exergy destruction was occurred the FR and SR due to the occurrence of several reactions in these units leading to the high irreversibility. However, the high exergy efficiency is occurred in the group of reactor units, while the group of heat exchanger units showed that low exergy efficiency. Because of the difference temperature in the heat exchanger units was very high, leading to the low exergy efficiency. While the input exergy of the reactor units was very high compared with the exergy destruction in these units, leading to the high exergy efficiency. The exergy efficiency of the

process could be improved by utilizing heat released from the exothermic reactors, FR and SR, to the heater for decreases the exergy destruction from the reactors. The exergy efficiency of the heat exchanger could be improved by using the different level of utility to decreases the temperature different in each heat exchanger unit. The energy and exergy efficiency of the process can be increased by increasing the CaO/CH_4 molar ratio and the steam feed to FR and SR, due to the amount of H_2 product was increased by increasing the CaO/CH_4 molar ratio and the steam feed to FR and SR. While increasing the FR temperature and Fe_3O_4/CH_4 molar ratio was created the optimal point of exergy efficiency due to the difference of the reaction occurred in system in the high and low FR temperature and Fe_3O_4/CH_4 molar ratio.

9.2 Recommendations

9.2.1 The inert solid should be added into the system to improve the stability of the oxygen carrier and adsorbent, and to improve the heat transfer from the solid circulation.

9.2.2. The network optimization and the heat integration considering the quality of utility and the use of the heat from the exothermic reaction should be performed to improve the energy and exergy efficiency of the process.

9.2.3. The non-ideal heat transfer and the size of solid should be considered in the future work to study the behavior of transport phenomenon in the reactors.

9.2.4. In present, the experimental data is quite limited, so in the future, the kinetic developed by using the experimental data should be used as a simulation tool to improve the reliability of the simulation.

9.2.5 The economic analysis of the process should be performed in the future work to determine the economic feasibility of the process.

9.2.6 The SECLR-WS process should be integrated with the PEMFC system to produce the couple of electricity and H_2. The integrated system is interesting because the H_2 product from the SECLR-WS process can be used directly in the PEMFC system to produces the electricity without additional unit.

REFERENCES

A. Phuluanglue, W. K., S. Wongsakulphasatch, W. Kiatkittipong, A. Arpornwichanop, and S. Assabumrungrat. (2015). Simulation of Modified Sorption Enhanced Chemical Looping Reforming for Hydrogen Production from Biogas. International Journal of Chemical, Environmental & Biological Sciences (IJCEBS), 3, 339-343.

Abad, A. (2015). Chemical looping for hydrogen production. 327-374.

Abad, A., Mattisson, T., Lyngfelt, A., and Johansson, M. (2007). The use of iron oxide as oxygen carrier in a chemical-looping reactor. Fuel, 86, 1021-1035.

Antzara, A., Heracleous, E., Bukur, D. B., and Lemonidou, A. A. (2015). Thermodynamic analysis of hydrogen production via chemical looping steam methane reforming coupled with in situ CO2 capture. International Journal of Greenhouse Gas Control, 32, 115-128.

Authayanun, S., Aunsup, P., Patcharavorachot, Y., and Arpornwichanop, A. (2014). Theoretical analysis of a biogas-fed PEMFC system with different hydrogen purifications: Conventional and membrane-based water gas shift processes. Energy Conversion and Management, 86, 60-69.

Balat, H., and Kırtay, E. (2010). Hydrogen from biomass – Present scenario and future prospects. International Journal of Hydrogen Energy, 35, 7416-7426.

Bhatia, K. K., and Wang, C.-Y. (2004). Transient carbon monoxide poisoning of a polymer electrolyte fuel cell operating on diluted hydrogen feed. Electrochimica Acta, 49, 2333-2341.

Bleeker, M. F., Kersten, S. R. A., and Veringa, H. J. (2007). Pure hydrogen from pyrolysis oil using the steam-iron process. Catalysis Today, 127, 278-290.

Bleeker, M. F., Veringa, H. J., and Kersten, S. R. A. (2010). Pure Hydrogen Production from Pyrolysis Oil Using the Steam−Iron Process: Effects of Temperature and Iron Oxide Conversion in the Reduction. Industrial & Engineering Chemistry Research, 49, 53-64.

Boles, M. A., and Yunus A. Cengel, D. (2014). Thermodynamics: An Engineering Approach: McGraw-Hill Education.

Bonilla-Petriciolet, A., Rangaiah, G. P., and Segovia-Hernández, J. G. (2011). Constrained and unconstrained Gibbs free energy minimization in reactive systems using genetic algorithm and differential evolution with tabu list. Fluid Phase Equilibria, 300, 120-134.

Boyano, A., Blanco-Marigorta, A. M., Morosuk, T., and Tsatsaronis, G. (2011). Exergoenvironmental analysis of a steam methane reforming process for hydrogen production. Energy, 36, 2202-2214.

Chen, S., Xue, Z., Wang, D., and Xiang, W. (2012). Hydrogen and electricity co-production plant integrating steam-iron process and chemical looping combustion. International Journal of Hydrogen Energy, 37, 8204-8216.

Chiesa, P., Lozza, G., Malandrino, A., Romano, M., and Piccolo, V. (2008). Three-reactors chemical looping process for hydrogen production. International Journal of Hydrogen Energy, 33, 2233-2245.

Cormos, C.-C. (2010). Evaluation of iron based chemical looping for hydrogen and electricity co-production by gasification process with carbon capture and storage. International Journal of Hydrogen Energy, 35, 2278-2289.

Dimian, A. C., Bildea, C. S., and Kiss, A. A. (2014). Pinch Point Analysis. 35, 525-564.

Dincer, I., and Rosen, M. A. (2013). Exergy Analysis of Hydrogen Production Systems. 347-362.

Ding, Y., and Alpay, E. (2000). Adsorption-enhanced steam–methane reforming. Chemical Engineering Science, 55, 3929-3940.

Dou, B., Song, Y., Wang, C., Chen, H., and Xu, Y. (2014). Hydrogen production from catalytic steam reforming of biodiesel byproduct glycerol: Issues and challenges. Renewable and Sustainable Energy Reviews, 30, 950-960.

Edrisi, A., Mansoori, Z., Dabir, B., and Shahnazari, A. (2014). Hydrogen, nitrogen and carbon dioxide production through chemical looping using iron-based oxygen carrier – A Green plant for H2 and N2 production. International Journal of Hydrogen Energy, 39, 10380-10391.

Effendi, A., Hellgardt, K., Zhang, Z., and Yoshida, T. (2005). Optimising H production from model biogas via combined steam reforming and CO shift reactions. Fuel, 84, 869-874.

Fan, J., Hong, H., Zhu, L., Wang, Z., and Jin, H. (2017). Thermodynamic evaluation of chemical looping combustion for combined cooling heating and power production driven by coal. Energy Conversion and Management, 135, 200-211.

Fan, J., Zhu, L., Jiang, P., Li, L., and Liu, H. (2016). Comparative exergy analysis of chemical looping combustion thermally coupled and conventional steam methane reforming for hydrogen production. Journal of Cleaner Production, 131, 247-258.

Flytzani-Stephanopoulos, M., and Voecks, G. E. (1983). Autothermal reforming of aliphatic and aromatic hydrocarbon liquids. International Journal of Hydrogen Energy, 8, 539-548.

Fraser, S. D., Monsberger, M., and Hacker, V. (2006). A thermodynamic analysis of the reformer sponge iron cycle. Journal of Power Sources, 161, 420-431.

Go, K., Son, S., Kim, S., Kang, K., and Park, C. (2009). Hydrogen production from two-step steam methane reforming in a fluidized bed reactor. International Journal of Hydrogen Energy, 34, 1301-1309.

Hufton, J., Mayorga, S., and Sircar, S. (1999). Sorption-enhanced reaction process for hydrogen production. AIChE Journal, 45, 248-256.

Ishida, M., and Jin, H. (1996). A Novel Chemical-Looping Combustor without NOx Formation. Industrial & Engineering Chemistry Research, 35, 2469-2472.

J.Y., X., M., C., and M., S. (2004). Calculation for physical and chemical exergy of flows in systems elaborating mixed-phase flows and a case study in an IRSOFC plant. International Journal of Energy Research, 28, 101-115.

Kasemanand, S., Im-orb, K., Tippawan, P., Wiyaratn, W., and Arpornwichanop, A. (2017). Exergy analysis of the biogas sorption-enhanced chemical looping reforming process integrated with a high-temperature proton exchange membrane fuel cell. Energy Conversion and Management, 149, 485-494.

Kathe, M. V., Empfield, A., Na, J., Blair, E., and Fan, L.-S. (2016). Hydrogen production from natural gas using an iron-based chemical looping technology: Thermodynamic simulations and process system analysis. Applied Energy, 165, 183-201.

Kemp, I. C. (2011). Pinch Analysis and Process Integration: A User Guide on Process Integration for the Efficient Use of Energy.

Khan, M. N., and Shamim, T. (2016). Investigation of hydrogen generation in a three reactor chemical looping reforming process. Applied Energy, 162, 1186-1194.

Lane, H. (1913). Process for the production of hydrogen. In: Google Patents.

Lima da Silva, A., Dick, L. F. P., and Lourdes Müller, I. (2012). Performance of a PEMFC system integrated with a biogas chemical looping reforming processor: A theoretical analysis and comparison with other fuel processors (steam reforming, partial oxidation and auto-thermal reforming). International Journal of Hydrogen Energy, 37, 6580-6600.

Linnhoff, B., and Hindmarsh, E. (1983). The pinch design method for heat exchanger networks. Chemical Engineering Science, 38, 745-763.

Lyngfelt, A., Leckner, B., and Mattisson, T. (2001). A fluidized-bed combustion process with inherent CO2 separation; application of chemical-looping combustion. Chemical Engineering Science, 56, 3101-3113.

Martavaltzi, C. S., Pampaka, E. P., Korkakaki, E. S., and Lemonidou, A. A. (2010). Hydrogen Production via Steam Reforming of Methane with Simultaneous CO2Capture over CaO−Ca12Al14O33. Energy & Fuels, 24, 2589-2595.

Martínez, I., Romano, M. C., Fernández, J. R., Chiesa, P., Murillo, R., and Abanades, J. C. (2014). Process design of a hydrogen production plant from natural gas with CO2 capture based on a novel Ca/Cu chemical loop. Applied Energy, 114, 192-208.

Medrano, J. A., Potdar, I., Melendez, J., Spallina, V., Pacheco-Tanaka, D. A., van Sint Annaland, M., and Gallucci, F. (2018). The membrane-assisted chemical looping reforming concept for efficient H 2 production with inherent CO 2 capture: Experimental demonstration and model validation. Applied Energy, 215, 75-86.

Messerschmitt, A. (1910). Process of producing hydrogen. In: Google Patents.

Muellerlanger, F., Tzimas, E., Kaltschmitt, M., and Peteves, S. (2007). Techno-economic assessment of hydrogen production processes for the hydrogen economy for the short and medium term. International Journal of Hydrogen Energy, 32, 3797-3810.

Mukherjee, S., Kumar, P., Yang, A., and Fennell, P. (2015). Energy and exergy analysis of chemical looping combustion technology and comparison with pre-combustion and oxy-fuel combustion technologies for CO 2 capture. Journal of Environmental Chemical Engineering, 3, 2104-2114.

Ogden, J. M. (2001). Review of small stationary reformers for hydrogen production.

Ortiz, M., de Diego, L. F., Abad, A., García-Labiano, F., Gayán, P., and Adánez, J. (2010). Hydrogen production by auto-thermal chemical-looping reforming in a pressurized fluidized bed reactor using Ni-based oxygen carriers. International Journal of Hydrogen Energy, 35, 151-160.

Perry, R., and Green, D. (2008). Perry's Chemical Engineers' Handbook, Eighth Edition: McGraw-Hill Education.

Peters, M. S., Timmerhaus, K. D., and West, R. E. (2003). Plant Design and Economics for Chemical Engineers: McGraw-Hill.

Phuluanglue, A., Khaodee, W., and Assabumrungrat, S. (2017). Simulation of intensified process of sorption enhanced chemical-looping reforming of methane: Comparison with conventional processes. Computers & Chemical Engineering, 105, 237-245.

Pimenidou, P., Rickett, G., Dupont, V., and Twigg, M. V. (2010). High purity H2 by sorption-enhanced chemical looping reforming of waste cooking oil in a packed bed reactor. Bioresour Technol, 101, 9279-9286.

Pipatmanomai, S., Kaewluan, S., and Vitidsant, T. (2009). Economic assessment of biogas-to-electricity generation system with H2S removal by activated carbon in small pig farm. Applied Energy, 86, 669-674.

Poku, M. Y. B., Biegler, L. T., and Kelly, J. D. (2004). Nonlinear Optimization with Many Degrees of Freedom in Process Engineering. Industrial & Engineering Chemistry Research, 43, 6803-6812.

Querol, E., Gonzalez-Regueral, B., and Perez-Benedito, J. L. (2013). Exergy Concept and Determination. 9-28.

Rakib, M. A., Grace, J. R., Lim, C. J., Elnashaie, S. S. E. H., and Ghiasi, B. (2010). Steam reforming of propane in a fluidized bed membrane reactor for hydrogen production. International Journal of Hydrogen Energy, 35, 6276-6290.

Ritter, J. A., and Ebner, A. D. (2007). State-of-the-Art Adsorption and Membrane Separation Processes for Hydrogen Production in the Chemical and Petrochemical Industries. Separation Science and Technology, 42, 1123-1193.

Rydén, M., and Arjmand, M. (2012). Continuous hydrogen production via the steam–iron reaction by chemical looping in a circulating fluidized-bed reactor. International Journal of Hydrogen Energy, 37, 4843-4854.

Ryden, M., and Lyngfelt, A. (2006). Using steam reforming to produce hydrogen with carbon dioxide capture by chemical-looping combustion. International Journal of Hydrogen Energy, 31, 1271-1283.

Ryden, M., Lyngfelt, A., and Mattisson, T. (2006). Synthesis gas generation by chemical-looping reforming in a continuously operating laboratory reactor. Fuel, 85, 1631-1641.

Rydén, M., Lyngfelt, A., and Mattisson, T. (2008). Chemical-Looping Combustion and Chemical-Looping Reforming in a Circulating Fluidized-Bed Reactor Using Ni-Based Oxygen Carriers. Energy & Fuels, 22, 2585-2597.

Rydén, M., and Ramos, P. (2012). H2 production with CO2 capture by sorption enhanced chemical-looping reforming using NiO as oxygen carrier and CaO as CO2 sorbent. Fuel Processing Technology, 96, 27-36.

Sahdev, M. (2012). Pinch Technology: Basics for Beginners.

Schomaker, A., Boerboom, A., Visser, A., and Pfeifer, A. (2000). Anaerobic digestion of agro-industrial wastes: information networks technical summary on gas treatment. AD_NETT Project FAIR-CT96-2083 (DG12-SSMI).

Shokrollahi Yancheshmeh, M., Radfarnia, H. R., and Iliuta, M. C. (2016). High temperature CO2 sorbents and their application for hydrogen production by sorption enhanced steam reforming process. Chemical Engineering Journal, 283, 420-444.

Smith, R. (2016). Chemical Process Design and Integration.

Song, C., Liu, Q., Ji, N., Kansha, Y., and Tsutsumi, A. (2015). Optimization of steam methane reforming coupled with pressure swing adsorption hydrogen production process by heat integration. Applied Energy, 154, 392-401.

Steinberg, M., and Cheng, H. C. (1989). Modern and prospective technologies for hydrogen production from fossil fuels. International Journal of Hydrogen Energy, 14, 797-820.

Svoboda, K., Siewiorek, A., Baxter, D., Rogut, J., and Pohořelý, M. (2008). Thermodynamic possibilities and constraints for pure hydrogen production by a nickel and cobalt-based chemical looping process at lower temperatures. Energy Conversion and Management, 49, 221-231.

Svoboda, K., Slowinski, G., Rogut, J., and Baxter, D. (2007). Thermodynamic possibilities and constraints for pure hydrogen production by iron based chemical looping process at lower temperatures. Energy Conversion and Management, 48, 3063-3073.

Szargut, J. (2005). Exergy Method: Technical and Ecological Applications: WIT Press.

Takenaka, S., Nomura, K., Hanaizumi, N., and Otsuka, K. (2005). Storage and formation of pure hydrogen mediated by the redox of modified iron oxides. Applied Catalysis A: General, 282, 333-341.

Thursfield, A., Murugan, A., Franca, R., and Metcalfe, I. S. (2012). Chemical looping and oxygen permeable ceramic membranes for hydrogen production – a review. Energy & Environmental Science, 5, 7421.

Tippawan, P., Thammasit, T., Assabumrungrat, S., and Arpornwichanop, A. (2016). Using glycerol for hydrogen production via sorption-enhanced chemical looping reforming: Thermodynamic analysis. Energy Conversion and Management, 124, 325-332.

Tugnoli, A., Landucci, G., and Cozzani, V. (2008). Sustainability assessment of hydrogen production by steam reforming. International Journal of Hydrogen Energy, 33, 4345-4357.

Udomchoke, T., Wongsakulphasatch, S., Kiatkittipong, W., Arpornwichanop, A., Khaodee, W., Powell, J., Gong, J., and Assabumrungrat, S. (2016). Performance evaluation of sorption enhanced chemical-looping reforming for hydrogen production from biomass with modification of catalyst and sorbent regeneration. Chemical Engineering Journal, 303, 338-347.

Voitic, G., and Hacker, V. (2016). Recent advancements in chemical looping water splitting for the production of hydrogen. RSC Adv., 6, 98267-98296.

Xiang, W., Chen, S., Xue, Z., and Sun, X. (2010). Investigation of coal gasification hydrogen and electricity co-production plant with three-reactors chemical looping process. International Journal of Hydrogen Energy, 35, 8580-8591.

Yahom, A., Powell, J., Pavarajarn, V., Onbhuddha, P., Charojrochkul, S., and Assabumrungrat, S. (2014). Simulation and thermodynamic analysis of chemical looping reforming and CO2 enhanced chemical looping reforming. Chemical Engineering Research and Design, 92, 2575-2583.

Yang, L., Ge, X., Wan, C., Yu, F., and Li, Y. (2014). Progress and perspectives in converting biogas to transportation fuels. Renewable and Sustainable Energy Reviews, 40, 1133-1152.

Yoon, S.-G., Lee, J., and Park, S. (2007). Heat integration analysis for an industrial ethylbenzene plant using pinch analysis. Applied Thermal Engineering, 27, 886-893.

Zamel, N., and Li, X. (2011). Effect of contaminants on polymer electrolyte membrane fuel cells. Progress in Energy and Combustion Science, 37, 292-329.

Zeng, L., He, F., Li, F., and Fan, L.-S. (2012). Coal-Direct Chemical Looping Gasification for Hydrogen Production: Reactor Modeling and Process Simulation. Energy & Fuels, 26, 3680-3690.

Zeppieri, M., Villa, P. L., Verdone, N., Scarsella, M., and De Filippis, P. (2010). Kinetic of methane steam reforming reaction over nickel- and rhodium-based catalysts. Applied Catalysis A: General, 387, 147-154.

Zhu, L., Zhou, M., Shao, C., and He, J. (2018). Comparative exergy analysis between liquid fuels production through carbon dioxide reforming and conventional steam reforming. Journal of Cleaner Production, 192, 88-98.

VITA

Mr. Natthaporn Saithong was born on May 23, 1993, in Bangkok, Thailand. He finished high school from Wat Suthiwararam School in 2012. During his undergraduate study, he had the opportunity to attend a student training program in the position of Plant Technical at PTT Global Chemical Public Company Limited, Rayong. He received his Bachelor's Degree in Chemical Engineering from Department of Chemical Engineering, Faculty of Engineering, Kasetsart University in 2016. After graduation, he pursued graduate study and received his Master's degree in Chemical Engineering from Department of Chemical Engineering, Faculty of Engineering, Chulalongkorn University under the supervision of Asst. Prof. Amornchai Arpornwichanop.